

2

AFWAL-TR-81-3036

LEVEL II

2

AD A108610



# CAVITY OSCILLATION IN CRUISE MISSILE CARRIER AIRCRAFT

H. W. BARTEL  
J. M. MC AVOY

LOCKHEED-GEORGIA COMPANY  
STRUCTURES TECHNOLOGY DIVISION  
MARIETTA, GEORGIA 30063

DTIC  
ELECTE  
S DEC 15 1981 D  
E

JUNE 1981

Final Report For Period August 1979 to April 1981

Approved for public release; distribution unlimited

FLIGHT DYNAMICS LABORATORY  
AIR FORCE WRIGHT AERONAUTICAL LABORATORIES  
AIR FORCE SYSTEMS COMMAND  
WRIGHT-PATTERSON AIR FORCE BASE, OHIO 45433

81 12 14 087

DTIC FILE COPY

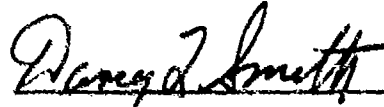
NOTICE

When Government drawings, specifications, or other data are used for any purpose other than in connection with a definitely related Government procurement operation, the United States Government thereby incurs no responsibility nor any obligation whatsoever, and the fact that the government may have formulated, furnished, or in any way supplied the said drawings, specifications, or other data, is not to be regarded by implication or otherwise as in any manner licensing the holder or any other person or corporation, or conveying any rights or permission to manufacture, use, or sell any patented invention that may in any way be related thereto.

This technical report has been reviewed and is approved for publication.

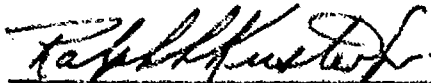


LEONARD L. SHAW  
Project Manager



DAVEY L. SMITH, Chief  
Structural Integrity Branch  
Structures & Dynamics Division

FOR THE COMMANDER:



RALPH L. KUSTER, JR., Colonel, USAF  
Chief, Structures & Dynamics Division

If your address has changed, if you wish to be removed from our mailing list, or if the addressee is no longer employed by your organization please notify AFWAL/FIBE, W-P AFB, OH 45433 to help us maintain a current mailing list.

Copies of this report should not be returned unless return is required by security considerations, contractual obligations, or notice on a specific document.

REPORT DOCUMENTATION PAGE		READ INSTRUCTIONS BEFORE COMPLETING FORM
1. REPORT NUMBER AFWAL-TR-81-3036	2. GOVT ACCESSION NO. D-A108610	3. RECIPIENT'S CATALOG NUMBER
4. TITLE (and Subtitle) CAVITY OSCILLATION IN CRUISE MISSILE CARRIER AIRCRAFT		5. TYPE OF REPORT & PERIOD COVERED Final Report August 1979 to April 1981
		6. PERFORMING ORG. REPORT NUMBER LG81ER0156
7. AUTHOR(s) Harold W. Bartel James M. McAvoy		8. CONTRACT OR GRANT NUMBER(s) F33615-79-C-3207
9. PERFORMING ORG. NAME AND ADDRESS Lockheed-Georgia Co. 86 S. Cobb Dr. Marietta, GA 30063		10. PROGRAM ELEMENT, PROJECT, TASK AREA & WORK UNIT NUMBERS 24010131
11. CONTROLLING OFFICE NAME AND ADDRESS Flight Dynamics Laboratory (AFWAL/FIBE) Air Force Wright Aeronautical Laboratories Wright-Patterson AFB, Ohio 45433		12. REPORT DATE JUNE 1981
		13. NUMBER OF PAGES
14. MONITORING AGENCY NAME & ADDRESS (if different from Controlling Office)		15. SECURITY CLASS. (of this report) Unclassified
		15a. DECLASSIFICATION/DOWNGRADING SCHEDULE
16. DISTRIBUTION STATEMENT (of this Report) Approved for public release; distribution unlimited.		
17. DISTRIBUTION STATEMENT (of the abstract entered in Block 20, if different from Report)		
18. SUPPLEMENTARY NOTES		
19. KEY WORDS (Continue on reverse side if necessary and identify by block number) cavity noise, cavity oscillation, cavity resonance, oscillatory pressures		
20. ABSTRACT (Continue on reverse side if necessary and identify by block number) This report discusses cavity oscillation in general, and particularly the problem of cavity oscillation in the missile bays of cruise missile carrier aircraft during missile launch. The missile bay configurations analyzed ranged from the complete interior volume of a large transport aircraft, to the bomb bay of a conventional bomber. All of the carrier aircraft cases evaluated were conceptual; no specific airframe models or manufacturers are identified. The principles and technology presented are not limited to missile bays; they are applicable to general cavities having free-stream flow velocities above Mach 0.4. It is observed that above Mach 0.4 the pressure fluctuations in an oscillating cavity may arise from: a) sustained periodic pressure fluctuations in the aperture shear layer that radiate noise into the cavity; b) sustained periodic pressure fluctuations in the aperture shear layer that couple with the cavity volume acoustic modes (this generally produces by far the most intense cavity oscillation). Theoretical/empirical techniques are presented for predicting oscillatory frequency, pressure level, pressure spatial distribution in the cavity, and the degree of alleviation achievable with suppressors. The information is based on extensive experimentation with subscale models having apertures of 2 <sup>nd</sup> to 6 <sup>th</sup> in a cold air wall-jet flow facility. A bibliography is included containing 145 listings.		

## PREFACE

This report was prepared by the Lockheed-Georgia Company, Marietta, Georgia, for the Flight Dynamics Laboratory, Air Force Wright Aeronautical Laboratories, Wright-Patterson Air Force Base, Ohio, under Contract F33615-79-C-3207. The work described herein is a continuing part of the Air Force Systems Command's exploratory development program to establish tolerance levels and design criteria for acoustic fatigue prevention in flight vehicles.

The work was directed under Work Unit 24010131, "Cruise Missile/Cavity Oscillation Environments." Mr. Leonard Shaw (AFWAL/FIBE) was the Project Engineer. The Lockheed Program Manager was Mr. Harold Bartel. The Principal Investigators were Mr. Harold Bartel and Mr. James M. McAvoy.

For internal control, this report is identified by Lockheed as LG81ER0156, and is the only publication prepared under this contract. Submittal of the technical report by the authors in April 1981 completed the technical effort, which was begun in August 1979.

Accession For	
NTIS GRA&I	<input checked="checked" type="checkbox"/>
DTIC TAB	<input type="checkbox"/>
Unannounced	<input type="checkbox"/>
Justification	
By	
Distribution/	
Availability Codes	
Dist	Avail and/or Special
A	

## TABLE OF CONTENTS

<u>Section</u>	<u>Title</u>	<u>Page</u>
	LIST OF FIGURES	vii
	SYMBOLS AND SUBSCRIPTS	xii
1.0	SUMMARY	1
2.0	INTRODUCTION	3
3.0	TECHNICAL DISCUSSION	4
3.1	Missile Bay Configurations	4
3.2	Historical Highlights	5
3.3	Approach to Methods Development	7
3.4	Testing Arrangement	7
3.4.1	Test Facility	7
3.4.2	Subscale Models	8
3.4.3	Data Acquisition	9
3.5	Exploratory Tests	11
3.5.1	Cavity Oscillation	11
3.5.2	Helmholtz Resonance	14
3.5.3	Cavity Acoustic Resonance	15
3.6	CMCA Missile Bay Model Tests	20

PRECEDING PAGE BLANK-NOT FILMED

TABLE OF CONTENTS (Contd)

<u>Section</u>	<u>Title</u>	<u>Page</u>
3.7	Development of Prediction Methods	23
3.7.1	Missile Bay Oscillation Frequency	23
3.7.2	Oscillation Mode Priority	28
3.7.3	Distortion	30
3.7.4	Correlation With Prior Experiments	31
3.7.5	Sound Pressure Level Prediction	32
3.7.6	Sound Pressure Spatial Variation	33
3.7.7	Broadband Noise	37
3.7.8	Clutter Effects	38
3.8	Cavity Oscillation Predictions	40
3.8.1	CMCA Cases	40
3.8.2	Sample Application of Methods	41
3.8.3	Results of Predictions	51
3.8.4	Required Alleviation	51
3.8.5	Effectiveness of Alleviation Devices	51
3.8.6	Revised Predictions	54
4.0	OBSERVATIONS AND CONCLUSIONS	55
5.0	RECOMMENDATIONS	57
6.0	REFERENCES	59
7.0	BIBLIOGRAPHY	61

# LIST OF FIGURES

<u>Figure</u>	<u>Title</u>	<u>Page</u>
1	Cavity Arrangements In Cruise Missile Carrier Aircraft and In Conventional Bombers	74
2	Long CMCA Missile Bays Selected For Analyses	75
3	Short CMCA Missile Bays Selected For Analyses	76
4	Aft Launch And Conventional CMCA Missile Bays Selected For Analyses	77
5	Generic Representation Of Missile Bays	78
6	Generic Representation Of Missile Bays	79
7	Wall-Jet Flow Facility	80
8	Aperture Viewed From Back Side Of Flow Plane, With A Test Model In Position	81
9	Typical Model Construction Concepts	82
10	Category 1 and Category 2 Models	83
11	Category 3 Model with Two Aperture Configurations, and Installation In Flow Stream	84
12	Category 4 Model With Spacers to Vary L/D	85
13	Response Spectra Measured At Various Flow Velocities. Rectangular Cavity, 18" x 5.75" x 5.75" With 0.5" Neck, Aperture Located At Down-stream End	86
14	Frequency And Mach Number Of Oscillatory Responses Exceeding 150 db, In Six Variations Of Rectangular Missile Bays	87
15	Frequency And Mach Number Of Responses In A Rectangular 18" x 5.75" x 5.75" Missile Bay With A 6" Aperture	88
16	Helmholtz Response In A Large Missile Bay Equipped With A Neck	89
17	Cavity Depth Correction For Depthwise Acoustic Modes In Conventional Bomb Bays	90
18	Cavity Depth Correction For Depthwise Acoustic Modes In Category 4 Missile Bays	91

# LIST OF FIGURES (Contd)

<u>Figure</u>	<u>Title</u>	<u>Page</u>
19	Fore-Aft Acoustic Resonance Frequencies Calculated And Measured In A 44" Missile Bay	92
20	CMCA Case 1 Response Test Spectra, Cylindrical Missile Bay 23.2" x 5.4" D	93
21	CMCA Case 2 Response Test Spectra, Rectangular Missile Bay 23.2" x 5.75" x 5.75"	94
22	CMCA Case 3 Response Test Spectra, Cylindrical Missile Bay 6" x 5.4" D	95
23	CMCA Case 4 Response Test Spectra, Rectangular Missile Bay 6" x 5.75" x 5.75"	96
24	CMCA Case 5 Response Test Spectra, Cylindrical Missile Bay 7" x .85" D, Aft Launch	97
25	CMCA Case 6 Response Test Spectra, Conventional Bomb Bay, 6" Aperture, 3" Depth	98
26	Computed Shear Layer And Acoustic Modes, Cylindrical Missile Bay, 21" x 5.4" D, With 6" Aperture	99
27	Cavity Oscillations Measured In A Cylindrical Missile Bay With Floor	100
28	Cavity Oscillations Measured In A Cylindrical Missile Bay, No Floor	101
29	Mach Number ( $M_i$ ) At Which The Strouhal Curves For Acoustic Modes And Shear Layer Modes Intersect	102
30	Strouhal Number ( $S_i$ ) At Which The Strouhal Curves For Acoustic Modes And Shear Layer Modes Intersect	102
31	Examples Of Oscillatory Sound Pressure Wave Distortion	103
32	Response Spectra Measured In A Cylindrical Missile Bay, 21" x 5.4" D, No Floor, 6" Aperture At Downstream End	104
33	SPL Spatial Variation Fore-Aft In 21" x 5.4" D Cylindrical Missile Bay, At .81 Mach, 320 And 640 Hertz Modes	105
34	SPL Spatial Variation Fore-Aft In 21" x 5.4" D Cylindrical Missile Bay, At .81 Mach, 960 And 1275 Hertz Modes	105



LIST OF FIGURES (Contd)

<u>Figure</u>	<u>Title</u>	<u>Page</u>
35	SPL Spatial Variation Fore-Aft In 21" x 5.4" D Cylindrical Missile Bay, At .81 Mach, 2550 And 3825 Hertz Modes	106
36	Rossiter's Measured Oscillatory Response (From Reference 2) Correlated With Predicted Acoustic Modes For L/D = 1 Cavity, L = 8"	107
37	Rossiter's Measured Oscillatory Response (From Reference 2) Correlated With Predicted Acoustic Modes For L/D = 2 Cavity, L = 8"	108
38	Rossiter's Measured Oscillatory Response (From Reference 2) Correlated With Predicted Acoustic Modes For L/D = 8 Cavity, L = 8"	109
39	Development Of Sound Pressure Level Empirical Prediction Curve	110
40	Normalized Maximum Oscillatory SPL In Cylindrical Missile Bays	110
41	Normalized Maximum Oscillatory SPL In Rectangular Missile Bays	111
42	Normalized Maximum Oscillatory SPL In Conventional Bomb Bays	111
43	Oscillatory SPL Variation With Mach Number Between Onset And Termination	112
44	Free Stream Dynamic Pressure, Standard Atmosphere	113
45	SPL Spatial Variation Fore-Aft In 21" x 5.4" D Cylindrical Missile Bay, At .71 Mach, 325 And 650 Hertz	114
46	SPL Spatial Variation Fore-Aft In 21" x 5.4" D Cylindrical Missile Bay, At .71 Mach, 975 And 1300 Hertz	114
47	SPL Variation Measured Fore-Aft In 21" x 5.4" D Cylindrical Missile Bay, At .71 Mach, 1600 And 1775 Hertz	115
48	SPL Variation Measured Fore-Aft In 21" x 5.4" D Cylindrical Missile Bay, At .71 Mach, 1950 And 2250 Hertz	115

LIST OF FIGURES (Contd)

<u>Figure</u>	<u>Title</u>	<u>Page</u>
49	Fore-Aft SPL Variation Given By Equation 34 Which Accounts For Broadband Noise Level, 21" Cylindrical Missile Bay	116
50	Broadband SPL At Downstream Wall Near Aperture	117
51	Depthwise Variation of Broadband SPL On Downstream End Wall	117
52	Effect Of Clutter On Frequency And Level Of Maximum Oscillation	118
53	Effect Of Clutter And Partial Blockage On Frequency And Level Of Maximum Oscillation	119
54	Shear Layer Oscillation Modes	120
55	CMCA Case 2 Predicted Acoustic Modes Superimposed On Shear Layer Modes	121
56	Speed Ranges Of Probable Modes Of Oscillation Predicted For CMCA Case 2	122
57	CMCA Case 2 Maximum Oscillatory Frequency And Maximum SPL Predicted For 25,000 Feet	123
58	CMCA Case 2 Maximum Oscillatory Sound Pressure Spectrum Predicted For .8M, 25,000 Feet	123
59	CMCA Case 2 Predicted Variation In SPL Fore-Aft, For .8M At 25,000 Feet	124
60	Predicted CMCA Missile Bay Oscillation Within The Speed Range Of .4M To 1.2M, At 25,000 Feet	125
61	Predicted CMCA Missile Bay Oscillation At .8 Mach Altitudes Of 25,000 And 37,000 Feet	126
62	CMCA Case 1 Predicted Fore-Aft Variation In SPL On Wall Opposite Aperture, For .8M At 25,000 Feet Altitude	127
63	CMCA Case 3 Predicted Fore-Aft Variation In SPL On Wall Opposite Aperture, For .8M At 25,000 Feet Altitude	128
64	CMCA Case 4 Predicted Fore-Aft Variation In SPL On Wall Opposite Aperture, For .8M At 25,000 Feet Altitude	128

LIST OF FIGURES (Contd)

<u>Figure</u>	<u>Title</u>	<u>Page</u>
65	CMCA Case 6 Predicted Fore-Aft Variation In SPL On Wall Opposite Aperture, For .8M At 25,000 Feet Altitude	129
66	CMCA Case 6 Predicted Depthwise Variation In SPL On Downstream Wall, For .8M At 25,000 Feet Altitude	130
67	Illustration Of Shear Layer Alteration Devices Examined	131
68	CMCA Case 1 Response Spectra With And Without Spoiler/Ramp Alleviation Devices	132
69	Illustration Of Selected Alleviation Devices For Long Missile Bays	133
70	Effect Of Selected Alleviation Device(s) On Maximum Oscillatory SPL	133
71	Predicted Maximum Levels Of CMCA Missile Bay Oscillation With And Without Alleviation; Launch At .8 Mach, 25,000 And 37,000 Feet Altitude	134

## SYMBOLS AND SUBSCRIPTS

### SYMBOLS

- a Missile bay normalized dimension in fore-aft or streamwise direction; ratio of aperture length to missile bay length;  $a = L_x / \ell_x$ .
- b Missile bay normalized dimension in depth direction; ratio of aperture length to missile bay depth;  $b = L_x / \ell_F$ .
- C Speed of sound in missile bay (feet per second).
- $C_\infty$  Speed of sound in freestream (feet per second).
- D Depth dimension in open bomb bays, or diameter of cylindrical missile bay model.
- dB Decibels, always referenced to  $2.9006 \times 10^{-9}$  psi (.0002 dynes per sq. cm.).
- $dB_r$  Decibel spectrum level.
- F Acoustic mode order term for modes in non streamwise direction. For enclosed rectangular missile bays,  $F = N_z$ . For enclosed cylindrical and semicylindrical missile bays,  $F = a_{m,n}$ . For open bomb bays,  $F = N_z/2$ .
- f Frequency in Hertz (cycles per second).
- g Gravitational acceleration constant.
- G Acoustic mode-dependent constant defined as,  $G = (a^2 N_x^2 + b^2 F^2)^{1/2}$ .
- H Mach-dependent constant defined as,  $H = (1 + .2M^2)^{1/2}$ .
- $K_v$  Ratio of convection velocity to freestream velocity. Herein,  $K_v = 0.57$ .

## SYMBOLS AND SUBSCRIPTS (Contd)

$L, L_x$	Aperture length in fore-aft or streamwise direction (feet).
$L_y$	Aperture width, crosswise to stream flow (feet).
$L_z$	Aperture neck or throat depth (feet).
$l_F$	Missile bay dimension in non-streamwise direction (feet). For enclosed rectangular bays, $l_F = l_z$ . For enclosed cylindrical and semicylindrical missile bays, $l_F = r$ . For open bomb bays, $l_F = l_{ze}$ .
$l_x$	Missile bay dimension in fore-aft or streamwise direction (feet).
$l_z$	Missile bay dimension in depth direction (feet).
$l_{ze}$	Acoustic effective depth in open bomb bays (feet).
$M$	Mach number.
$m$	Tangential acoustic mode integer in cylindrical and semicylindrical enclosures; $m = 0, 1, 2, 3$ , etc. (all integers).
$N_R$	Shear layer pressure oscillation mode integer in Rossiter equation; $N_R = 1, 2, 3$ , etc.
$N_S$	Shear layer pressure oscillation mode integer in Spee equation; $N_S = 1, 2, 3$ , etc.
$N_x$	Fore-aft acoustic mode integer. In all missile bays $N_x = 0, 1, 2, 3$ , etc. (all integers).
$N_z$	Depthwise acoustic mode integer. In enclosed rectangular missile bays, $N_z = 0, 1, 2, 3$ , etc. (all integers). In open bomb bays, $N_z = 0, 1, 3, 5$ etc. (odd integers only).

## SYMBOLS AND SUBSCRIPTS (Contd)

n	Radial acoustic mode integer in cylindrical and semicylindrical enclosures; $n = 0, 1, 2, 3$ etc. (all integers).
P	Pressure in pounds per square inch.
q	Dynamic pressure in pounds per square inch.
R	Universal gas constant; 53.35 for air.
r	Radius of cylindrical or semicylindrical missile bay (feet).
S	Strouhal number; defined as $S = fL/U$ .
SPL	Sound pressure level, in decibels.
T	Temperature, degrees Rankine.
U	Free-stream velocity (feet per second).
$U_c$	Convection velocity (feet per second). herein $U_c = .57 U$ .
x	Station or position fore-aft in missile bay, with $x = 0$ at downstream wall, in units consistent with $L_x$ .
z	Station or position depthwise in missile bay, with $z = 0$ at aperture, in units consistent with $L_z$ .
$\alpha$	$L/D$ - dependent constant in Rossiter equation. Herein, $\alpha = .25$ .
$a_{mn}$	Acoustic mode constant for cylindrical and semicylindrical enclosures. Quantified in Section 3.5.3.
$\gamma$	Ratio of specific heats; for air, $\gamma = 1.395$ .

### SYMBOLS AND SUBSCRIPTS (Contd)

- $\eta_x$  Fore-aft location in missile bay, defined as  $x/l_x$ .
- $\eta_z$  Depthwise location in missile bay, defined as  $z/l_z$ .
- $\xi$  Empirical exponent, defined as  $22 / (SPL_{max} - SPL_B)$ .
- $\rho$  Density of gas.

## SYMBOLS AND SUBSCRIPTS (Contd)

### SUBSCRIPTS

- B Denotes broadband or random noise.
- F Denotes the dimension direction that is consistent with the acoustic mode order term F.
- i Denotes the intersection of Strouhal curves for shear layer and acoustic modes.
- m Denotes tangential acoustic modes.
- max Denotes the spatial maximum sound pressure level during cavity oscillation.
- n Denotes radial acoustic modes.
- o Denotes onset of an oscillation
- R Denotes shear layer oscillation, as described by Rossiter.
- S Denotes shear layer oscillation, as described by Spee.
- r Denotes random spectrum level.
- t Denotes termination of an oscillatory condition. Also denotes total when related to temperature.
- st Denotes static.
- x Denotes fore-aft or streamwise direction.
- y Denotes direction crosswise to stream flow.



### SYMBOLS AND SUBSCRIPTS (Contd)

- $z$  Denotes depthwise direction.
- $ze$  Denotes "effective" dimension.
- $\infty$  Denotes free-stream properties.
- $\eta$  Denotes a fore-aft or depth position in missile bay.

## 1.0 SUMMARY

Approximately 30 combinations of missile bay configurations and candidate Cruise Missile Carrier Aircraft (CMCA) were identified and studied. The missile bay configurations were grouped into four categories related to missile bay shapes and launch techniques. All but one (the conventional bomb bay) represented new cavity configurations and flow conditions not addressed by the available literature. It became necessary to evaluate the oscillatory behavior of the "unconventional" missile bays, using inexpensive subscale models, to determine the applicability or degree of inadequacy of existing cavity analysis methods.

Experiments were conducted using a wall-jet flow facility with a variety of cylindrical and rectangular models of approximately 1/40 scale. These experiments provided evidence that two different phenomena -- shear layer oscillation and acoustic resonance within the cavity enclosure -- combine to cause cavity oscillation. Prior research has shown that vortices are shed from the aperture upstream lip and propagate past the aperture, producing travelling oscillatory pressure waves whose frequency increases with flow Mach number. Acoustic resonance frequency within the cavity enclosure is almost constant -- it changes only as total temperature changes with Mach number -- a small change at subsonic speeds. Sustained cavity oscillation occurs when the shear layer oscillation frequency coincides with a cavity acoustic resonance frequency. Then the two reinforce each other to cause oscillatory pressures that can easily exceed 170 dB (an rms pressure of 132 pounds per square foot).

Methods for estimating the shear layer oscillation frequency and the acoustic resonance frequency were assembled and combined into analytical/graphical procedures for determining the Mach numbers where the two coincide. This approach resulted in a method for predicting both cavity oscillation frequency and critical Mach number. Graphical descriptions of sound pressure level as a function of dynamic pressure and Mach number were obtained from model tests representing various types of missile bays. Means for rapidly predicting the oscillatory pressure levels in missile bays were determined from the tests. Analytical expressions for the varia-

tion in sound pressure level over the length and/or depth of missile bays were developed and verified in model tests.

From the large number of CMCA candidates identified, six significantly different cases were analyzed. The cavity oscillation environment in each of these six cases was predicted using the analysis methodology developed. It was found that five of the cases would encounter discrete fluctuating pressures at frequencies ranging from 5 to 50 Hertz, and at levels on the order of 150 to 170 dB -- intense enough to cause structural damage. Devices for modifying the shear layer over the aperture were identified for these five cases and tested on subscale models. Cavity oscillatory pressure levels were reduced 10 to 30 dB with the devices selected, and based on these results the cavity oscillation environments estimated for the five "problem" CMCA cases were revised.

The quality and accuracy of cavity oscillation prediction analyses were enhanced as a result of this program. Further improvement is still needed. Recommended subjects of future development work include: detailed experimental investigation of the oscillating shear layer and interaction with acoustic resonance pressure oscillations; refinement and implementation of an acoustic finite element analysis method for quantifying acoustic resonance frequency and mode shape in irregularly shaped enclosures; optimizing suppression by locating spoilers so as to modify effective aperture lengths to mismatch frequencies of shear layer oscillation and acoustic resonance.

## 2.0 INTRODUCTION

In studies of Cruise Missile deployment, one of the options under consideration is to transport and launch the missiles using existing transport aircraft that have been modified to provide this capability. While this option has obvious advantages, the transport aircraft modified to the Cruise Missile Carrier Aircraft (CMCA) configuration will be exposed to harsh acoustical environments that have not been considered previously. In this study the environment of concern is cavity oscillation during missile launch. The entire fuselage interior (or a fraction thereof) will be subjected to the effects of high velocity flow past the launch aperture and can experience intense fluctuating pressures at frequencies in the range of 5 to 50 Hertz. The cavity resonance problem has been investigated in depth for the conventional bomb bay (the special case of a rectangular enclosure having one entire wall open to stream flow and a length-to-depth ratio usually greater than three). In the CMCA missile bays however, wide variations in size and shape are likely, i.e., the missile bay may be much longer than the aperture; the aperture may be located anywhere along the bay length; the length to depth ratio may be less than three; the missile bay may open to the aperture via a "neck"; the missile bay cross section may be cylindrical, semicylindrical, rectangular, or even irregular.

Two arbitrary CMCA concepts are exemplified in Figure 1 to illustrate their degree of departure from a conventional bomb bay (also shown). Very little prior development work has been done on cavities representing the CMCA variations, so the character of cavity resonance in CMCA's was unknown and not predictable. Nevertheless, the potential for severe resonance and resultant damage was clear. Thus, a need existed for analysis methods that would afford preliminary estimates of the frequency, amplitude, and spatial variation of the cavity oscillatory pressures. The effort described herein was undertaken to develop those analysis methods.

### 3.0 TECHNICAL DISCUSSION

#### 3.1 MISSILE BAY CONFIGURATIONS

For cruise missile carriers derived from aircraft already developed and in service, the missile bay configurations are governed by two considerations: the type of airframe; and the missile launch system.

Airframes can be classified as:

- o Cargo aircraft adaptations characterized by a low continuous floor, high wing, and large internal volume.
- o Passenger aircraft adaptations characterized by a high continuous floor, low wing, and large internal volume.
- o Bomber aircraft adaptations characterized by an integral bomb bay of limited volume.

Missile launch systems can be classified as:

- o Carriage launchers fixed in position, translating missiles for axial ejection through aft doors or tubes.
- o Linear launchers fixed in position, translating missiles for ejection through bottom.
- o Rotary launchers fixed or moved into position, rotating to eject missiles through bottom or side.

A wide variety of candidate CNCA systems can be configured from combinations of these various airframe and missile launch systems. More than 30 were identified during the course of this effort. From this collection, six representative configurations were selected for analysis. The six analysis cases are shown in Figures 2, 3, and 4, along with pertinent descriptive data. In Section 3.8 the cavity oscillation prediction methods developed herein are applied to these six cases.

For the development of prediction methods, it was concluded that all likely missile bay configurations could be grouped into the four simplified cavity arrangements illustrated in Figures 5 and 6. The bulk of the initial experimental work therefore utilized models representing these four cavity categories.

### 3.2 HISTORICAL HIGHLIGHTS

Some of the earliest investigations of cavity resonance were directed toward quantifying the noise radiated away from cavities, with analytical prediction techniques becoming available in the early 1960's. Investigations of aircraft cavity oscillation frequency and level were intensified in the early 1950's for the B-47 and Canberra bombers and have continued at a moderate pace to the present time.

In 1962, Plumblee, Gibson, and Lassiter (Reference 1) developed a method to predict cavity response based on a strong mathematical treatment, with results supported by model tests. They hypothesized that acoustic modes within the cavity were driven by boundary-layer turbulence resulting in intense pressure fluctuations. Subsequent efforts to apply the method of Plumblee, et al. proved their method to be more applicable to what later became defined as "deep" cavities. Notably, though, the method provides a way to calculate depthwise as well as lengthwise acoustic modes in a rectangular enclosure having one entire wall open to high-speed flow.

In 1964, J. E. Rossiter (Reference 2) conducted experiments that identified the source of excitation as vortices shedding from the upstream edge of the aperture. He formulated an analytical expression for the cavity oscillation frequency that has been widely used for "shallow" cavities.

In 1970, Heller, Holmes, and Covert (Reference 3) modified and improved Rossiter's formula to correct for the speed of sound in the cavities. In 1975, Smith and Shaw (Reference 4) formulated an empirical sound pressure level prediction scheme.

Since then, cavity oscillation problems in the bomb bays of aircraft such as the F-111A and B-1 bombers and in miscellaneous weapons pods have led to the undertaking of several related cavity noise investigations (References 5, 6, 7, and 8). By and large, those investigations were directed toward problems associated with rectangular, shallow cavity configurations. The results of those investigations have been used extensively to define and refine empirical methods for the prediction of sound pressure level and frequency. One shortcoming of these methods was the inability to predict the onset of cavity oscillation. Investigators using these predictions usually qualified their results with the words, "If an oscillation occurs, it will be at the predicted frequency."

NASA-sponsored work has been done by Block, Heller, and Tam concerning, among other things, the extension of Rossiter's work to predict cavity oscillations below Mach 0.4 for cavities such as open landing gear wheel wells. Considerable work on cavity oscillations has also been contributed by the academic community, dealing with cavity oscillations in aerospace vehicles, wind tunnel walls, and ships. Professor S. A. Elder (References 9 and 10) is currently conducting Navy-sponsored work at the U.S. Naval Academy.

In 1978, Rockwell and Naudascher (Reference 11) correlated the modes obtained by Rossiter in his original work (for  $L/D = 2$ ) with the longitudinal acoustic resonance in Rossiter's cavity. They assumed that all six walls were hard and neglected depth mode response. Improved correlation is obtained (and shown herein) when the modified Rossiter formula is used in conjunction with a more precise accounting of the acoustic resonances.

### 3.3 APPROACH TO METHODS DEVELOPMENT

The literature applicable to cavity oscillation was reviewed for data and methodology useful in analyses and in alleviating or suppressing oscillation. A listing of the more noteworthy publications is in the Bibliography. The subject matter of the literature reviewed encompassed full-scale aircraft bomb bays, wing-mounted pod cavities, optical instrument recesses in the surfaces of aircraft and missiles, scaled models, rectangular cutouts in wind tunnels and water tables, slots and irregular cutouts in wind tunnel walls, architectural acoustics, and musical instruments. The literature on cavity oscillation generally fell into either of two groups: one dealing specifically with aircraft bomb bays; the other dealing with more general cavities but exposed to low-velocity flow. Thus, despite the range of subject matter evaluated, very little information was found to be directly applicable to CMCA cavity oscillation analysis. Because of this disparity, the formulation of the CMCA cavity oscillation prediction methodology relied heavily on subscale model tests.

### 3.4 TEST ARRANGEMENT

Primary considerations in the subscale model tests were low overall cost, ease of configuration change, real-time processing of data on-line, and direct observation of the cavity behavior.

#### 3.4.1 Test Facility

The principal feature of the test facility was a semi-free cold air rectangular jet nozzle with an integral flow plane, capable of continuous operation at velocities exceeding Mach 1.2. The overall arrangement is shown in Figures 7 and 8.

A cylindrical plenum chamber was positioned upstream of the nozzle, with an internal contraction cone to transition from a cylindrical to a rectangular cross-section. A honeycomb section was positioned at the upstream end of the contraction cone to straighten the flow entering the nozzle. The supply line was brought into the plenum chamber through the side with a 90°



turn directing the flow back against the domed end, thus dispersing the flow throughout the plenum before entry into the honeycomb. The nozzle flow rate was governed by a manually controlled pneumatic regulator valve in the supply line.

A flow-plane which contained the aperture was contiguous to one wall of the nozzle and was mounted in a vertical plane. A flow fence made of heavy aluminum tooling plate was positioned on each side of the aperture to form, in conjunction with the flow-plane, a deep channel projecting downstream from the nozzle exit. This channel arrangement constrained the flow on three sides while allowing expansion and secondary air entrainment opposite the aperture. It produced the effect of a divergent nozzle at the aperture without having a wall opposite the aperture to reflect pressure fluctuations or cause acoustic resonance effects. The aperture (or opening) in the flow plane was located slightly downstream of the nozzle exit (see Figure 7). The models were attached to the back side of the flow plane, with their opening positioned over the flow-plane aperture (see Figure 8). Thus, the models were outside the flow to avoid physical interference with the airstream. The velocity distribution across the aperture was considerably improved over that available from a free-jet nozzle, as speed over the aperture deviated less than one percent from the velocity at the center of the aperture for all speeds below Mach 1.0. This is illustrated in Figure 9 for a nominal flow velocity of Mach 0.87. The boundary layer was examined at various speeds and locations to verify that the flow was uniform. A velocity profile obtained at the upstream lip of the aperture is also shown in Figure 9. The width of the flow field over the aperture was three times the aperture width. The depth of the flow field over the aperture was 1.3 times the aperture length. The flow-plane thickness at the aperture was 0.080 inch.

#### 3.4.2 Subscale Models

In the preliminary experiments the scaled models were configured to represent the variations in the four categories of missile bays discussed in paragraph 3.1. This was achieved with four basic model geometries: (1) A cylindrical cross section model (representing categories 1 and 2) with re-

locatable end plugs and removable floors which provided variation in cavity length, neck length, and aperture location upstream/downstream (see Figure 10); (2) a rectangular cross section model (representing categories 1 and 2) with relocatable end plugs, removable "ceiling" plugs and removable spacers to vary cavity length, cavity depth, neck length, and aperture location upstream/downstream (see Figure 10); (3) a cylindrical (tubular) fuselage model mounted completely immersed in the nozzle flow (representing Category 3) with removable end fittings employing different aperture shapes and locations to vary cavity length and flow direction relative to the aperture (see Figure 11); and (4) a narrow rectangular cross-section model (representing Category 4) with cavity width equal to aperture width and with removable spacers available to vary cavity depth (see Figure 12). The models were constructed either from 3/4 inch plywood, 1/2 inch plexiglass, or rolled aluminum sheet. In every case checks were made to verify that structural vibrations did not contribute to the oscillatory pressure response of the models.

#### 3.4.3 Data Acquisition

The instrumentation and the test procedures were tailored to define sound pressure spectra inside the missile bays over a Mach range of 0.4 to 1.2 and a dynamic pressure range of 200 to 2000 psf.

Microphones (1/4 inch) were located inside the models to sense pressure fluctuations. In some instances, the microphones were permanently fixed in the models. For spatial surveys, the microphones were mounted in tubular probes that were repositioned in discrete increments. The microphone signals were amplified or attenuated as necessary for maximum signal-to-noise ratio, using B&K Model 2603 microphone amplifiers. The microphone data analyses were obtained on-line with Nicolet Scientific Corporation Model 446A Fast Fourier Transform computing analyzers and companion digital plotters.

The cavity response and the properties of the flow were recorded at stabilized flow conditions. The frequency response spectra were continuously monitored on a scope display for on-line identification of

critical velocities where response changes and response maxima occurred. Total head and static pressure sensors were mounted in the flowstream in the vicinity of the aperture. A pitot-static survey over the aperture was used to calibrate the fixed pressure probes to accurately indicate velocity at the aperture. Flowstream temperature was measured in the plenum upstream of the contraction nozzle, where the velocity was approximately 5% of the velocity at the aperture and was never in excess of Mach 0.065. An alternate temperature measurement was made slightly downstream of the aperture.

During initial calibration runs and exploratory tests of the models, the gradual changes in cavity oscillation frequency due to total temperature change were seen to be quite small. The abrupt changes in frequency due to mode change were also sometimes quite small. Such small changes were concealed in 1/3-octave frequency analyses. Multiple resonance peaks were sometimes closely spaced and, likewise, were not identifiable with 1/3-octave analyses. In full-scale aircraft cavity work where the frequencies might be on the order of 5 to 50 Hertz, 1/3-octave analyses may suffice. In subscale model testing however, narrow-band spectrum analysis is essential. Therefore, the plans to use 1/3-octave analyses for certain data processing and presentations were abandoned in favor of narrowband spectrum analyses. Digital spectrum analyzers were used that employed 400 line resolution over the analysis range; whereby an analysis from 0 to 5K Hertz had a bandwidth of only 12.5 Hertz, 0 to 10K had 25 Hertz, etc. Checks were made to verify that the analysis bandwidth was always wider than the cavity response peaks, to insure that the level indicated by the analyzer at the peak was therefore the true level of the response.

The transition of the cavity oscillation from one mode to another was sometimes not detected unless Mach number (flow velocity) was changed in very small increments, so as to reveal when one mode subsided and another emerged. It was therefore necessary to examine cavity response at small increments of Mach No., or to continuously record the cavity response as the velocity was increased in order to identify the critical Mach number. Both techniques were used throughout the experiments.

### 3.5 EXPLORATORY TESTS

The initial experiments were structured to determine that the test setup and the subscale models provided satisfactory data and agreement with published results. Six variations of rectangular cross-section missile bays were tested. These models had aperture lengths of 1/2 foot. A typical set of sound pressure level response spectra for a range of Mach numbers is shown in Figure 13. The frequencies of the response "peaks" for six variations are plotted in Figure 14. The general clustering of the data in certain frequency ranges is similar to that reported by other investigators.

#### 3.5.1 Cavity Oscillation

The solid lines in Figure 14 show the cavity oscillation frequency versus Mach number obtained with the modified Rossiter equation (reference 3), for the first 3 modal orders ( $N_R = 1, 2, \text{ and } 3$ ). The modified Rossiter equation is

$$f = \frac{U_\infty}{L} \left[ \frac{N_R - \alpha_R}{M(1 + 0.2M^2)^{-1/2} + \frac{1}{K_v}} \right] \quad (1)$$

For moderate cavity length-to-depth ratios and flow velocities above about Mach 0.5, the appropriate values for the constants  $\alpha_R$  and  $K_v$  are 0.25 and 0.57 respectively.  $U_\infty$  is free-stream velocity;  $L$  is aperture length;  $N_R$  is modal integer (1, 2, 3 etc.); and  $M$  is freestream Mach number. The subscript  $R$  denoting Rossiter has been added to avoid confusion since these symbols are also used in other equations herein. The cavity oscillation frequency given by the Spee equation (References 12 and 13) is also shown in Figure 14 for the first 3 modal orders. The Spee equation is

$$\tan \left[ \frac{2\pi f N_S L}{U_c} \right] = \frac{2\pi f N_S L}{U_c} \quad (2)$$

where  $U_c$  is shear layer mean particle velocity, in this case taken to be convection velocity which Rossiter suggested to be 57 percent of free-

stream velocity. While the Spee relation gave fair agreement with the data in this comparison, it generally did not fit the data as well as the Rossiter equation. The modified Rossiter equation was, therefore, preferred in subsequent data correlations. Figure 14 also shows that the cavity oscillation frequency may coincide roughly with any of the first three modal orders given by the Rossiter equation. However, there is no indication of the mode most likely to respond for a given cavity and flow condition. There is also considerable scatter in the data. Thus, the frequency of oscillation is not predicted accurately with the modified Rossiter equation alone.

A detailed study of the data revealed that over the velocity range where a mode of cavity oscillation occurred, the frequency of oscillation often remained nearly constant rather than increasing in accord with the Rossiter equation, and generally coincided with one of the cavity acoustic resonances through a broad speed range.

An illustration of this behavior is shown in Figure 15 for a rectangular 18" x 5.75" x 5.75" missile bay model, having a 1/2 inch neck with a one-by-six inch aperture located at the downstream end of the cavity. The shear layer oscillation frequency given by the Rossiter equation is shown by the lines for  $N_R = 1, 2,$  and  $3$ . The fore/aft acoustic resonance frequencies are shown by the lines for  $N_x = 1, 2, 3, 4,$  and  $5$ . Complex acoustic modes are shown for  $N_x = 1$  through  $6$ , and  $N_z = 1$ . The frequencies at which strong cavity oscillation occurred were obtained from the spectra of Figure 13 and are indicated by the solid symbols. Frequencies at which weaker oscillation occurred (weaker but still clearly an oscillatory condition) are indicated by the open symbols. From several such experiments, it was concluded that the shear layer instability or oscillation frequency increases with Mach number approximately in accord with the modified Rossiter equation. However, in the absence of any reinforcement from acoustic resonance, the shear layer oscillation is comparatively weak. At certain velocities when the shear layer oscillation frequency approaches a cavity acoustic resonance frequency, the shear layer oscillation sometimes "locks on" that acoustic resonance. Throughout a definite velocity range, the coupled shear layer/cavity oscillation occurs at the acoustic resonance

frequency. During this "lock on" condition, the shear layer oscillation is reinforced and fluctuating pressures in the cavity become very intense.

Prior investigators have offered different descriptions of the mechanism involved during this oscillatory condition. Some descriptions have dealt with flow turbulence, some with captive vortices in the cavity, some with pure vortex shedding, some with fluid inflow/outflow, and some with reversed flow and forward propagating pressure disturbances within the cavity. From the current tests, it is believed that any of the previously described mechanisms can occur under the right circumstances. It is also believed that in some cases more complex mechanisms are involved. It was observed that strong oscillation occurred in cavity configurations where none of the aforementioned mechanisms seem plausible.

Neither an experimental nor theoretical study of the aperture hydrokinetics was within the scope of this effort. The following rationalization is thus based on the current experiments and observations of the behavior of a variety of widely differing cavity configurations responding in many different resonant modes.

The vortices that are shed from the upstream edge of the aperture give rise to comparatively weak oscillatory pressure waves that convect downstream over the aperture. The vortex convection velocity, hence wavelength, increases with convected distance. As a result of the changing wavelength over the aperture, a range of frequencies is available to "lock-onto" cavity acoustic modes.

As the frequency of the convecting shear layer pressure wave nears the frequency of an acoustic resonance in the cavity, the intensity of the acoustic resonance standing pressure wave increases. At some frequency, the standing wave reaches a level sufficient to "regulate" (in an unknown manner) the shedding of the vortices, thus causing the shear layer pressure oscillation frequency to coincide with the acoustic resonance frequency. At this time, the acoustic pressure increases the shear layer oscillatory pressure, which in turn increases the acoustic pressure until the cavity response quickly reaches a stable but very intense level. As long as flow

conditions are such that the acoustic resonance pressure wave can regulate the shear layer oscillation, the process will be sustained.

During this condition where the shear layer pressure wave is reinforced to very intense levels, the pressures impressed on the cavity volume can become severely distorted. Such a distorted wave contains higher harmonics of the wave frequency, and readily excites higher multiples of the cavity resonance involved.

As Mach number increases, the vortex shedding rate and hence the frequency of shear layer oscillation is maintained until a velocity is reached where the acoustic resonance pressure waves can no longer regulate or control the shear layer oscillation. At this velocity, the "locked-on" condition breaks down and the shear layer oscillation frequency reverts to the now higher frequency as identified from the modified Rossiter equation. The oscillatory pressure then immediately subsides to a relatively weak level. Often however, a higher-order acoustic resonance within the cavity is available that coincides with the now higher shear layer oscillation frequency, wherein the shear layer oscillation simply "locks onto" another acoustic resonance. Intense levels are then sustained at another frequency. In large missile bays with many acoustic resonances available, the cavity oscillatory condition can exist at almost all speeds above about Mach 0.4 by simply transitioning from one mode to another as flow conditions change.

As a result of many experiments, it was concluded that the formulation of missile bay analysis methods would first require a satisfactory means for quantifying the cavity acoustic resonance frequencies. In addition to the cavity acoustic modes, the Helmholtz mode is possible in certain classes of cavities. Both are considered in the following sections.

### 3.5.2 Helmholtz Resonance

The Helmholtz mode of an enclosure with an aperture may be characterized as a single degree-of-freedom vibration system consisting of a spring and mass. The spring rate is determined by the elastic fluid in the enclosure

volume, and the mass is determined by the portion of air defined by the aperture/neck geometry. Part of the fluid at the entry and exit to the neck moves in unison with the fluid within the neck to make up this mass. An end correction to account for the extra mass has been investigated by Alster (Reference 14) for the case of zero flow. However, the literature offers very little for the case of parallel subsonic flow past the aperture. Since some of the CMCA missile bays involve volumes with a well-defined neck, the behavior of the Helmholtz mode was examined in experiments. The test data contained clear evidence of the Helmholtz mode at very low speeds. The frequency of the Helmholtz mode was found to be lowest at zero velocity and increased as speed was increased. The response level of the Helmholtz mode was observed to always decrease above a certain flow velocity. Any evidence of the Helmholtz mode was gone at speeds well below the lowest launch speed. A typical Helmholtz response behavior is exemplified in Figure 16 for a missile-bay model containing a long neck (representative of a through-the-floor launch configuration). The response is very sharp at  $M = 0.09$  through  $M = 0.12$ , but is harder to identify at  $M = 0.24$  and completely missing at  $M = 0.38$ . This type of behavior at low Mach number was observed on most of the missile-bay models containing well-defined necks, but it was increasingly more difficult to identify as neck lengths decreased to zero. As a result of these tests and observations, it is concluded that the Helmholtz resonance can be neglected in the speed range of interest to CMCA analysts.

### 3.5.3 Cavity Acoustic Resonance

Acoustic resonances in a cavity are normal modes of vibration of the air occupying the cavity volume, and hereinafter are sometimes called acoustic modes, or simply "modes". In a normal-mode vibration system, an infinite number of resonant modes are possible. Any particular mode characterizes a distinct spatial variation of the pressure in the air; likewise, a standing wave characterizes an acoustic resonance.

To examine the connection between cavity oscillation frequency and cavity acoustic resonance frequencies available, it was first necessary to establish a means for determining the acoustic resonances. Two approaches



are available: (1) the use of acoustic finite element methods and (2) the use of the classical equations for standard shapes. The works of Craggs (Reference 15), Wolf (Reference 16), and Petyt (Reference 17) have demonstrated the feasibility of using acoustic finite element theory to calculate resonance frequency and mode shape. While the finite element method is capable of handling any shape, its use requires a medium-capacity high-speed computer and a large amount of input is needed to thoroughly define the geometry of the missile bay. The classical approach is fast and convenient when the missile bay is idealized with an equivalent rectangular or cylindrical cross section. The frequencies and mode shapes are then calculated for the idealized geometry using the classical equations available from any good text on acoustics (see, for example, P. M. Morse, Reference 18). This idealization affords considerable saving in time. The limited number of calculations required can be made quickly on a desk calculator. Since virtually no lateral acoustic resonance participation occurs, the lateral degrees of freedom may be neglected. The lengthwise and depthwise modes can be readily determined once the characteristic dimensions are known. The inexact nature of other aspects of the cavity oscillation phenomenon tend to favor the use of the classical equations.

An investigation of missile-bay model resonance frequencies under flow conditions (discussed subsequently) led to the conclusion that the classical equations produced acceptable results. It was also concluded that most CNCA missile-bay shapes could be reasonably represented by one of the ideal shapes for which equations are available. This approach was, therefore, used in this program.

For wide rectangular enclosures where the aperture open area is small relative to the surrounding wall area, the cavity can be treated as fully enclosed. The frequency is determined from:

$$f = \frac{C}{2} \left[ \left( \frac{N_x}{l_x} \right)^2 + \left( \frac{N_z}{l_z} \right)^2 \right]^{1/2} \quad (3)$$

where  $N_x$  and  $N_z$  are mode integers 0, 1, 2, 3, 4, etc. for the fore-aft direction and the depthwise direction respectively,  $C$  is speed of sound in the cavity, and  $l_x$  and  $l_z$  are the cavity dimensions.

For cylindrical enclosures with the diameter large in comparison to the aperture width, acoustic resonance frequency is given by:

$$f = \frac{C}{2} \left[ \left( \frac{N_x}{\ell_x} \right)^2 + \left( \frac{a_{mn}}{r} \right)^2 \right]^{1/2} \quad (4)$$

where  $N_x$  is mode integer 0, 1, 2, 3, 4, etc. for the fore-aft direction;  $a_{mn}$  is a mode-dependent coefficient tabulated below for the tangential and radial mode integers,  $m$  denotes tangential modes and  $n$  denotes radial modes;  $C$  is speed of sound in the cavity, and  $r$  is cylinder radius.

Values of  $a_{mn}$  for cylindrical enclosures are :

	$n = 0$	$n = 1$	$n = 2$	$n = 3$	$n = 4$
$m = 0$	0.0	1.22	2.23	3.24	4.24
$m = 1$	.586	1.70	2.71	3.73	4.73
$m = 2$	.972	2.13	3.17	4.19	5.20
$m = 3$	1.34	2.55	3.61	4.64	5.66
$m = 4$	1.69	2.95	4.04	5.08	6.11
$m = 5$	2.04	3.35	4.45	5.51	6.55
$m = 6$	2.39	3.74	4.86	5.93	6.98
$m = 7$	2.73	4.12	5.26	6.35	7.41
$m = 8$	3.07	4.49	5.66	6.76	7.83

For semicylindrical enclosures, where the aperture open area can be neglected, the acoustic modes are given by the same expression as for cylinders. However, it should be noted that in semicylinders the tangential resonance node lines will be located at specific angles relative to the diametrical plane. And if the aperture is located at one of the node lines, the corresponding modes will not occur.

For conventional bomb bays, where the aperture opening constitutes one entire wall of the enclosure, the uncorrected acoustic resonance frequency is given by

$$f = \frac{C}{2} \left[ \left( \frac{N_x}{l_x} \right)^2 + \left( \frac{N_z}{2l_z} \right)^2 \right]^{1/2} \quad (5)$$

where  $N_x$  is mode integer 0, 1, 2, 3, 4, etc. for the fore-aft direction and  $N_z$  is odd mode integer 0, 1, 3, 5, 7, etc. for the depthwise direction. In the fore-aft direction, the cavity responds as would any other rectangular enclosure. In the depth direction, the cavity responds in a manner very similar to a one-end-open tube.

However, conventional bomb bays are usually shallow with length-to-depth ratio (L/D) equal to three or more. They depart rather drastically from a simple one-end-open tube. Even in a large CMCA with a missile bay of the conventional type, L/D will likely equal two or more. In these cavities, the effects of flow across the aperture make rather large "end" corrections necessary to obtain agreement between theoretical and experimental depth mode acoustic resonances. Plumblee et al. investigated depth mode response (Reference 1) and developed a complex theoretical method that related depth mode frequency to acoustical impedance at the aperture. The method appears to work well for deep cavities but is less suitable for L/D of about two or more. For a given set of aperture and cavity conditions, an approximation can be obtained simply by relating the observed frequency to the theoretical frequency given by the equation for an open-end tube. The differences between observed and calculated frequencies can be used to obtain a depth dimension correction. The depth dimension correction shown in Figure 17 was obtained from East's work (Reference 19). However, the depth dimension corrections determined during exploratory tests of Category 4 conventional bomb bays were found to differ somewhat from East's data. Based on the results of these tests, a depth mode correction was developed which is shown in Figure 18. This correction was determined from tests of six Category 4 missile bays that responded in the depth mode. The Figure 18 depth dimension correction is to be applied to all orders of the depthwise acous-

tic resonances, as well as to the complex modes (fore/aft modes coupled with depth modes). Equation 5 is then modified to give the corrected acoustic resonance frequency for conventional bomb bays:

$$f = \frac{C}{2} \left[ \left( \frac{N_x}{l_x} \right)^2 + \left( \frac{N_z}{2l_{ze}} \right)^2 \right]^{1/2} \quad (6)$$

where  $l_{ze}$  is the effective depthwise dimension, obtained from Figure 18.

The above equations were used to calculate the acoustic resonance frequencies for selected missile-bay model configurations for static (no-flow) conditions. The models were excited with small speakers to measure the acoustic resonances. The measured resonance frequencies agreed very closely with the theory. Similar close agreement between calculated and measured frequencies was observed at flow velocities where the broad band flow noise excited the cavity acoustic modes. This was particularly true for the fore-aft modes, which often tend to influence the cavity oscillation. At flow velocities above Mach 0.4 the measured enclosure resonance frequencies deviated from the values calculated for zero flow, due to changes in the speed of sound,  $C$ , in the air within the missile bay. The properties for the air within the missile bay are the same as for free stream air that has been decelerated to zero velocity. Thus, the missile bay air temperature is the same as the free stream total temperature  $T_t$  (assuming dry air and no losses, or 100 percent recovery); whereby, the speed of sound in the missile bay is given approximately by:

$$C = (g \gamma R T)^{1/2} = 49 (T_t)^{1/2} \quad (7)$$

where  $T_t$  is free-stream total temperature in degrees Rankine.

In CNCA cavity oscillation analyses, the parameters known from the flight conditions are speed (Mach No.), altitude, and speed of sound in the outside air at the altitude. It is, therefore, convenient to relate the speed of sound in the missile bay,  $C$ , to the speed of sound in the outside air,  $C_\infty$ , at the flight altitude. The air within the missile bay has the same properties as outside static air that has been accelerated to the aircraft forward speed, whereby the temperature of the air within the

missile bay is given by total temperature  $T_t$ . Thus:

$$T_t = T_{st} \left( 1 + \frac{\gamma-1}{2} M^2 \right) \quad (8)$$

where  $T_{st}$  is static temperature of the outside air at the altitude in question. Then, assuming polytropic compression of dry air for which the ratio of specific heats,  $\gamma = 1.395$ , the speed of sound in the missile bay is given approximately by

$$C = 49 \left[ T_{st} (1 + 0.2M^2) \right]^{1/2} \quad (9)$$

And since the speed of sound in the outside air is

$$C_\infty = 49 (T_{st})^{1/2} \quad (10)$$

the speed of sound in the cavity becomes

$$C = C_\infty (1 + 0.2M^2)^{1/2} \quad (11)$$

The acoustic resonance frequencies in the selected missile bay models were then calculated using the speed of sound in the model, and were found to agree very well with measured data. Figure 19 shows a comparison of calculated and measured lengthwise resonance frequencies at Mach 0.9, where the broadband flow noise was exciting the fore-aft acoustic modes. In this spectrum analysis from 0 to 2000 Hertz, the first 12 orders are evident and the measured and calculated frequencies agree very well.

### 3.6 CNCA MISSILE BAY MODEL TESTS

The general oscillatory behavior of large cavities (large relative to the aperture area) was investigated in the exploratory tests. Those tests provided the information and direction needed to determine the format of the prediction/analysis methods. CNCA models representing candidate missile-bay configurations were then tested to obtain the data needed to reinforce the frequency analysis methods and, more importantly, to provide additional oscillatory sound pressure level data applicable to CNCA missile bays. These SPL data, in combination with some of the exploratory test

data, served to establish empirical relations for describing SPL dependency on dynamic pressure, Mach number, and configuration for describing sound pressure spatial variation, and for determining oscillatory mode priority, distortion effects, and broadband noise level.

Six small inexpensive models were configured and tested that represented the six CMCA cases selected for analysis in Section 3.1. Response spectra were obtained over the Mach range of 0.4 to 1.2. Sample spectra are included and discussed herein.

CMCA Case 1 - This was a long model, fully cylindrical in cross section. No floor, ceiling, or missile payload was simulated. The missile bay or cavity was 23.2 inches long streamwise and 5.4 inches in diameter. The cavity end bulkheads were flat, parallel, and normal to the centerline; the centerline was parallel to the aperture and the stream flow. The aperture was six inches long streamwise, one inch wide and 0.080 inch deep. The aperture downstream edge coincided with the cavity downstream end bulkhead.

Sound pressure level spectra at increments of Mach number are shown in Figure 20. The microphone was located at the downstream bulkhead, on the wall opposite the aperture.

CMCA Case 2 - This was a long model, square in cross-section. It included a full-length simulated floor that resulted in a "neck" between the aperture and the cavity. There was no missile payload. The cavity was 23.2 inches long streamwise, 5.75 inches wide, and 5.75 inches deep. The end bulkheads were flat, parallel, and normal to the centerline; the centerline was parallel to the aperture and the stream flow. The aperture was six inches long streamwise and one inch wide. The neck was 1.39 inches deep. The aperture downstream edge and the neck downstream wall were aligned with the cavity end bulkhead.

Sound pressure level spectra at increments of Mach number are shown in Figure 21. The microphone was located at the downstream bulkhead on the ceiling opposite the aperture.

CMCA Case 3 - This model was a minimum length variation of Case 1; fully cylindrical in cross section. No floor, ceiling, or missile payload was simulated. The cavity was six inches long streamwise (same length as the aperture) and 5.4 inches in diameter. In all other respects, the model was identical to Case 1.

Sound pressure level spectra at increments of Mach number are shown in Figure 22.

CMCA Case 4 - This model was a minimum length variation of Case 2; square in cross section, and included a full-length simulated floor that resulted in a neck between the aperture and the cavity. There was no missile payload. The cavity was six inches long streamwise (same as the aperture), 5.75 inches wide, and 5.75 inches deep. In all other respects, the model was identical to Case 2.

Sound pressure level spectra at increments of Mach number are shown in Figure 23.

CMCA Case 5 - This was a long model, fully cylindrical in cross-section. No floor, ceiling, or missile payload was simulated. The model represented an aft-opening, rearward-ejection-launch type of missile bay. The end opening was skewed out through the cylinder. An elliptical aperture resulted. The entire model was immersed in the flow stream. The cavity centerline was parallel to the stream flow, and the plane of the aperture was at about 20 degrees to the centerline. The cavity was 5.57 inches long at the shortest point on the circumference of the slanted opening, and 8.47 inches at the longest point. It was 0.85 inch in diameter, with 0.080 inch wall thickness.

Sound pressure level spectra at increments of Mach number are shown in Figure 24. The microphone was located at the upstream bulkhead on the cavity centerline.

CMCA Case 6 - This was a conventional bomb-bay type of cavity. The cross section was rectangular, the length-to-depth ratio was 2.0. The cavity and

aperture were six inches long and one inch wide. The end bulkheads were normal to the aperture; the aperture and opposite wall were parallel to the stream flow. There was no missile payload.

Sound pressure level spectra at increments of Mach number are shown in Figure 25. The microphone was located at the downstream bulkhead on the wall opposite the aperture centerline.

### 3.7 DEVELOPMENT OF PREDICTION METHODS

#### 3.7.1 Missile Bay Oscillation Frequency

As discussed in section 3.5.1, cavity oscillation may be either the result of a shear layer instability oscillation that exists independent of any acoustic resonance within the missile bay or, more likely, it may be the result of a shear layer oscillation driving a missile bay acoustic resonance wherein the acoustic resonance sound pressures regulate or control the shear layer instability frequency. Analytical relations for the frequency of the shear layer oscillation and the frequency of the missile bay acoustic resonances are discussed in sections 3.5.1 and 3.5.3.

The frequency of the shear layer pressure oscillation in terms of Mach number is given by Equation (1), whereby

$$f = \frac{MC_\infty}{L} \left[ \frac{N_R - .25}{M(1 + .2M^2)^{-1/2} + 1.75} \right] \quad (1)$$

The expressions (Equations 3, 4, and 6) for acoustic resonance frequency vary slightly, depending on missile bay type and/or shape. In the interest of simplifying the use of these equations in predictions, it is advantageous to standardize to a single expression of the form

$$f = \frac{C}{2} \left( \frac{N_x^2}{l_x^2} + \frac{F^2}{l_F^2} \right)^{1/2} \quad (2)$$

where lateral acoustic modes have been neglected. For rectangular missile bays,  $F = N_z = 0, 1, 2, 3$ , etc.; for cylindrical and semi-cylindrical



missile bays,  $F = \alpha_{mn}$ , as defined in section 3.5.3; for conventional bomb bays (one entire wall open),  $r = N_z / 2L_{ze}$  with  $N_z = 0, 1, 3, 5, 7$ , etc., odd integers only. Since speed of sound in the free stream,  $C_\infty$ , is more readily available than speed of sound in the missile bay,  $C$ , the acoustic resonance frequency in terms of free-stream speed of sound is (combining equations (12) and (13))

$$f = \frac{C_\infty}{2} (1 + .2M^2)^{1/2} \left( \frac{N_x^2}{l_x^2} + \frac{F^2}{l_F^2} \right)^{1/2} \quad (14)$$

With equations (12) and (14), the frequencies of the shear layer pressure oscillation and the various acoustic resonance modes in a missile bay can be calculated and plotted as a function of Mach number on a single plot as was done in Figure 15. The intersections of the shear layer oscillation curves with the acoustic resonance curves identify the possible frequencies of oscillation, and the corresponding Mach number.

Because  $C_\infty$  is altitude-dependent, it becomes necessary to repeat the entire process at every altitude of interest. Also, there can be many acoustic resonances available in some missile bays. As a result, the curve plotting process and the identification of curve intersections can become extremely burdensome. It is, therefore, advantageous to normalize the frequency expressions in terms of Strouhal number and to make certain definitions and substitutions which simplify the calculations. The modified Rossiter equation for shear layer oscillation in terms of Strouhal number is:

$$S = \frac{N_R - .25}{M(1 + .2M^2)^{-1/2} + 1.75} \quad (15)$$

The missile bay acoustic resonance (recognizing that  $S = fL_x/U$ , and  $C_\infty = U/M$ ) in terms of Strouhal number is:

$$S = \frac{L_x}{2M} (1 + .2M^2)^{1/2} \left( \frac{N_x^2}{l_x^2} + \frac{F^2}{l_F^2} \right)^{1/2} \quad (16)$$

By definition, let  $(1+.2M^2)^{1/2} = H;$  (17)

$$\frac{L_x}{l_x} = a; \frac{L_x}{l_F} = b; \quad (18)$$

whereby 
$$\left( \frac{N_x^2}{l_x^2} + \frac{F^2}{l_F^2} \right)^{1/2} = \frac{(a^2 N_x^2 + b^2 F^2)^{1/2}}{L_x}; \quad (19)$$

and let 
$$(a^2 N_x^2 + b^2 F^2)^{1/2} = G. \quad (20)$$

Then by substitution the modified Rossiter equation for shear layer oscillation in terms of Strouhal number is:

$$S = \frac{N_R - .25}{\frac{M}{H} + 1.75} \quad (21)$$

and the missile bay acoustic resonance in terms of Strouhal number is:

$$S = \frac{GH}{2M} \quad (22)$$

By using equations 21 and 22, shear layer oscillation modes and acoustic resonance modes have been calculated for a representative missile bay model and are shown in Figure 26. This example is for a cylindrical missile bay large in comparison to aperture length, wherein a number of intersections occur, as denoted by encirclements. This same model was tested with and without a fuselage floor. Strong well-defined cavity oscillations are identified by the data symbols and corresponding SPLs in Figures 27 and 28.

It is seen that when sustained cavity oscillation occurs, the measured Strouhal number tracks the calculated acoustic mode Strouhal number, and as speed increases the cavity oscillation shifts as the shear layer oscillation Strouhal curve comes into the proximity of different acoustic modes.

At the intersections of the Strouhal curves for shear layer oscillation and acoustic resonance, i.e. where the two frequencies coincide,

$$\frac{N_R - .25}{\left(\frac{M}{H}\right)_i + 1.75} = \frac{GH_i}{2M_i} \quad (23)$$

where subscript "i" denotes intersection. By algebraic manipulation,

$$\left(\frac{H}{M}\right)_i = \frac{2(N_R - .25) - G}{1.75G} \quad (24)$$

This is a useful interim form, in that the quantity  $(H/M)_i$  involves only the intersection Mach number, and the right side involves only the dimensional and modal-order parameters relating to shear layer and acoustic resonance frequencies. Since, by definition,

$$\left(\frac{H}{M}\right) = \frac{(1 + .2M^2)^{1/2}}{M}; \quad \left(\frac{H}{M}\right)^2 = \frac{1 + .2M^2}{M^2} \quad (25)$$

and by further manipulation, the intersection Mach number is

$$M_i = \left[ \left(\frac{H}{M}\right)_i^2 - .2 \right]^{-1/2} \quad (26)$$

From equation 22, the Strouhal number where intersection occurs is:

$$S_i = \frac{G}{2} \left(\frac{H}{M}\right)_i \quad (27)$$

A value of  $G$  can be calculated from Equation 20 for each acoustic resonance mode in the missile bay, and substituted into Equation 24 to obtain a value of  $(H/M)_i$  for each intersection of the shear layer oscillation curves ( $N_R = 1, 2, 3$ , etc.) and the acoustic resonance mode curves. The values of  $(H/M)_i$  thus obtained are then substituted into Equation 26 to yield the Mach number at which each intersection occurs. The corresponding Strouhal number at which an intersection occurs is obtained from Equation 27. As a convenience to aid in these calculations, values of  $M_i$  and  $S_i$  may be obtained directly from Figures 29 and 30 for Mach numbers up to 2.0, shear layer modes up to the 5th order, and  $G$  values up to 4.0.

The values of  $M_i$  and  $S_i$  for each potential cavity oscillatory condition (each intersection) have been considered independently of altitude. The frequency in cycles per second commensurate with each intersection is determined from

$$f = \frac{SU}{L} = \frac{S_i M_i C_\infty}{L} = \frac{GHC_\infty}{2L} \quad (28)$$

Values of  $C_\infty$  are obtained from standard atmospheric tables.

In the exploratory tests, it was observed that cavity oscillation often began at Mach numbers less than  $M_i$  and as speed increased, oscillation continued beyond  $M_i$ . A study was conducted to determine the range (on either side of the intersection Mach number) over which sustained cavity oscillation occurred. From this study of scaled model test data, empirical expressions were developed that defined the onset and termination of cavity oscillation in terms of Strouhal number and Mach number. The expressions are as follows, where subscript "o" denotes onset of oscillation and "t" denotes termination:

$$S_o = S_i + .25 \left[ N_R (1 + M_i) \right]^{-1/2} \quad (29)$$

$$M_o = \left[ \frac{4S_o^2}{G^2} - .2 \right]^{-1/2} \quad (30)$$

$$S_t = S_i - .2 \left[ N_R (1 + M_i) \right]^{-1/2} \quad (31)$$

$$M_t = \left[ \frac{4S_t^2}{G^2} - .2 \right]^{-1/2} \quad (32)$$

### 3.7.2 Oscillation Mode Priority

The prediction methodology presented herein yields many "intersections", and each identifies a potential condition of cavity oscillation. However, from the model tests and from full-scale aircraft experience, it is clear that when many modes are possible certain modes of cavity oscillation occur more readily than others. The identification of the "preferred" cavity oscillation condition is made according to the following hierarchy.

Shear layer pressure oscillation mode priority:

<u>Priority</u>	<u>Mode</u>
A	$N_R=2$
B	$N_R=1$
C	$N_R=3$
D	$N_R=4$

Acoustic mode priority in conventional bomb bays:

1st	$0,0,N_z$
2nd	$N_x,0,N_z$
3rd	$N_x,0,0$

Acoustic mode priority in rectangular missile bays:

1st	$N_x,0,N_z$
2nd	$N_x,0,0$
3rd	$0,0,N_z$

Acoustic mode priority in cylindrical and semicylindrical missile bays:

1st	$N_x,0,0$
2nd	$N_x,m,n$

Examine each shear layer oscillation frequency curve for intersections with acoustic mode curves, and assign to each intersection a letter-number priority wherein the letter denotes shear layer mode priority and the number denotes acoustic mode priority. In those Mach ranges where more than one intercept exists, the preferred cavity oscillation condition is the one of highest priority. The shear layer mode priority is given preference over acoustic mode priority.

### 3.7.3 Distortion

When sustained cavity oscillation occurs, there is often a strong response of higher-order acoustic modes; modes that are an even integer higher than the principal mode being driven by the shear layer oscillation. This is evident in the model test data cited previously, Figures 27 and 28. In Figure 28 for example, at Mach 0.8 the second-order shear layer oscillation is driving the fourth-order, fore-aft acoustic mode at 1275 Hertz, and the cavity is also responding at 2550, 3825, 5100, and 6375 Hertz; the second, third, and fourth multiples of the 4,0,0 acoustic mode. These responses cannot be attributed to higher-order shear layer excitation, because the higher-order shear layer frequencies are not exact integer multiples of the second-order mode that is driving the cavity. Instead, the strong responses of the higher-order acoustic modes are attributed to distortion. A typical example of severe distortion of the pressures at the downstream wall is shown in Figure 31. The cavity pressures exhibit a "saw toothed" wave shape during one half-cycle and a "flattening" or "clipping" during the other half-cycle. A second example shows the absence of severe distortion near a node plane where the pressures are lower. As is known from Fourier analysis, a distorted periodic wave contains higher harmonics of the fundamental frequency. A distorted periodic pressure impressed on the cavity readily excites higher multiples of the cavity acoustic mode involved in regulating the shear layer oscillation. The higher frequency "spikes" visible on the wave in Figure 31 are the higher-order mode pressures that the microphone sensed at that location. The cavity spectral analyses are shown in Figure 32. At Mach .81 it is seen that the principal mode is at 1275 Hertz, and the second, third, fourth, fifth, sixth, and seventh multiples of 1275 Hertz are responding strongly due to distortion excitation. These higher multiples are verified as being genuine acoustic modal responses by the pressure distributions shown in Figures 33, 34, and 35. There it is seen that the pressure distributions in the cavity at both the low and high frequencies are consistent with the corresponding acoustic modes. In Figures 33 and 34, the pressure distributions show weak response (about 145 dB) of the first, second, and third-order acoustic modes and strong response (about 165 dB) of the fourth-order acoustic mode. In each case a theoretical cosine curve is plotted with the curve peaks

scaled to the maximum level of the measured data. Clearly, the trend of each data set follows the theoretical cosine variation for the mode represented. At 2550 Hertz, the second multiple of the principal mode, the pressure distributions are seen in Figure 35 to agree quite well with the eighth order cosine curve, indicating that there is, in fact, an eighth order acoustic mode responding. At 3825 Hertz the twelfth order mode is not verified, but neither is it refuted due to an inadequate number of survey points. Obviously, an inordinate number of measurements would be required to identify these high multiples of the principal mode.

Distortion induced response was observed in a number of the subscale model tests, usually when cavity sound pressure levels exceeded 155 to 160 dB and invariably when the level exceeded 165 dB. However, resources did not permit sufficient study to develop reliable techniques for precisely predicting either the occurrence or level of these distortion induced modes. As a guide, one can expect distortion-induced higher-order modes to occur at Mach numbers above .65 when the cavity oscillation level at the principal mode exceeds 160 dB. Expect the second, third, and fourth multiples of the principal mode to be about the same level as the principal mode. Expect the fifth multiple and above to decrease about three dB per multiple. Generally, if levels are severe enough to result in distortion-induced response, the levels will be intolerable and alleviation will be required.

#### 3.7.4 Correlations With Prior Experiments

The cavity oscillation frequency prediction methodology was applied to conventional bomb-bay-type cavities, both deep and shallow, for which test data were available in the literature. Some of the results of Rossiter's work (Reference 2) are shown in Figures 36, 37, and 38 to illustrate the coupling of shear layer modes with acoustic modes. In Figure 36, the first five acoustic modes calculated for Rossiter's deep cavity ( $L/D = 1$ ) are shown as solid lines. The first six modes of the shear layer oscillation (as given by the modified Rossiter equation) are shown by dashed lines. The solid symbols denote cavity oscillation that Rossiter observed.



The depth mode (0,0,1) is seen to be low enough to couple strongly with the first "Rossiter" mode. When the second "Rossiter" mode coupled with the first complex streamwise/depth acoustic mode (1,0,1) at about  $M = 0.9$ , the first "Rossiter" mode subsided. Calculated modes and test results are shown in Figure 37 for an intermediate depth ( $L/D = 2$ ). In this case, the first complex acoustic mode (1,0,1) coupled with the third "Rossiter" mode near  $M = 0.55$ , and with the second "Rossiter" mode near  $M = 0.8$ . Note also that concurrent with the coupled shear layer/acoustic mode oscillation, there was pure shear layer oscillation as indicated by the open symbols. In Figure 38, which is for a very shallow cavity ( $L/D = 8$ ), the first depthwise acoustic resonance frequency was so high it was completely out of consideration for shear layer coupling. Only the first two fore-aft acoustic modes are within the range of interest, and there was no evidence of coupling of the shear layer oscillation with these acoustic modes. Here, only pure shear layer oscillation occurred. It is also interesting that, in the  $L/D = 8$  case, Rossiter's data showed that where there was no apparent acoustical coupling, the sound pressure level was significantly reduced from the SPL produced in the deeper cavities. This was true despite the fact that, with decreasing cavity depth, the transducer used to measure sound pressures was located inherently closer to the oscillating shear layer.

### 3.7.5 Sound Pressure Level Prediction

Sound pressure level prediction methods were developed empirically from the test results for 10 subscale models that were tested with variations on aperture position and neck length. The oscillatory sound pressure levels were normalized to dynamic pressure,  $q$ , and plotted against Mach number for each test as illustrated in the composite plot in Figure 39. "Best-fit" curves were constructed through the maxima on such composite plots. These best-fit curves were then grouped together according to type of missile bay configuration such as cylindrical enclosed, rectangular enclosed, and rectangular with one wall open. Straight-line envelopes were fitted to these groups of best-fit curves and are shown in Figures 40, 41, and 42. Such envelopes were arranged to reflect conservative estimates of the normalized fluctuating pressure level; they are conservative in that most

of the cavity oscillation levels did not exceed these envelopes. Also, it is expected that subscale models with clean, smooth, hard walls would exhibit slightly higher levels than would a full-scale aircraft having irregular, cluttered interior surfaces. Each envelope can be represented by an equation as indicated in Figures 40, 41, and 42, to facilitate calculation of level. These curves and equations yield the level only at the intersection Mach number,  $M_i$ . For preliminary design estimates, it would probably be prudent to use the intersection level throughout the speed range in which a particular cavity oscillation mode is sustained. However, an empirically developed approximation of the level behavior on either side of the intersection Mach number is shown in Figure 43 and may be used for estimating missile bay environments as a function of launch speed.

The values of  $20 \log P/q$  obtained from Figures 40, 41, and 42 are dependent on speed and altitude. Sound pressure levels (dB referenced to  $2.9006 \times 10^{-9}$  psi) are obtained from

$$SPL = 20 \log P/q + 171 + 20 \log q \quad (33)$$

where  $q = \rho M^2 C_p^2 / 2$  in pounds per square inch. Values of  $\rho$  and  $C_p$  are obtained from standard atmospheric tables, or  $q$  may be obtained directly from a reference plot such as shown in Figure 44. The cavity oscillation sound pressure level thus obtained is a discrete frequency level, as discussed in section 3.4.3.

### 3.7.6 Sound Pressure Spatial Variation

The sound pressure level spatial distributions were investigated by conducting pressure surveys for the various response modes within the subscale model missile bays. Examples are shown in Figures 33 through 35 for a Category 1 missile bay where, in addition to the principal mode response, distortion was driving higher multiples of the principal mode. The missile bay was surveyed at Mach 0.81 and the principal mode was at 1275 Hertz, as shown by the spectra in Figure 32. The fourth-order fore-aft acoustic resonance was being driven by the second-order shear layer oscillation. The theoretical cosine curves shown in Figure 34 descend to zero at the nodes, but the measured data descend only to the broadband noise floor.

which averages around 135 dB in the 25 Hertz analysis bandwidth. The broadband noise also adds to the level of the oscillation to some extent on either side of the mode. This has the effect of flattening the sound pressure distribution curve.

In Figure 28, a different oscillatory condition is seen at Mach 0.71. There, the second-order shear layer oscillation is driving the third-order fore-aft acoustic resonance. The spectrum analysis in Figure 32 shows this principal mode to be at 975 Hertz. As was the case at Mach 0.81, the spectrum analysis also shows strong response at a higher multiple of the principal mode, in this case 1950 Hertz, twice the principal mode frequency. Sound pressure surveys of the Mach 0.71 oscillatory condition are shown in Figures 45 through 48. The first- and second-order fore-aft acoustic modes are shown in Figure 45 to be responding weakly (about 145 dB maximum). The principal mode (3,0,0 responding at about 165 dB maximum) is shown in Figure 46, along with weak response (about 145 dB maximum) of the (4,0,0) mode. The measured frequencies are accurate to  $\pm 12.5$  Hertz (since the analysis bandwidth in this case was 25 Hertz) and agree very well with the calculated frequencies shown in Figure 26. The calculated frequencies for the 2,1,0 and the 5,0,0 modes are nearly equal (1580 and 1588 Hertz respectively from Figure 26) and both, though weak at 145 dB maximum, are discernible in the Figure 47 survey for 1600 Hertz. The 3,1,0 mode calculated to be 1731 Hertz is weak, but also evident in the Figure 47 survey for 1775 Hertz. The Figure 48 survey for 1950 Hertz is most interesting. It clearly shows strong response (159 dB maximum) of a fourth-order fore-aft acoustic mode. However, the pure fourth-order fore-aft mode would be expected at about 1300 Hertz, not 1950. This is seen in Figure 26 to be the 4,1,0 mode which was calculated as 1923 Hertz. This response frequency is the second multiple of the principal mode, evidenced by the Figure 32 spectra, but note in Figure 28 that neither of the "Rossiter" curves coincide with this response mode. This response is induced by distortion at the 975 Hertz frequency. However, in this instance, the distortion excites a complex mode, the 4,1,0, rather than the 6,0,0, the second multiple of the principal mode. A final pressure distribution survey is shown in Figure 48 for the 7,0,0 mode responding at 2250 Hertz. The 7,0,0 mode, which has 7 minima and 8 maxima, is weak (about 144 dB) but is still discernible.

These pressure distribution surveys clearly show the acoustic modal participation in the cavity response. They also show that the spatial variation of the measured pressures agrees well with the theoretical cosine curve distribution when the cosine curve is scaled to the maximum SPL. As is always the case, the levels near the nodes are influenced by broadband noise, and this must be taken into account.

In cavity oscillations involving depthwise acoustic resonance, the oscillatory sound pressures were always a maximum at the wall opposite the aperture, and decreased predictably toward the aperture. All depthwise surveys were for cases involving first-order depth mode response. Resources did not permit investigations of higher-order depth mode responses, but such spatial distributions would logically be expected to follow the classical wave shape, as does the first-order mode. The node locations in depthwise pressure distributions are based on the "effective" depth determined from Figure 18 and not the geometric depth.

Based on these surveys and observations, empirical expressions were developed for predicting the spatial variation of the sound pressures on the cavity wall surfaces, for the principal mode of cavity oscillation.

In the fore-aft direction, the sound pressure variation along the wall opposite the aperture is given by:

$$SPL_{\eta_x} = SPL_B + \left[ SPL_{max} - SPL_B \right] \left[ 1 - \cos \left( N_x \pi \eta_x \right) \right]^\xi \quad (34)$$

where

$\eta_x = \frac{x}{L_A}$ , nondimensional fore-aft position; fraction of cavity length.

$SPL_B$  = Broadband sound pressure spectrum level, dB<sub>r</sub>, at the wall opposite the aperture, on the end bulkhead.

$SPL_{max}$  = Oscillatory sound pressure level at the end bulkhead on the wall opposite the aperture.

$N_x$  = Fore-aft acoustic mode integer; 1, 2, 3, etc.

$$\xi = \frac{22}{SPL_{max} - SPL_B}$$

Equation 34 is valid for any enclosed rectangular, cylindrical, and semi-cylindrical missile bay and for conventional bomb bays. For pure fore-aft modes (no depth mode response) the fore-aft pressure variation is the same at any depth, but the broadband level used in the equation must be for the applicable depth. Fore-aft sound pressure distributions were calculated using Equation 34 for comparison with the theoretical cosine curve and to show the limiting effect of the broadband noise. The comparison is shown in Figure 49. The two cases considered are the principal modes of response in the 21-inch-long cylindrical missile bay at Mach 0.71 and 0.81.

In the depthwise direction, the sound pressure variation on the end bulkhead in enclosed rectangular missile bays is given by the same expression, with the subscripts redefined to denote the depth directions, e.g.:

$$SPL_{\eta_z} = SPL_B + \left[ SPL_{max} - SPL_B \right] \left[ \left| \cos(N_z \pi \eta_z) \right| \right]^5 \quad (35)$$

$\eta_z = \frac{z}{L_z}$ , nondimensional depthwise position; fraction of cavity depth.

$N_z$  = depth acoustic mode integer; 1, 2, 3, etc.

$SPL_B$  = broadband sound pressure level, dB<sub>r</sub>, at  $\eta_z$

In conventional bomb-bay cavities, the depthwise sound pressure variation at the end bulkhead is given by:

$$SPL_{\eta_z} = \left[ SPL_B + SPL_{max} - SPL_B \right] \left[ \left| \cos \frac{N_z \pi (1 - \eta_z)}{2 \left( \frac{ze}{L_z} \right)} \right| \right]^5 \quad (36)$$

where

$N_z$  = depth acoustic mode integer; 1, 3, 5, 7, etc.

For pure depth modes (no fore-aft mode response), the depthwise pressure variations given by Equations 35 and 36 are the same at any fore-aft position in the missile bay, but the broadband noise level used in the equations must be for the proper depth and fore-aft position.

The expressions for depthwise SPL variation in enclosed cylindrical and semi-cylindrical missile bays are more complex and were not developed, because the principal response mode in such missile bays will rarely involve tangential and radial modes. The radial frequencies are too high to be driven by the probable shear layer oscillation. The tangential modes are highly damped and will normally not be excited.

When the cavity oscillation involves combined fore-aft and depth mode response (complex modes), the pressure variation at the surface will still be as given by Equations 34, 35, and 36. However, to obtain pressure variations at points within the interior volume (away from the surfaces), the fore-aft and depth mode equations must be combined. While not overly difficult, the equations are cumbersome and were not developed here, since the level of a complex mode at any "interior" point in a cavity will always be less than the level near the surface. In preliminary analyses, the maximum levels should be of primary concern. An illustration of complex mode pressure variation within an enclosure can be found in Reference 20.

### 3.7.7 Broadband Noise

In the subscale model tests, it was observed that the broadband noise level did not vary substantially among missile-bay categories one, two, and four. The single most important parameter was microphone location relative to the aperture downstream edge. Normalized broadband noise level near the downstream edge of the aperture is shown in Figure 50 as a function of Strouhal number, where the characteristic dimension is the aperture length. For locations more remote from the aperture, the broadband noise levels will be lower. To account for this, Figure 51 was constructed from the test data to permit empirical corrections of the Figure 50 levels.

Broadband noise data were obtained from spectrum analyses for each missile-bay model tested. However, when normalized to dynamic pressure and plotted as a function of Strouhal number, the data did not collapse to a single band or cluster. The implication is that broadband level in the cavity is not directly dependent on  $q$ . Instead, the level at low Mach number is higher than the dynamic pressure warrants and is being influenced by other

sources such as upstream flow noise, valve noise, etc., or, at the high Mach numbers the subscale models and flow facility provided unusually clean flow at the aperture that resulted in low broadband noise in the missile bay. A comparison with published data for full-scale aircraft and for wind tunnel tests of subscale models revealed that the published broadband noise levels generally equaled or exceeded the levels measured here. This raised the suspicion that the published data might also be contaminated by extraneous sources, which is not unlikely when one recognizes that the wind tunnels and the full-scale aircraft both involve intense extraneous sources that could radiate noise into the cavity. This suspicion precluded the use here of the published broadband noise data, since the objective is to predict the broadband noise level due solely to the flow over, or into, the cavity. (The user must "add in" the extraneous noise from his particular engines, airframe structure, aperture doors, etc. to arrive at the most realistic prediction of his environment.) The presently measured broadband noise levels are therefore presented and are considered adequate since the broadband noise is of secondary importance compared to the discrete levels that exist during cavity oscillation.

#### 3.7.8 Clutter Effects

A full complement of cruise missiles could be expected to displace as much as one-half of the air in the missile bay, or block up to one-half of the cross sectional area, depending on the configuration. The missiles might also be expected to disperse the sound waves and decrease the strength of the sound pressures at resonance. A missile positioned over the aperture might be expected to decrease the efficiency of the shear layer excitation of the cavity acoustic resonances. However, experimental investigations did not always substantiate these expectations.

The photo in Figure 52 illustrates an extreme case of clutter in a short, rectangular missile bay model. The sound pressure spectra in Figure 52 show the effect of the missiles on oscillatory response. The SPL is decreased about 5 dB, and the response frequency is decreased about 13 percent. In Figure 53, the photo illustrates the case of missiles positioned very near the aperture but not interfering with the flow. The companion

response spectra show a 10 dB reduction in SPL and a 10 percent reduction in oscillatory frequency.

The reduction in frequency is consistent with Parker's observations (Reference 21) in his experiments related to acoustic resonances in heat exchangers. The presence of the clutter (missiles) reduces the speed of sound in the missile bay, thus reducing the acoustic mode frequencies. The reduction in sound pressure level is attributable to scattering and damping.

These effects on SPL and frequency are significant. The frequency change is particularly important, since a lower frequency can result in a lower speed (Mach number) at which the oscillation occurs. Whether or not oscillation will occur at any given speed is, therefore, influenced by the missile payload on board. In a CMCA, the significance of clutter and/or partial blockage will depend on the configuration. However, the determination of clutter effects is best done experimentally during the detailed design phase.



### 3.8 CAVITY OSCILLATION PREDICTIONS FOR SELECTED CRUISE MISSILE CARRIER AIRCRAFT (CMCA)

#### 3.8.1 CMCA Cases

Six CMCA cases were selected for analysis, as discussed in Section 3.1. The general arrangement of the missile bays, and the pertinent descriptive data are shown for each case in Figures 2 through 4. Since the prediction methods provide the means for analyzing cavity oscillation at any desired temperature/altitude/speed/dynamic pressure conditions, the six CMCA cases were analyzed for typical conditions to provide comparative data and a demonstration of the methods. The analyses and the conditions applied were as follows:

- o Determine the speeds at which each missile-bay oscillation condition occurs and determine the frequency and SPL of the oscillation. Do this for 25,000 feet altitude, standard atmosphere, for speeds ranging from  $M=0.4$  to 1.0.
- o At nominal launch conditions of Mach 0.8 at 25,000 feet, determine the missile-bay oscillatory frequencies and corresponding SPL's, and the broadband noise level, to obtain a sound pressure spectrum at a representative location. Determine sound pressure spatial variation.
- o At a second launch condition of Mach 0.8 at 37,000 feet, determine the missile-bay oscillation frequencies and corresponding SPL's.
- o Assume that the missile bay is empty; there are no baffles or partitions in the launchers or missile bays; and neglect the effects of aperture doors.

### 3.8.2 Sample Application of Prediction Procedures

In the interest of clarity and for illustration, a rather elementary step-by-step application of the cavity oscillation prediction procedure follows for CMCA Analysis Case 2. Because of the geometry of Case 2, many modes are possible. While this makes it more burdensome to analyze, it is a comprehensive example; thus its selection.

missile bay:  $l_x = 100$  feet;  $l_y = 16$  feet;  $l_z = 9$  feet  
aperture/neck:  $L_x = 26$  feet;  $L_z = 6$  feet;  $L_y = 6$  feet

#### Geometry:

1. Case 2 constitutes a long, rectangular cross-section cavity exposed to parallel stream flow, via a well-defined neck. Dimensions are:

#### Frequency Calculations:

2. Calculate values of  $H$  using Equation 17, at Mach increments of 0.1M for the speed range of interest, e.g.,

M	.4	.5	.6	.7	.8	.9	1.0	1.1	1.2
H	1.016	1.025	1.035	1.048	1.062	1.078	1.095	1.114	1.135

3. Calculate values of shear layer oscillation Strouhal number at each Mach number increment for each shear layer mode through  $N_R=5$ , using Equation 15 and the values of  $M$  and  $H$  established from Step 2, e.g.,

Mach #	.4	.5	.6	.7	.8	.9	1.0	1.1	1.2
$N_e=1$	.348	.332	.316	.302	.288	.276	.264	.252	.241
$N_e=2$	.812	.774	.738	.705	.673	.643	.615	.588	.562
$N_e=3$	1.276	1.216	1.160	1.108	1.058	1.011	.967	.924	.884
$N_e=4$	1.739	1.658	1.582	1.510	1.442	1.379	1.318	1.260	1.205
$N_e=5$	2.203	2.100	2.003	1.913	1.827	1.746	1.670	1.596	1.526

4. Construct a "master" plot (that can be copied and used repeatedly) of shear layer oscillation Strouhal number versus Mach number using the values tabulated in Step 3, e.g., see Figure 54.
5. Calculate values of  $G$  using Equation 20. Use the appropriate definition of  $F$  consistent with the missile bay cross-section. (See Section 3.7.1 or the list of definitions/symbols). Tabulate  $G$  for each fore-aft acoustic mode through  $N_x=10$ , each depthwise acoustic mode through  $N_z=2$ , and each complex acoustic mode through  $N_x=2, N_z=2$ , e.g.:

$N_x$	1	2	3	4	5	6	7	8	9	10	0	1	2	0	1	2
$F$	0	0	0	0	0	0	0	0	0	0	1	1	1	2	2	2
$G$	.26	.52	.78	1.04	1.3	1.56	1.82	2.08	2.34	2.60	2.89	2.90	2.94	5.78	5.78	5.80

6. For each acoustic mode order calculate values of acoustic mode Strouhal number at each Mach number increment. Use the values of  $H$  and  $G$  tabulated in Steps 2 and 5, with Equation 22, e.g.:

Mach No.	.4	.5	.6	.7	.8	.9	1.0	1.1	1.2
$N_x=1, N_z=0$	.330	.266	.224	.195	.173	.156	.142	.132	.123
$N_x=2, N_z=0$	.660	.533	.448	.389	.345	.311	.285	.263	.246
$N_x=3, N_z=0$	.991	.799	.673	.584	.518	.467	.427	.395	.369
$N_x=4, N_z=0$	1.321	1.066	.897	.779	.690	.623	.569	.527	.492
$N_x=5, N_z=0$	1.651	1.332	1.121	.973	.863	.779	.712	.658	.615
$N_x=6, N_z=0$	1.981	1.599	1.345	1.168	1.035	.934	.854	.790	.738
$N_x=7, N_z=0$	2.311	1.865	1.570	1.362	1.208	1.090	.996	.922	.861
$N_x=8, N_z=0$	2.642	2.132	1.794	1.557	1.381	1.246	1.139	1.053	.984
$N_x=9, N_z=0$	2.972	2.398	2.018	1.752	1.553	1.401	1.281	1.185	1.107
$N_x=10, N_z=0$	3.302	2.665	2.242	1.946	1.726	1.557	1.423	1.317	1.230
$N_x=0, N_z=1$	3.670	2.962	2.493	2.163	1.918	1.731	1.582	1.463	1.367
$N_x=1, N_z=1$	3.683	2.972	2.501	2.171	1.925	1.737	1.588	1.468	1.371
$N_x=2, N_z=1$	3.734	3.013	2.536	2.201	1.951	1.761	1.610	1.489	1.390
$N_x=0, N_z=2$	7.341	5.924	4.985	4.327	3.836	3.462	3.115	2.927	2.733
$N_x=1, N_z=2$	7.341	5.924	4.985	4.327	3.836	3.462	3.165	2.927	2.733
$N_x=2, N_z=2$	7.366	5.945	5.002	4.342	3.850	3.474	3.176	2.937	2.743

7. Plot the values of Strouhal number computed in Step 6 on a copy of the plot of shear layer oscillation Strouhal numbers constructed in Step 4. Identify or note the approximate intersections of the shear layer mode curves and the acoustic mode curves, (see Figure 55). Each intersection defines a potential cavity oscillation mode.
8. From among the intersections noted in Step 7, list the more probable cavity oscillation modes using the shear layer/acoustic mode hierarchy discussed in Section 3.7.2, e.g.:

<u>Mach Range</u>	<u>Probable Oscillation Mode</u> ( $N_R$ ) ( $N_x$ , $N_z$ )	<u>Priority</u>
$M \leq .4$	$N_R=1, N_x=1, N_z=0$	B2
<del>—.4 to .7 —</del>	<del><math>N_R=3, N_x=4, N_z=0</math></del>	<del>C2</del>
.4 to .7	$N_R=2, N_x=3, N_z=0$	A2
<del>—.4 to .7 —</del>	<del><math>N_R=3, N_x=5, N_z=0</math></del>	<del>C2</del>
.7 to 1.0	$N_R=2, N_x=4, N_z=0$	A2
.7 to 1.0	$N_R=3, N_x=6, N_z=0$	C2
<del>—.7 to 1.0 —</del>	<del><math>N_R=3, N_x=7, N_z=0</math></del>	<del>C2</del>
$M \geq 1.0$	$N_R=2, N_x=5, N_z=0$	A2
$M \geq 1.0$	$N_R=1, N_x=2, N_z=0$	B2
$M \geq 1.0$	<del><math>N_R=3, N_x=8, N_z=0</math></del>	<del>C2</del>

Note that at any speed range there are ample modes available having A, B, or C priority, and in this case it is unnecessary to list the D priority modes. Identify one or two top-priority modes in each range and rule out all others, e.g., the dashed lines.

The application of the mode hierarchy rules to select the probable modes can be deferred until Step 11 if preferred, where a graphical presentation of the intersections will be available and all of the prevailing conditions can be visualized. However, doing so in this step reduces the amount of calculation in Step 9.

9. Compute and tabulate the Mach numbers and Strouhal numbers of onset, intersection, and termination for each of the probable cavity oscillation modes identified in Step 8, using the equations below which were obtained from Section 3.7.1:

$N_R$	$N_x$	$N_z$	$G$	$\left(\frac{H}{M}\right)_i$	$M_i$	$S_i$	$S_o$	$S_t$	$M_o$	$M_t$
1	1	0	.26	2.73	.372	.355	.568	.184	.230	.745
1	2	0	.52	1.08	1.021	.280	.456	.139	.590	3.414
2	3	0	.78	1.99	.515	.776	.920	.661	.432	.612
2	4	0	1.04	1.35	.784	.702	.834	.596	.649	.948
2	5	0	1.3	.97	1.166	.631	.751	.535	.939	1.447
3	6	0	1.56	1.44	.729	1.120	1.230	1.032	.661	.803

$$G = (a^2 N_x^2 + b^2 F^2)^{1/2}, \text{ calculated in step 5.}$$

$$\left(\frac{H}{M}\right)_i = \frac{2(N_R - .25) - G}{1.75G}$$

$$M_i = \left[ \left(\frac{H}{M}\right)_i^2 - .2 \right]^{-1/2}$$

$$S_i = \frac{G}{2} \left(\frac{H}{M}\right)_i$$

$$S_o = S_i + .25 \left[ N_R (1 + M_i) \right]^{-1/2}$$

$$S_t = S_i - .2 \left[ N_R (1 + M_i) \right]^{-1/2}$$

$$M_o = \left[ \frac{4S_o^2}{G^2} - .2 \right]^{-1/2}$$

$$M_t = \left[ \frac{4S_t^2}{G^2} - .2 \right]^{-1/2}$$

10. Using the plot prepared in Step 7, and the values of  $M_o$ ,  $M_i$ , and  $M_t$  computed in Step 9, indicate the speed range over which each probable mode would respond, as shown by the shading in Figure 56.
11. Inspect Figure 56, apply the cavity oscillation mode hierarchy described in Section 3.7.2, and conclude the following: Priority A and B modes are available throughout the speed range; therefore, rule out all others. The cavity oscillation modes predicted are the (2)(3,0), the (2)(4,0), the (2)(5,0), the (1)(1,0), and the (1)(2,0).
12. Compute the cavity oscillation frequencies using Equation (28),  $f = S_i M_i C_\infty / L$ , where  $C_\infty$  is obtained from reference tables to be 1016 ft/sec at 25,000 ft, and 968 ft/sec at 37,000 ft. Obtain the following:

Mode ( $N_R$ )( $N_x, N_z$ )	Onset Mach	Intersection Mach	Termination Mach	Frequency @ 25000 Ft Hertz	Frequency @ 37000 Ft Hertz
(2)(3,0)	.432	.515	.612	15.6	14.9
(2)(4,0)	.649	.784	.948	21.5	20.5
(2)(5,0)	.939	1.166	1.447	28.7	27.3
(1)(1,0)	.230	.372	.745	5.2	5.0
(1)(2,0)	.590	1.021	3.414	11.2	10.7

#### Sound Pressure Level Derivations:

13. Enter Figure 41 at the intersection Mach number for each cavity oscillation mode (or use the equations noted on Figure 41) and obtain the normalized maximum sound pressure levels at intersection as follows:

Mode ( $N_R$ )( $N_x, N_z$ )	Intersection Mach	20 log P/q dB
(2)(3,0)	.515	-30.7
(2)(4,0)	.784	-23.1
(2)(5,0)	1.166	-26.4
(1)(1,0)	.372	-19.6
(1)(2,0)	1.021	-25.1

14. Determine dynamic pressure  $q$  (in pounds per square inch) at each intersection Mach number for the desired altitude of 25000 feet, and convert normalized sound pressure level ( $20 \log P/q$ ) to SPL for each mode, as follows:

$$\text{SPL} = 20 \log P/q + 20 \log q + 170.75$$

$$q = \frac{M^2 \rho C_\infty^2}{2}; \text{ obtain } \rho \text{ and } C \text{ from reference tables}$$

Mode ( $N_R$ )( $N_x, N_z$ )	Intersection Mach	$q$ (PSI) @ 25,000 Ft	SPL (dB) @ 25,000 Ft
(2) (3,0)	.515	1.01	150
(2) (4,0)	.784	2.35	155
(2) (5,0)	1.166	5.19	159
(1) (1,0)	.372	.53	146
(1) (2,0)	1.021	3.98	158

15. To calculate SPL for each cavity oscillation mode, at speeds both below and above intersection, use Figure 43 to obtain the correction to be applied to the intersection SPL. For convenience enter Figure 43 at five speeds, whereby  $\Delta \text{dB}$  is:

$M$	$M_o$	$\frac{M_o + M_i}{2}$	$M_i$	$\frac{M_i + M_t}{2}$	$M_t$
$\Delta \text{dB}$	-7	-2	0	-2	-10

Using  $SPL @ M = SPL @ M_1 + \Delta dB$ , and disregarding Mach numbers that are well below .4 and above 1.2, the resulting sound pressure levels are:

Mode ( $N_R$ )( $N_x, N_z$ )	Mach Number	SPL @ 25K ft	Mode ( $N_R$ )( $N_x, N_z$ )	Mach Number	SPL @ 25K ft
(2)(3,0)	$M_0 = .432$	143	(1)(1,0)	$M_0 = .230$	
	$M_1 + M_0 = .473$	148		$M_1 + M_0 = .301$	
	2			2	
	$M_1 = .515$	150		$M_1 = .372$	146
	$M_1 + M_1 = .563$	148		$M_1 + M_1 = .558$	144
	2			2	
	$M_1 = .612$	140		$M_1 = .745$	136
(2)(4,0)	$M_0 = .649$	148	(1)(2,0)	$M_0 = .590$	151
	$M_1 + M_0 = .716$	153		$M_1 + M_0 = .805$	156
	2			2	
	$M_1 = .784$	155		$M_1 = 1.021$	158
	$M_1 + M_1 = .866$	153		$M_1 + M_1 = 2.217$	
	2			2	
	$M_1 = .948$	145		$M_1 = 3.414$	
(2)(5,0)	$M_0 = .939$	152			
	$M_1 + M_0 = 1.052$	157			
	2				
	$M_1 = 1.166$	159			
	$M_1 + M_1 = 1.306$				
	2				
	$M_1 = 1.447$				

16. Plot the maximum SPL's obtained in Step 15 versus Mach number, to obtain a graphical summary of oscillatory levels at any launch speed at 25000 feet altitude, as shown in Figure 57. If desired, the levels may be combined to obtain an envelope of overall oscillatory level versus launch speed, neglecting broadband noise. Recall that the frequencies were determined in Step 12.



17. To obtain the oscillatory SPL's versus launch speed at any other altitude, such as 37,000 feet, the levels obtained in Step 15 are adjusted according to the change in q:

$$SPL_{37,000} = SPL_{25,000} + 20 \text{ LOG} \left( \frac{q_{37,000}}{q_{25,000}} \right) = SPL_{25,000} - 4.8 \text{ dB}$$

Environment at Selected Launch Speed of .8M; 25,000 Feet Altitude:

18. From Step 12, or from Figure 57 obtained in Step 16, determine for .8M at 25,000 feet, that the missile bay will respond in two modes: the (2)(4,0) and the (1)(2,0). The frequency of these two modes will vary slightly from the frequencies at the intersection Mach numbers. Obtain frequency at 0.8M using Equation 28 and G from Step 9:

$$f_{(2)(4,0)} = \frac{(1.04)(1016)}{(2)(26)} (1 + 2 \times 0.8^2)^{1/2} = 21.6 \text{ Hz}$$

$$f_{(1)(2,0)} = \frac{(52)(1016)}{(2)(26)} (1 + 2 \times 0.8^2)^{1/2} = 10.8 \text{ Hz}$$

19. From Figure 57 derived in Step 16, determine the spatial maximum sound pressure level at 0.8M for the 10.8 Hertz mode to be 156 dB, and for the 21.6 Hertz mode to be 154.5 dB.
20. Determine normalized broadband sound pressure level (1/3-octave-band level) for each mode frequency from Figure 50. For the 10.8 Hertz mode, enter Figure 50 at  $S = fL/MC_\infty = 0.34$  and read  $20 \log P/q = -40\text{dB}$ . For the 21.6-Hertz mode,  $S = .69$  and  $20 \log P/q = -38\text{dB}$ . These levels are at the downstream wall near the aperture.

21. Obtain 1/3-octave broadband sound pressure level,  $SPL_B$ , from the normalized level using

$$SPL_B = 20 \text{ LOG } \frac{P}{q} + 20 \text{ LOG } q + 170.75$$

At .8M and 25000 ft,  $q = 2.44$  and  $SPL_B$  at 21.6 Hertz is 140.5dB.  
At 10.8 Hertz it is 138.5 dB.

22. Convert the 1/3-octave broadband noise level to spectrum level,  $dB_r$ , using

$$\text{spectrum SPL} = 1/3 \text{ octave SPL} - 10 \log (1/3 \text{ octave BW})$$

Obtain the following:

Frequency Hertz	1/3 Octave SPL - dB	1/3 Octave BW - Hz	Spectrum SPL - $dB_r$
10.8	138.5	2.2	135
21.6	140.5	4.4	134

23. Determine the broadband noise level at the wall opposite the aperture using Figure 51. Enter Figure 51 at  $z/L_x = 15/26 = 0.58$ ; obtain a correction of  $dB = -13$ . Levels along the opposite wall are therefore 13 dB less than at the downstream wall near the aperture, whereby at 10.8 Hertz, opposite-wall spectrum level is 122  $dB_r$ , and at 21.6 Hertz it is 121  $dB_r$ . Repeat Steps 20,21,22, and 23 at any other frequencies desired.

24. Construct a cavity response spectrum plot to summarize levels at .8M, 25,000 ft., using frequencies and levels available from Steps 18, 19, and 23. The result is shown in Figure 58. To obtain the spectrum plot for any other altitude (at 0.8M), adjust the oscillatory levels and the broadband levels to account for change in  $q$  as done in Step 17.

25. Determine the spatial variation of the oscillatory sound pressure levels along the missile-bay wall opposite the aperture using Equation 34.

$$SPL_{\eta_x} = SPL_B + \left( SPL_{\max} - SPL_B \right) \left[ \left| \cos N_x \pi \eta_x \right| \right]^{\frac{22}{SPL_{\max} - SPL_B}}$$

Obtain  $SPL_B$  from Step 23, obtain  $SPL_{\max}$  from Step 19, obtain  $N_x$  from Step 18, whereby for the 10.8 Hertz mode,

$$SPL_{\eta_x} = 122 + 34 \left[ \left| \cos 2\pi \eta_x \right| \right]^{.645}$$

and for the 21.6 Hertz mode,

$$SPL_{\eta_x} = 121 + 33.5 \left[ \left| \cos 4\pi \eta_x \right| \right]^{.658}$$

Calculate the following levels at the spatial locations indicated:

Mode ( $N_x$ )( $N_y$ )( $N_z$ )	Frequency Hertz	dB at $\eta_x$ ; $\eta_x = x/l$										
		.0	.1	.2	.3	.4	.5	.6	.7	.8	.9	1.0
(1)(2,0)	10.6	136	152	138	138	152	156	152	138	138	152	156
(2)(4,0)	21.6	154.5	136	150	150	136	154.5	136	150	150	136	154.5
Approximate Overall		158	152	150	150	152	158	152	150	150	152	158

26. Construct a plot of level versus spatial position along the missile bay wall opposite the aperture to summarize the cavity environment at .8M, 25,000 feet, using the values obtained in Steps 23 and 25. The result is shown in Figure 59.

### 3.8.3 Results of Predictions

The cavity oscillation prediction procedure, as applied to CMCA Case 2 and described in the previous section, was used to analyze CMCA Cases 1,3,4, and 6 (see Figures 2, 3, and 4) in accord with the conditions noted in Section 3.8.1. Case 5 was not analyzed due to the absence of any sustained oscillation in either the exploratory tests or the CMCA model tests discussed in Section 3.6. A summary of the predicted oscillatory conditions that could occur at 25,000 feet is shown in Figure 60 for each CMCA case. The Mach number at which each oscillation begins (onset), maximizes (intersection), and ends (termination) is tabulated along with the maximum sound pressure levels and corresponding frequencies.

A summary of the oscillatory modes and their levels and frequencies for launch at Mach 0.8, 25,000 feet and for launch at Mach 0.8, 37,000 feet is shown in Figure 61 for each CMCA case. The predicted spatial variations of the SPL's for launch at Mach 0.8 at 25,000 feet are shown in Figures 62 through 66 for each case.

### 3.8.4 Required Alleviation

It can be seen in Figure 60 that maximum oscillatory levels at 25,000 feet exceed 150 dB in all cases. These oscillations are essentially discrete frequency pressure fluctuations that could have a pronounced effect on aircraft integrity, depending on how closely the oscillation frequencies match the airframe structural resonance frequencies. For this program, it was presumed that the predicted levels would be intolerable and that alleviation devices would be required for all cases analyzed.

### 3.8.5 Effectiveness of Alleviation Devices

As discussed earlier, cavity oscillations in CMCA's involve two basic physical phenomena: shear layer oscillation and missile bay acoustic resonances. In some very shallow cavities, the potential for missile bay acoustic modes is severely limited and the shear layer oscillation appears capable of sustaining itself at moderate levels independent of acoustic modes. Also, it is impractical to eliminate acoustic modes in an en-

closure. Thus, the shear-layer oscillation is the phenomenon that is best altered to achieve cavity noise suppression. The approach to the suppression of cavity oscillation in CMCA's is, thus, similar to the approach used heretofore on conventional bomb bays. The shear-layer oscillation frequency is characterized by the aperture length in the streamwise direction and the freestream velocity. With these quantities known, the frequencies of potential oscillation can be obtained from the modified Rossiter equation, but very little information about the physical aspects of the coupling with acoustic resonances is available. Based on flow observations using oil streaks, shadowgraphs, and water tables, some investigators have surmised that the introduction of turbulence into the shear layer could effectively destroy the shear layer and, therefore, suppress cavity oscillations. The thickness of the shear layer is increased by turbulence, and in some cases cavity oscillation sound pressure levels are reduced. Solid and porous spoilers, leading- and trailing-edge airfoils and ramps, and combinations thereof have been used for suppression devices on bomb-bay-type cavities with various degrees of success.

Cursory CMCA model tests were conducted to evaluate turbulence generating devices of the type illustrated in Figure 67. These tests consisted of "on-line" comparisons of cavity response level at a few speeds. This activity led to the observation that location, size, and orientation were more important than the degree of turbulence created by a particular device. In other words, a solid spoiler fence oriented normal to the flow at a favorable position upstream of the aperture leading edge might be more effective than a sawtooth device of similar overall geometric proportions. Turbulence alone did not seem to be of prime importance in cavity oscillation suppression. Instead, it appeared that the characteristic length of the unattached shear layer was the more important parameter in maximizing suppression. Additional cursory tests were then conducted to evaluate an upstream spoiler with and without a downstream ramp. From these tests it was observed that the upstream spoiler fence, when moved ahead of the aperture leading edge, evidently became the upstream origin for the shear layer. The shear layer characteristic length was thus increased, leading to a reduction in the shear layer oscillation frequency. Suppression was derived by "mismatching" or decoupling the shear layer from the responding acoustic mode. Ramps positioned downstream of the aperture present a

condition whereby the characteristic length is indistinct. The unattached shear layer length changes as its point of reattachment wanders fore-aft on the sloped ramp surface. The "Rossiter" modal frequencies for the original aperture are thus altered. When no acoustic modes were available below the principle mode frequency, the suppression devices that increased "apparent" aperture length were very effective. In large missile bays with many acoustic modes below the principle cavity oscillation mode, an upstream spoiler and a downstream ramp usually caused the shear-layer oscillation to couple with a lower-order acoustic mode.

The coupling with lower-order modes is illustrated in Figure 68 which shows the response of a model representing CMCA Case 1, i.e., a long cylindrical missile bay. Note that at Mach 0.62, the unsuppressed cavity oscillation involves the second- and third-order fore-aft acoustic modes. As speed is increased to Mach 0.77, the oscillation involves the fourth-order acoustic mode. At Mach 0.90, it involves the fifth-order acoustic mode. However, when fitted with an upstream spoiler and a downstream ramp, the cavity oscillation at Mach 0.63 involves the first-, second-, and third-order acoustic modes. Beyond that speed, the cavity oscillation continues to involve the third-order acoustic mode. With the increased "apparent" aperture length due to the presense of the spoiler and ramp, the reduced shear layer oscillation frequency no longer couples with the fourth- and fifth-order acoustic modes. Also, note that the unsuppressed cavity spectrum at Mach 0.90 Mach shows responses of the higher multiples of the principal acoustic mode, specifically the second and third multiples of the fifth-order acoustic mode. These responses are due to distortion. With suppression, the levels do not become intense enough to become distorted, and no distortion response is evident.

As a result of these tests and observations, the alteration of the shear layer to increase the "apparent" aperture length was the suppression approach selected, using a spoiler-type fence upstream. For large missile bays having many acoustic modes an airfoil-shaped ramp was added downstream of the aperture. Figure 69 illustrates these devices.

From test trials of these devices, it was concluded that the spoiler height

should be at least 7 percent of the aperture length, and position should be about 25 percent of the aperture length ahead of the aperture leading edge. The fore-aft position of the spoiler appears to be even more important than height. If an airfoil ramp is located downstream, the height of the ramp should be approximately equal to the height of the spoiler.

Subscale models representative of each CMCA analysis case were then tested with these devices in place to determine their effectiveness throughout the speed range of interest. Case 3 was evaluated first, and in this instance a substantial trial-and-error experimental effort was made to optimize the position of the upstream spoiler for minimum SPL. Nearly total suppression was obtained in the Mach range of 0.75 to 0.80, as shown in Figure 70. However, there were not sufficient resources to optimize the spoiler locations for every CMCA case. The other cases were all evaluated with the same spoiler location that was best for Case 3. In those cases, less suppression was therefore achieved at the Mach 0.80 range, as is evident in Figure 70. In each case, however, substantial suppression was obtained at certain velocities, and it is expected that the regions of substantial suppression could be shifted to any velocity desired by optimizing the size and location of the suppression devices. This remains to be demonstrated, however. So for purposes of revising the predicted SPL's in the CMCA cases analyzed, the noise reductions shown in Figure 70 were used as shown without allowance for optimizing the devices in each case.

#### 3.8.6 Revised Predictions

The SPL's predicted for 0.8 Mach and summarized in Figure 61 were adjusted according to the Figure 70 SPL reductions obtained experimentally. The resulting revised SPL's are shown in Figure 71 for 0.8 Mach at 25,000 and 37,000 feet. These results are only for illustrative purposes. The frequencies were not revised, since further research is necessary to demonstrate the relations between spoiler/ramp locations, apparent aperture length, and shear layer oscillation frequency. Broadband noise levels would likewise be affected by alleviation devices, and were not revised due to the lack of prediction methods applicable to suppressed cases.

Noteworthy trends, results, and behaviors observed during the course of this effort are delineated below. The order of presentation relates to subject matter rather than degree of importance.

All missile-bay test models that had parallel stream flow over an aperture were found to experience intense cavity oscillation.

In an oscillating cavity, the acoustic mode pressures appear to "regulate" the shear layer pressure oscillations, such that the shear layer can drive the acoustic mode over an appreciable Mach range.

The strongest cavity oscillation occurs when the frequency of shear layer pressure oscillation coincides with a cavity acoustic resonance. With correct representation of the two frequencies in terms of Strouhal number versus Mach number, the intersection of the two Strouhal curves identifies the oscillation frequency and Mach number.

The strongest cavity oscillation usually involves the second mode of the shear layer pressure oscillation.

When depthwise, lengthwise, and complex acoustic modes are "available," the shear layer pressure oscillation usually "prefers" to drive the complex mode.

A substantial "end correction" to the depth dimension is necessary in order to use the classical equations to compute depth-wise acoustic modes in a conventional bomb bay.

Higher multiples of the cavity oscillation frequency often occur when the oscillatory pressure waveform becomes severely distorted. As many as 15 of these "overtones" are not uncommon.

Helmholtz response is evident in large missile bays, but only at low velocities. As velocity increases, the sound pressure level of response



decreases, and above .2M the Helmholtz resonance rapidly vanishes. The Helmholtz resonance frequency is lowest at  $M = 0$ , and increases with Mach number.

The fore-aft spatial distribution of sound pressures in the missile-bay volumes is approximately a cosine wave shape; the number of wave minima depends on the acoustic modal order.

The highest oscillatory sound pressure level observed in the subscale model tests was 184 dB.

Five conceptual full-scale CMCA missile-bay cases were analyzed, and the predicted oscillatory sound pressure levels ranged from 143 to 178 dB, at frequencies ranging from 5 to 40 Hertz. In all five cases, the levels were judged to be excessive and to require alleviation.

Flow-modification devices for alleviating cavity oscillation were found to be effective if optimized in terms of size and fore-aft position relative to the upstream and downstream edges of the aperture.

The rearward missile-launch configurations having the aperture at the end, wherein the separated stream flow does not reattach downstream, were free of cavity oscillation.

Cavity response must be surveyed in small Mach number increments (one to three percent in critical regions) to identify transitions from one acoustic mode to another.

In spectrum analyses very narrow bandwidths are necessary to identify the correct acoustic mode involved.

## 5.0 RECOMMENDATIONS

Some of the results and observations arising from this effort are cause for altered thought and revised approaches to the overall cavity oscillation problem. For example, earlier published hypotheses regarding cavity excitation derived from studies of shallow bomb bays are not valid for cavity volumes that are larger than the product of aperture area and cavity depth, nor for deep cavities responding in a pure depth mode where the acoustic pressure wave meets the aperture/shear layer as a plane wave front. Yet, such cavities are very prone to oscillation. Further development work in a number of areas is warranted.

Experimental investigations are recommended to study the overall process of shear layer and acoustic pressure wave interaction. In particular, study the way the acoustic pressure waves regulate the vortex shedding process; study the change in shear layer pressure wave length (or convection velocity) over the length of the aperture; investigate the mechanism that produces severe distortion of the pressure wave; and the relative importance of various streamwise segments of the convecting shear-layer pressure wave in driving cavity acoustic resonances.

In some cases the modified Rossiter equation for shear layer oscillation frequency is inaccurate. Refinement for these cases is recommended.

The classical equations for cavity volume acoustic resonance frequencies are adequate for preliminary estimates. However, rarely does an actual aircraft cavity fully conform to the shape that the classical equations correctly represent. The method of acoustic finite element analysis should provide improved accuracy in the determination of acoustic modes in practical missile bays. The finite element methods should be implemented, and the results need to be checked with experiments to evaluate the validity of boundary assumptions and simplifications made to minimize machine computation time.

The extensive structural modifications necessary to ensure that airframes can tolerate intense cavity oscillation warrants a significant development

activity on suppression. The recommended study of the interaction of the shear layer and acoustic pressure waves would provide some of the insight needed. Activities that may warrant pursuit are: optimizing location and orientation of devices that vary the effective length of the aperture so as to mismatch the shear-layer oscillation from the cavity acoustic resonance frequency; development of concepts to prevent the shear layer pressure waves from interacting with cavity volume acoustic modes, and development of concepts to increase absorption and/or decrease the responsiveness of critical acoustic modes.

It is recommended that the cavity environment analysis methods developed and reported herein be applied to full-scale aircraft cases for which cavity oscillation data either already exist or can be inexpensively obtained, to validate the methods and determine whether the important parameters scale correctly.

Analytical development work is recommended that will lead to a mathematical description of the shear layer time-variant pressure distribution over the aperture area.

## 6.0 REFERENCES

1. Plumblee, H.E., Gibson, J.S., and Lassiter, L.W., "A Theoretical and Experimental Investigation of the Acoustical Response of Cavities in an Aerodynamic Flow," WADD-TR-61-75, USAF March 1962.
2. Rossiter, J.E., "Wind Tunnel Experiments on the Flow Over Rectangular Cavities at Subsonic and Transonic Speeds," ARC R&M No. 3438 (Oct. 1964).
3. Heller, H.H., Holmes, G., Covert, E.E., "Flow-Induced Pressure Oscillations in Shallow Cavities," AFFDL-TR-70-104, Dec. 1970.
4. Smith, D.L., and Shaw, L.L., "Prediction of the Pressure Oscillations in Cavities Exposed to Aerodynamic Flow," AFFDL-TR-75-34, October 1975.
5. Maurer, O., "Device to Reduce Flow-Induced Pressure Oscillations in Open Cavities," U.S. Patent - 3934846, 27 Jan. 1976.
6. Shaw, L.L., and Smith, D.L., "Aero-Acoustic Environment of a Store in an Aircraft Weapons Bay," AFFDL-TR-77-18, March 1977.
7. Clark, R.L., "Evaluation of F-111 Weapon Bay Aero-Acoustic and Weapon Separation Improvement Techniques," AFFDL-TR-79-3003, Feb. 1979.
8. Tipton, A.G., "Weapons Bay Cavity Noise Environments Data Correlation and Prediction for the B-1 Aircraft," AFWAL-TR-80-3050, June 1980.
9. Elder, S.A., "Self-Excited Depth Mode Resonance for a Wall-Mounted Cavity in Turbulent Flow," J. Acoustical Soc. of America, Vol. 64, No. 3, pp. 877-890, September 1978.
10. Elder, S.A., "Forced Vibrations of a Separated Shear Layer with Application to Cavity Flow-Tone Effects," Journal Acoustical Society of America, Vol. 67, No. 3, March 1980.
11. Rockwell, D., and Naudascher, E., "Review--Self-Sustaining Oscillations of Flow Past Cavities," Trans. of the ASME, Vol. 100, pp. 152-165, June 1978.
12. Nyborg, Wesley L., "Self-maintained Oscillations in A Jet Edge System," I.J. Acoust. Soc. America, Vol. 26, No. 2, March 1954, pp. 174-182.
13. Spee, B.M., "Wind Tunnel Experiments on Unsteady Cavity Flow at High Subsonic Speeds, Separated Flows," Part II, AGARD CP No. 4, May 1966, pp. 941-974.
14. Alster, M., "Improved Calculation of Resonant Frequencies of Helmholtz Resonators," J. of Sound and Vibration, Vol. 24, No. 1, pp. 63-85 1972.

15. Craggs, A., "The Use of Simple Three-Dimensional Acoustic Finite Elements for Determining the Natural Modes and Frequencies of Complex Shaped Enclosures," J. of Sound and Vibration, 23, 331-339, 1972.
16. Wolf, J.A. and Nefske, D.J., "NASTRAN Modeling And Analysis of Rigid And Flexible Walled Acoustic Cavities," In NASTRAN: Users Experience, NASA TM X-3278, Sept. 1975.
17. Petyt, M., Lea, J., and Koopman, G.H., "A Finite Element Method for Determining the Acoustic Modes of Irregular Shaped Cavities," J. Sound and Vibration, 45(4), 495-502, 1976.
18. Morse, P.M., "Vibration and Sound," 2nd Edition, McGraw Hill Book Co., Inc., New York, 1948.
19. East, L.F., "Aerodynamically Induced Resonance in Rectangular Cavities," Journal of Sound and Vibration, Vol. 3, No. 3, pp. 277-287, 1966.
20. Beranek, L.L., "Noise And Vibration Control," McGraw-Hill Book Co., Inc., New York, N. Y., 1971, Section 8.5.
21. Parker, R., "Acoustic Resonances In Passages Containing Banks of Heat Exchanger Tubes," Jou. of Sound and Vibration, 57(2), 245-260, 1978

## 7.0 BIBLIOGRAPHY

Elder, S.A., "Forced Vibrations of a Separated Shear Layer with Application to Cavity Flow-Tone Effects," Journal Acoustical Society of America, Vol. 67, No. 3, March 1980.

Tipton, A.G., "Weapons Bay Cavity Noise Environments Data Correlation and Prediction for the B-1 Aircraft," AFWAL-TR-80-3050, June 1980.

Clark, R.L., "Evaluation of F-111 Weapon Bay Aero-Acoustic and Weapon Separation Improvement Techniques," AFFDL-TR-79-3003, Feb. 1979.

Dowell, E.H., "Master Plan for Prediction of Vehicle Interior Noise," Paper 79-0582, AIAA 5th Aeroacoustics Conference, March 1979.

Hankey, W.L. and Shang, J.S., "Analysis of Pressure Oscillations in an Open Cavity," AIAA Jou., Vol. 18, No. 8, Paper 79-0136, Jan. 1979.

Richards, T.L. and Jha, S.K., "A Simplified Finite Element Method for Studying Acoustical Characteristics Inside a Car," J. of Sound and Vibration, 63 (1), 1979, pp. 61-72.

Shaw, L.L., "Suppression of Aerodynamically Induced Cavity Pressure Oscillations," AFFDL-TR-79-3119, November 1979.

Unruh, J.F., "A Finite Element Subvolume Technique for Structural-Borne Interior Noise, etc.," AIAA Paper No. 79-0585, 1979.

Wilby, J.F., and Pope, L.D., "Prediction of the Acoustic Environment in the Space Shuttle Payload Bay," AIAA Paper No. 79-0643, March 1979.

Balashov, I.F., Berenberg, V.A., Romanov, V.A., "Study on Transient Processes and Time of Oscillation Establishment in Open Cavities" (Russian), Optika i Spektroskopiya, Vol. 44, No. 2, Pgs. 312-319, 1978.

- Cabot, R.C., "Computer Aided Computation of Room Resonances," Bibl. Audio Eng. Soc. J. 26:537-46, July-Aug. 1978.
- Elder, S.A., "Self-Excited Depth Mode Resonance for a Wall-Mounted Cavity in Turbulent Flow," J. Acoustical Soc. of America, Vol. 64, No. 3, pp. 877-890, September, 1978.
- Joppa, P.D., and Fyfe, I.M., "A Finite Element Analysis of the Impedance Properties of Irregular Shaped Cavities with Absorptive Boundaries," J. of Sound and Vibration, 56(1), 1978, pp. 61-66.
- Kanellopoulos, J.D., and Fikioris, J.G., "Acoustical Resonant Frequencies in an Eccentric Spherical Cavity," Bibl. Diag. Acoustical Soc. America J. 64:286-97, July 1978.
- Koval, L.R., "Effects of Cavity Resonances on Sound Transmission Into a Thin Cylindrical Shell," Jour. of Sound and Vibration 58 (1), 23-33, 1978.
- Nefske, D.J. and Howell, L.J., "Automotive Noise Reduction Using Finite Element Methods," Paper No. 78-0365, Presented at the SAE Congress and Exposition, Detroit, Mich., Feb. 1978.
- Parker, R., "Acoustic Resonances in Passages Containing Banks of Heat Exchanger Tubes," Jou. of Sound and Vibration, 57(2), 245-260, 1978.
- Petyt, M., and Lim, S.P., "Finite Element Analysis of the Noise Inside a Mechanically Excited Cylinder," Inter. Jou. for Numerical Methods in Engineering, Vol. 13, (109-122), 1978.
- Rockwell, D., and Naudascher, E., "Review—Self-Sustaining Oscillations of Flow Past Cavities," Trans. of the ASME, Vol. 100, pp. 152-165, June 1978.
- Sarohia, V., and Massier, P.F., "Effect of Angle of Attack on Cavity Flow Oscillations," JPL Publication 79-19, California Institute of Technology, Pasadena, California, Oct. 1978.

- Scheiman, James, "Acoustical Measurements of a Large Cavity in a Wind Tunnel," NASA TM 78658, May 1978.
- Tam, C.K.W., and Block, P.W., "On Tones and Pressure Oscillations Induced by Flows Over Rectangular Cavities," Journal of Fluid Mechanics, Vol. 89, Nov. 1978.
- Block, P.J.W., "Measurements of the Tonal Component of Cavity Noise and Comparison with Theory." NASA TP-1013, 1977.
- DeMetz, F.C., and Farabee, T.M., "Laminar and Turbulent Shear Flow Induced Cavity Resonances," AIAA Paper 77-1293, Oct. 1977.
- Dowell, E.H., Gorman, G.P., and Smith, D.A., "Acoustoelasticity: General Theory Acoustic Natural Modes and Forced Responses to Sinusoidal Excitations, Including Comparison with Experiment," J.S.V. 52(4) 519-542, 1977.
- Holger, D.K., Wilson, T.A., and Beavers, G.S., "Fluid Mechanics of the Edgetone," Journal of Acoustical Society of America, Vol. 62, Number 5, pps. 1116-1128, Nov. 1977.
- Junger, M.C., "Model Scaling Laws for Sound Absorptive Boundaries," Bibl. Diag., Acoustical Soc. Am. J. 62:209-11, July 1977.
- Kagawa, J., Yamabuchi, T., and Mori, A., "Finite Element Simulation of an Axisymmetric Acoustic Transmission System with a Sound Absorbing Wall," J. of Sound and Vibration, 53(3), 1977, pp. 357-374.
- Rockwell, D., "Prediction of Oscillation Frequencies for Unstable Flow Past Cavities," (EN), Univ. Karlsruhe, Inst. Hydromech/D-7500, Karlsruhe/Fed. Rep. Ger. Journal of Fluids Engineering-Transactions of the ASME Series 1, Vol. 99, No. 2, pps. 294-300, 1977.
- Morel, T. "Experimental Study of a Jet-Driven Helmholtz Oscillator," General Motors Research Laboratories GMR-2362, July 1977.



Sarohia, V., and Massier, P.F., "Control of Cavity Noise," Journal of Aircraft, Sept. 1977.

Sarohia, V., and Massier, P.F., "Investigation of Pressure Oscillations in Axi-Symmetric Cavity Flows," Harry Diamond Laboratories Report HDL-CR-77-025-1, Sept. 1977, 48P.

Shaw, L.L., and Smith, D.L., "Aero-Acoustic Environment of a Store in an Aircraft Weapons Bay," AFFDL-TR-77-18, March 1977.

White, R.E., and Norton, D.J., "The Momentum Transfer of Incompressible Turbulent Separated Flow Due to Cavities with Steps," 261P, NACA-CR-151590, TEES-1086-TR-77-02, Dec. 1977.

Yu, Y.H., "Measurement of Sound Radiation from Cavities at Subsonic Speeds," Journal of Aircraft, Sept. 1977.

Benepe, D.B., and Richtman, R.T., "Study of Weapons Bay Environment Suppression Devices for F-111 Aircraft," F2H-12-13919, Gen. Dynamics, Ft. Worth, Texas, Aug. 1976.

Bliss, D.B., and Hayden, R.E., "Landing Gear and Cavity Noise Prediction," NASA Contractor Report: NASA CR-2714, 1976.

Block, Patricia J.W., "Noise Response of Cavities of Varying Dimensions at Subsonic Speeds," NASA Technical Note: NASA TN D-8351, 1976.

Craggs, A., "A Finite Element Method for Damped Acoustic Systems: An Application to Evaluate the Performance of Reactive Mufflers," Jour. Sound and Vibration, Vol 48, 377-392 1976.

Craggs, A., and Stead, G., "Sound Transmission Between Enclosures - A Study Using Plate and Finite Elements," Acoustics, Vol 35, 89-98, 1976.

Dougherty, W.S. Jr., Anderson, C.F., "An Experimental Study On Suppression of Edgetones from Perforated Wind Tunnel Walls", AIAA Paper 76-50, Fourteenth AIAA Aerospace Sciences Mtng., Jan. 1976.

Harden, J.C., and Mason, J.P., "A Vortex Model of Cavity Flow," AIAA Paper No. 76-524, 3rd Aeroacoustic Conf., July 1976.

Hersh, A.S., and Walker, B., "The Acoustical Behavior of Helmholtz Resonators Exposed to High Speed Grazing Flows," AIAA Paper No. 76-536, July 1976.

Hughes, R.C., and Haering, R.R., "Acoustic-Resonance in Composite Cavities," Journal of the Acoustical Society of America, Vol. 59, No. 2, Pgs. 452-458, Feb. 1976.

Maurer, O., "Device to Reduce Flow-Induced pressure Oscillations in Open Cavities," U.S. Patent - 3934846, 27 Jan. 1976.

Petyt, M., Lea, J., and Koopman, G.H., "A Finite Element Method for Determining the Acoustic Modes of Irregular Shaped Cavities," J. Sound and Vibration, Vol 45(4), 495-502, 1976.

Sanders, W.G., "The Effect of Cavity Opening Geometry on Air-Flow Induced Cavity Resonances," David Taylor Naval Ship R&D Center, May 1976.

Sarohia, V., "Experimental Investigations of Oscillations in Flows Over Shallow Cavities," AIAA Paper 76-182, Jan. 1976.

Tam, C.K.W., "The Acoustical Modes of a Two-dimensional Rectangular Cavity," Jou. Sound and Vibration 49, 353-364.

Woolley, J.P., and Karamcheti K., "The Two-Dimensional Development of Flow in the Presence of Periodic or Random Fluctuations with Application to the Calculation of Cavity Tones," Feb. 1976, 97P. (Neilson Engr. & Research) TRIII

Block, P.J.W., and Heller, H., "Measurements of Farfield Sound Generated from a Flow-Excited Cavity," NASA TM-X-3292, 1975.

Clark, R.L., "Weapons Bay Turbulence Reduction Techniques," AFFDL-TN-75147-FKM, Dec. 1975.

Franke, M.E., and Carr, D.L., "Effect of Geometry on Open Cavity Flow-Induced Pressure Oscillations," AIAA Paper 75-492, March, 1975.

Heller, H.H., and Bliss, D.B., "Aerodynamically Induced Pressure Oscillations in Cavities - Physical Mechanisms and Suppression Concepts," AFFDL-TR-74-133, Feb. 1975.

Ingard, U., And Singhal, V.K., "Effect of Flow on the Acoustical Resonance of an Opened-Ended Duct," Bibl. Diags., Acoustical Soc. Am. J. 58:788-93, Oct. 1975.

Kovaszny, L.S.G., Chih-Ming, Ho, "Static Pressure Rise In Acoustically Driven Cavities, AIAA Journal, Vol 13, Oct. 1975.

Mungur, P., and Whitesides, J.L., "Influence of Grazing Flow on Duct Wall Normal Impedances," AIAA 2nd Aero-Acoustics Conf. paper 75-494, March 1975.

O'Brien, V., "Unsteady Separation Phenomena in a Two-Dimensional Cavity," "AIAA Journal", Vol. 13, No. 3, March 1975.

Panton, R.L. and Miller, John M., "Excitation of a Helmholtz Resonator by a Turbulent Boundary Layer," J. Acoustical Soc. of America, Vol. 58, No. 4, pp. 800-806, 1975.

Sarohia, V., "Experimental and Analytical Investigation of Oscillations in Flows Over Cavities," PhD. Thesis, Calif. Institute of Technology, Pasadena, California, 1975.

Smith, D.L., and Shaw, L.L., "Prediction of the Pressure Oscillations in Cavities Exposed to Aerodynamic Flow," AFFDL-TR-75-34, October 1975.

Young, C.I.J., and Crocker, M.J., "Prediction of Transmission Loss in Mufflers by the Finite Element Method," Jou. of the Acoustical Soc. of America, 57, 144-8, 1975.

Carr, D.L., "An Experimental Investigation of Open Cavity Pressure Oscillations," M.S. Thesis, Air Force Institute of Technology, Wright-Patterson AFB, Ohio, 1974.

Maurer, O., "Investigation and Reduction of Open Weapon Bay Pressure Oscillations, Etc.," AFFDL-TR-74-101-FYA, January 1974.

McCanless, G.F., and Boone, J.R., "Noise Reduction in Transonic Wind Tunnels," Jou. Acoust. Soc. of Am. Vol. 56, No. 5, Nov. 1974, pp. 1501-1510.

Shaw, L.L., Smith, D.L., et al, "Aero-Acoustical Environment of a Rectangular Cavity with a Length to Depth Ratio of Four," AFFDL-TM-74-19-FYA, Jan. 1974.

Smith, D.L., Shaw, L.L., et al, "Aero-Acoustical Environment of Rectangular Cavities with Length to Depth Ratios of Five and Seven," AFFDL-TM-74-79-FYA, April 1974.

Van Kuren, J.T., et al, "Acoustic Phenomena of Open Cavity Airborne Cassegrainian Telescopes," AIAA Paper 74-195, January 30, 1974.

Bilanin, A.J., and Covert, E.E., "Estimation of Possible Excitation Frequencies for Shallow Rectangular Cavities," AIAA Journal, Vol. 11, No. 3, pp. 347-351, March 1973.

Craggs, A., "An Acoustic Finite Element Approach for Studying Boundary Flexibility and Sound Transmission Between Irregular Enclosures," J. Sound and Vib., 30, 343-357 (1973)

Coltman, J.W., "Mouth Resonance Effects In the Flute," J. Acoust. Soc. Am., Vol 54, pp 417-420, 1973.

Franke, M.E., et al., "Jet Driven Cylindrical Cavity Oscillators," ASME Journal Dyn. Systems, Meas. and Control, June 1973.

Shuka, T., and Ishihara, K., "The Analysis of the Acoustical Field In Irregularly Shaped Rooms by the Finite Element Method," J. Sound and Vib., 29 (1), 1973, pp. 67-76.

Stull, F.D., Curran, E.T., and Velkoff, H.R., "Investigation of Two-Dimensional Cavity Diffusers," AIAA Paper, Palm Springs, Calif., July 1973.

Wooley, J.P., and Karamcheti, K., "A Study of Narrow Band Noise Generation by Flow Over Ventilated Walls in Transonic Wind Tunnels," AFOSR-TR-73-0503, Feb. 1973.

Wooley, J.P., and Karamcheti, K., "The Role of Jet Stability in Edgetone Generation," AIAA Paper 73-628, 1973.

Alster, M., "Improved Calculation of Resonant Frequencies of Helmholtz Resonators," J. of Sound and Vibration, Vol. 24, No. 1, pp. 63-85, 1972.

Betts, P.C., "Self-Induced Oscillations in an Open Water Channel with Slotted Walls," J. Fluid Mechanics, Vol. 55, Part 3, 1972, pp. 401-417.

Craggs, A., "The Use of Simple Three-Dimensional Acoustic Finite Elements for Determining the Natural Modes and Frequencies of Complex Shaped Enclosures," J. of Sound and Vibration, 23, 331-339, 1972.

Gerlach, C.R., "Vortex Excitation of Metal Bellows," ASME J. Engineering for Industry," Feb. 1972, pp. 87-94.

O'Brien, V., "Closed Streamlines Associated with Channel Flow Over a Cavity," Physics of Fluids, Vol. 15, Dec. 1972, pp. 2089-2097.

Anon., "Final Report Wall Effects in Cavity Flows," Cal. Inst. of Tech. Div. of Engr. and App. Sci., AFSC FGN Tech. Div. (Translation), Paper E111A).

Beranek, L.L., Noise and Vibration Control, McGraw-Hill, 1971.

Buell, D.A., "An Experimental Investigation of the Airflow Over a Cavity with Antiresonance Devices," NASA TN-D-6205, March 1971.

Craggs, A., "The Transient Response of a Coupled Plate - Acoustic System Using Plate and Acoustic Finite Elements," J. of Sound and Vibration, 15, 509-528, 1971, (NASA CR1421, 1969).

Heller, H.H., Holmes, D.G., and Covert, E.E., "Flow Induced Pressure Oscillations in Shallow Cavities," Journal of Sound and Vibration, Vol. 18, 1971, pp. 454-552.

Koopman, G., and Pollard, H., "Model Studies of Helmholtz Resonances in Rooms with Windows and Doorways," J. of Sound and Vibration, 16(4), 489-503, 1971.

Miles, J.B., and Watson, G.H., "Pressure Waves for Flow Induced Acoustic Resonance in Cavities," Univ. of Missouri, Columbia, AIAA Journal, Vol. 9, No. 7, July 1971., p 1402-4.

Zienkiewicz, O.C., "The Finite Element Method in Engineering Science," McGraw-Hill, London, 1971.

Covert, E.E., "An Approximation Calculation of the Onset Velocity of Cavity Oscillations," AIAA Journal 8, (12), 2189-2194 Dec. 1970.

McGregor, O.W., and White, R.A., "Drag of Rectangular Cavities in Supersonic and Transonic Flow Including the Effects of Cavity Resonance," AIAA Journal, pp. 1959-1964, Nov. 1970.

Craggs, A., "The Transient Response of Coupled Acousto-Mechanical Systems," NASA CR-1421, Aug. 1969.

Dowell, E.H., "Transmission of Noise From a Turbulent Boundary Layer Through a Flexible Plate Into a Closed Cavity," J. Acoustical Soc. of America, 46, 238-252, 1969.

Heidmann, M.F., "Empirical Characterization of Some Pressure Wave Shapes in Strong Traveling Transverse Acoustic Modes," NLRC Report No. NASA-TM-X-1716, Jan. 1969.

Karamcheti, K., et al., "Some Features of An Edge-Tone Flow Field," NASA SP-207, pp 275-304, July 1969.

Mehta, U.B., and Lavan, Z., "Flow in a Two Dimensional Channel with a Rectangular Cavity," NASA CR-1245, Jan., 1969.

Yao-Tsu Wu, T., Whitney, A.K., and Lin, J.D., "Final Report Wall Effects in Cavity Flows," ONR Dept. of Navy Report No. E-111A.5, Aug. 1969.

Coltman, J.W., "Sounding Mechanism of the Flute and Organ Pipe," Journal of the Acoustical Society of America, Vol. 44, No. 4, 1968.

Morozov, M.G., "Acoustical Emission of Cavities in Supersonic Airflow," (Translation USSR Original 1960), FTD-MT-24-296-68, WPAFB, Ohio, Oct. 1968.

Phillips, B., "Effects of High-Wave Amplitude and Mean Flow On A Helmholtz Resonator," NASA-TM-X-1582, 1968.

Bennett, R.L., "An Experimental Investigation of Standing Vortices in an Open Cavity," M.S. thesis (Naval Postgraduate School, Monterey, Calif.), Unpublished, 1967.

Mason, V., "On the Use of Rectangular Finite Elements," Inst. Sound Vib. Res. Rep. I.S.A.V., 161, 1967.

East, L.F., "Aerodynamically Induced Resonance in Rectangular Cavities," Journal of Sound and Vibration, Vol. 3, No. 3, pp. 277-287, 1966.

Spee, B.M., "Wind Tunnel Experiments on Unsteady Cavity Flow at High Subsonic Speeds, Separated Flows," Part II, AGARD CP No. 4, pp. 941-974, May 1966.

Bodger, W.K., and Jones, C.M., "Aerodynamic Wind Throb in Passenger Cars," SAE Transactions Number 73, 1965.

Ketler, D.J., "Coupled Panel/Cavity Vibrations," AIAA Journal 3, 2163-2164, 1965.

Michalke, A., J. Fluid Mech., 23, pp. 521-544, 1965.

Weiss, R.F., and Florsheim, B.H., "Flow in a Cavity at Low Reynolds Number," Physics of Fluids, Vol. 8, 1965, pp. 1631-5.

Rossiter, J.E., "Wind Tunnel Experiments on the Flow Over Rectangular Cavities at Subsonic and Transonic Speeds," ARC R&M No. 3438, Oct. 1964.

Mauil, D.J., and East, L.F., "Three-Dimensional Flow in Cavities," Journal of Fluid Mechanics, Vol 16, p.620, 1963.

Covert, E.E., "An Analytical Investigation of Cavity Oscillations - Cavities with Unobstructed Openings and Discontinuous Velocity Profiles," M.I.T. Tech. Report 38, Oct. 1962.

Dunham, W.H., "Flow Induced Cavity Resonance in Viscous Compressible and Incompressible Fluids," 4th Symposium Nav. Hydro. ONR ACR-92 1057-1081, 1962.

Plumlee, H.E., Gibson, J.S., and Lassiter, L.W., "A Theoretical and Experimental Investigation of the Acoustical Response of Cavities in an Aerodynamic Flow," WADD-TR-61-75, March, 1962.

Rossiter, J.E. and Kurn, A.G., "Wind Tunnel Measurements of the Unsteady Pressures in and Behind a Bomb Bay (Canberra)," ARC Paper No. CP728, Oct. 1962.

Bland, R.E., and Skudrzyk, E.J., "Experimental Study of Flow-Induced Vibrations at a Cavity Opening," T.M. 19. 3360.07 ORL, Univesity Park, Pa., May 1961.



Eldred, K., Roberts, W., and White, R., "Structural Vibrations in Space Vehicles," WADD Tech. Report 61-62, March 1961.

Powell, A., "On the Edgetone," Journal of the Acoustical Society of America, Vol. 33, No. 4, pp. 395-409, 1961.

Tach, D.H., Smith, M.W., and Lambert, R.F., "Wall Pressure Fluctuation in Turbulent Airflow," Journal of Acoustical Society of America, Vol. 33, No. 4, April 1961.

Harrington, M.C. and Dunham, W.H., "Studies of the Mechanism for the Flow-Induced Cavity Resonance," Journal Acoust. Soc. America, Vol. 32, No. 7, July 1960, p. 921.

Anon., "The Investigation of Canopy-off Cockpit Buffeting in the B-47 Airplane," Boeing Report D-2688, 1952.

Curle, N., "Mechanisms of Edge Tones," Proc. of the Royal Society of London, Series A, Vol. 216, p. 412, 1953.

Doak, Philip E., "Sound Waves in Parabolic Rooms," Proc. Okla. Acad. Sci., XXXI(1950) 111-112.

Fail, R., Owen, R.B., and Eyre, R.C.W., "Low-speed Tunnel Tests on the Flow in Bomb Bays and Its Effect on Drag and Vibration," ARC RAE Report No. Aero 2511 17412, May 1954.

Karamcheti, K., "Acoustical Radiation from Two-Dimensional Rectangular Cutouts in Aerodynamic Surfaces," NACA TN 3487, August 1955.

Leopold, M.J., and Baker, R.W., "A Report on Research Directed Toward the Design, Development, Construction, and Testing of Aerodynamic Cavities," M.I.T. Naval Supersonic Lab., Tech. Report 417 (Nov. 1959).

Morse, P.M., and Bolt, R.H., "Sound Waves in Rooms," Rev. Mod. Physics 16:70-150, April 1944.

Morse, P.M., Vibration and Sound, 2nd Edition, McGraw Hill Book Co., Inc., New York, 1948.

Norton, D.A., "Investigation of B-47 Bomb Bay Buffeting," Boeing Report D-12675, Feb. 15, 1952.

Nyborg, Wesley L., et al., "Acoustical Characteristics of Jet-Edge and Jet-Edge Resonator Systems," J. Acoust Soc Am; Vol 24, No. 3, May 1958.

Nyborg, Wesley L., "Self-maintained Oscillations in A Jet Edge System," Jou. Acoust. Soc. America Vol. 26, No. 2, March 1954, pp. 174-182.

Owen, T.B., "Techniques of Pressure-Fluctuation Measurements Employed in the RHE Low-Speed Wind-Tunnels," NATO Report 172, (AGARD), March 1958.

Rayleigh, J.W.S., The Theory of Sound, Chapter 16, "Theory of Resonators," 1878, Dover Reprint 1945.

Richardson, E.G., Editor; Technical Aspects of Sound, Vol. 1, Chapter 18, "Mechanical Musical Instruments," Elsevier Publishing Co., 1953.

Roshko, A., "Some Measurements of Flow in a Rectangular Cutout," NACA TN 3488, Aug. 1955.

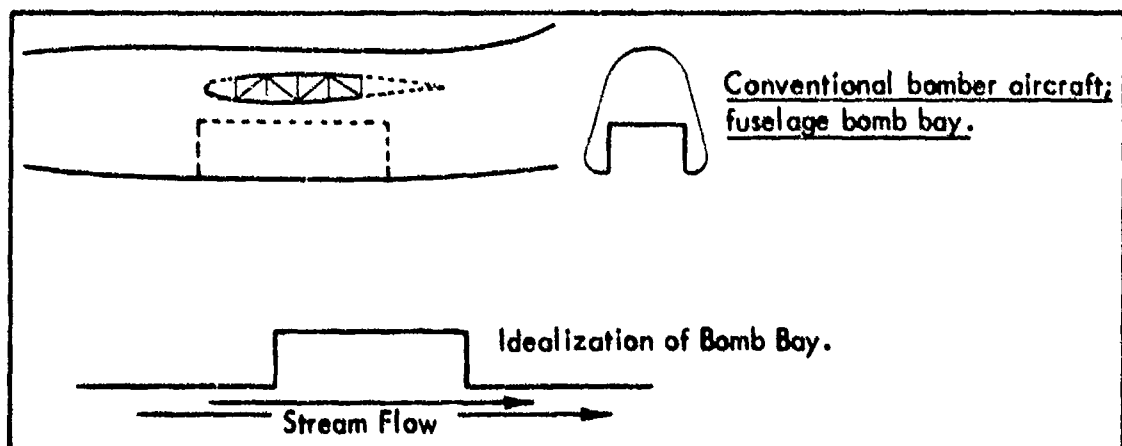
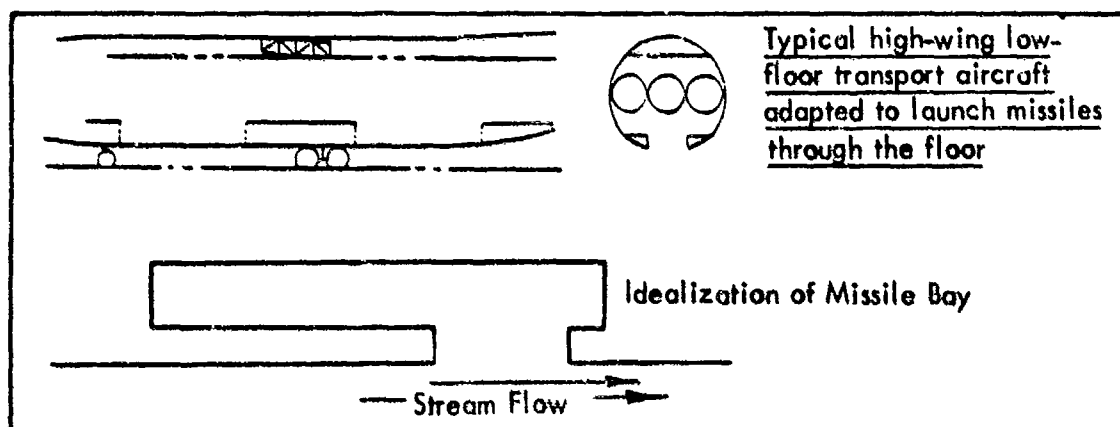
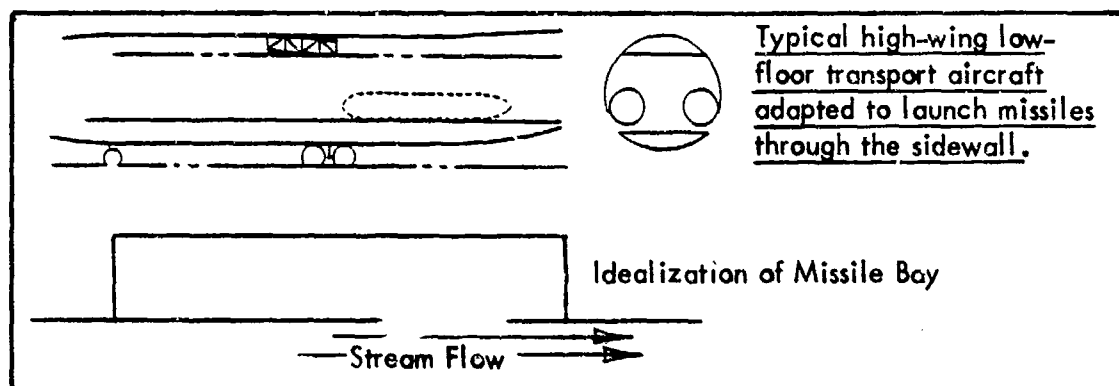


Figure 1. Cavity Arrangements in Cruise Missile Carrier Aircraft and in Conventional Bombers

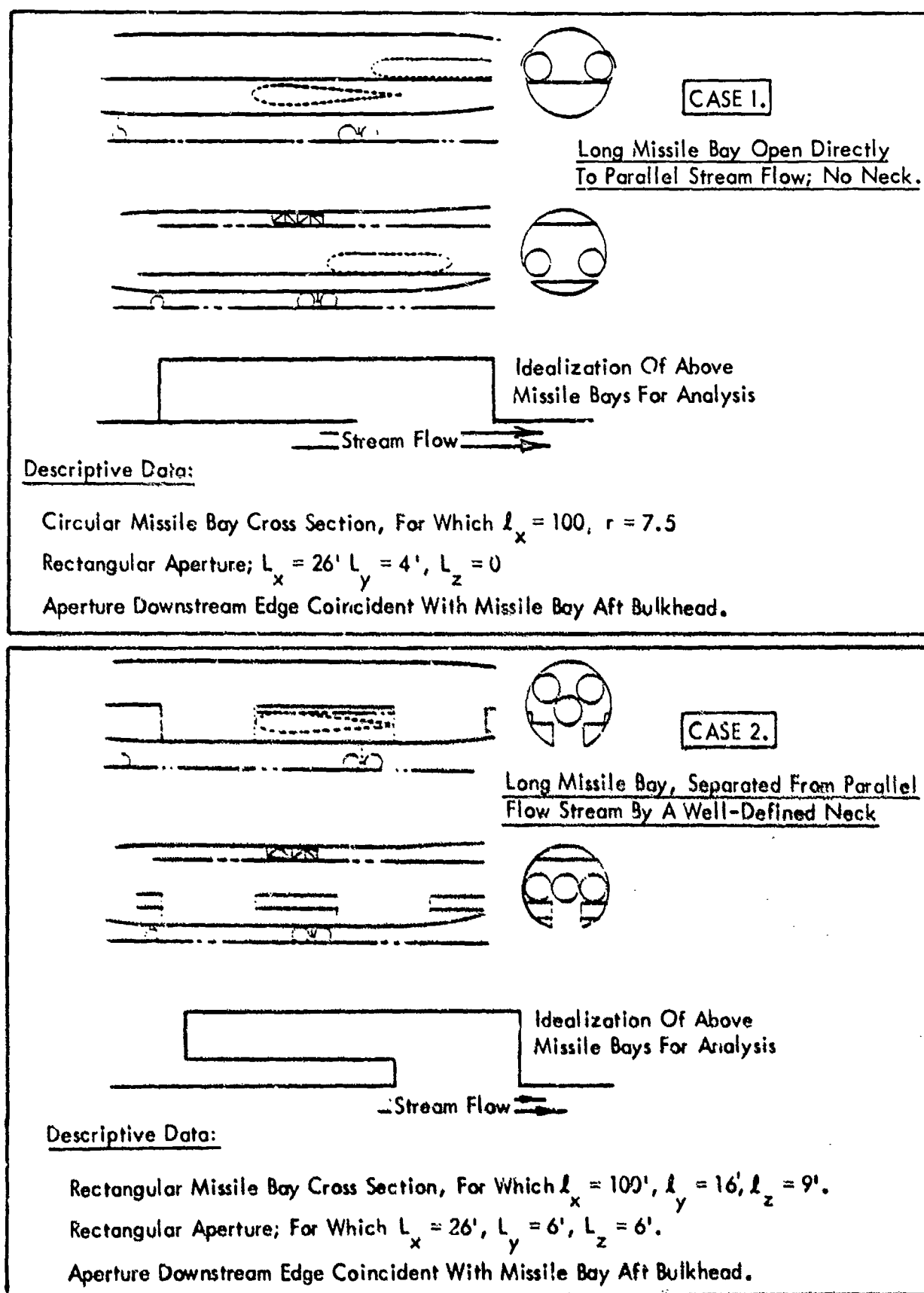


Figure 2. Long CMCA Missile Bays Selected For Analysis

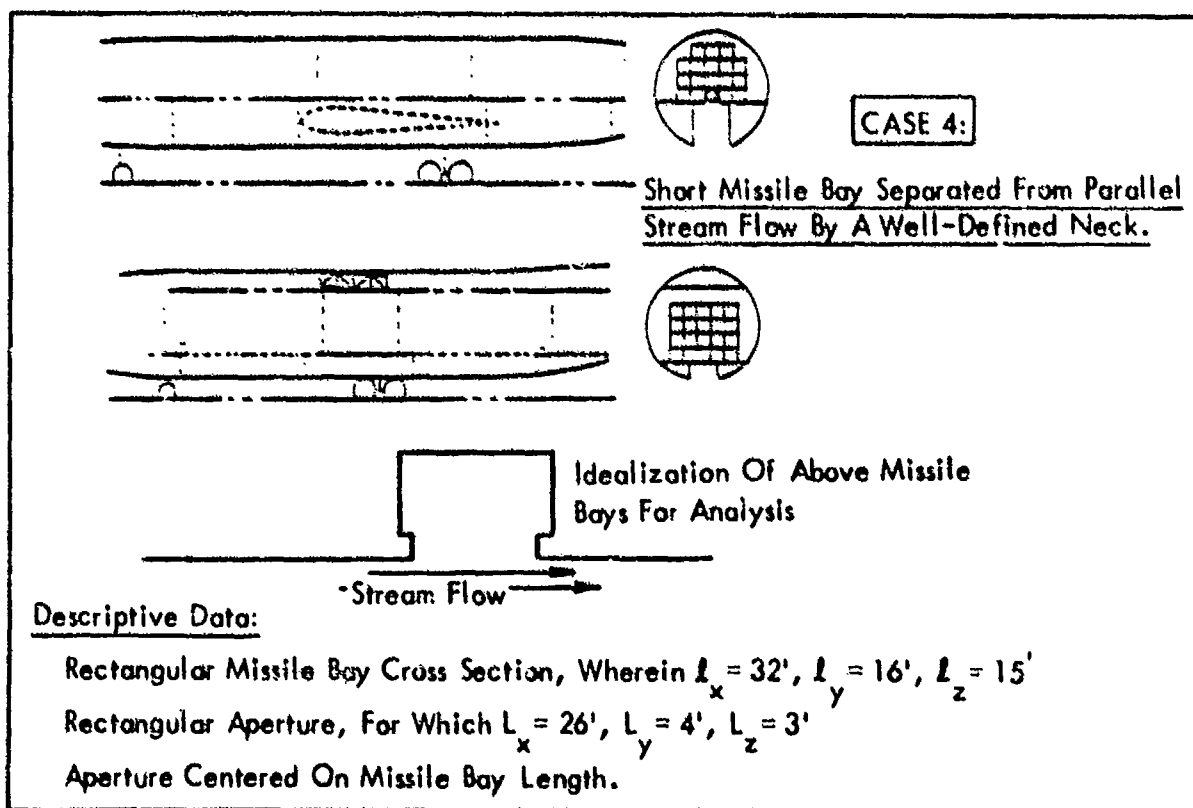
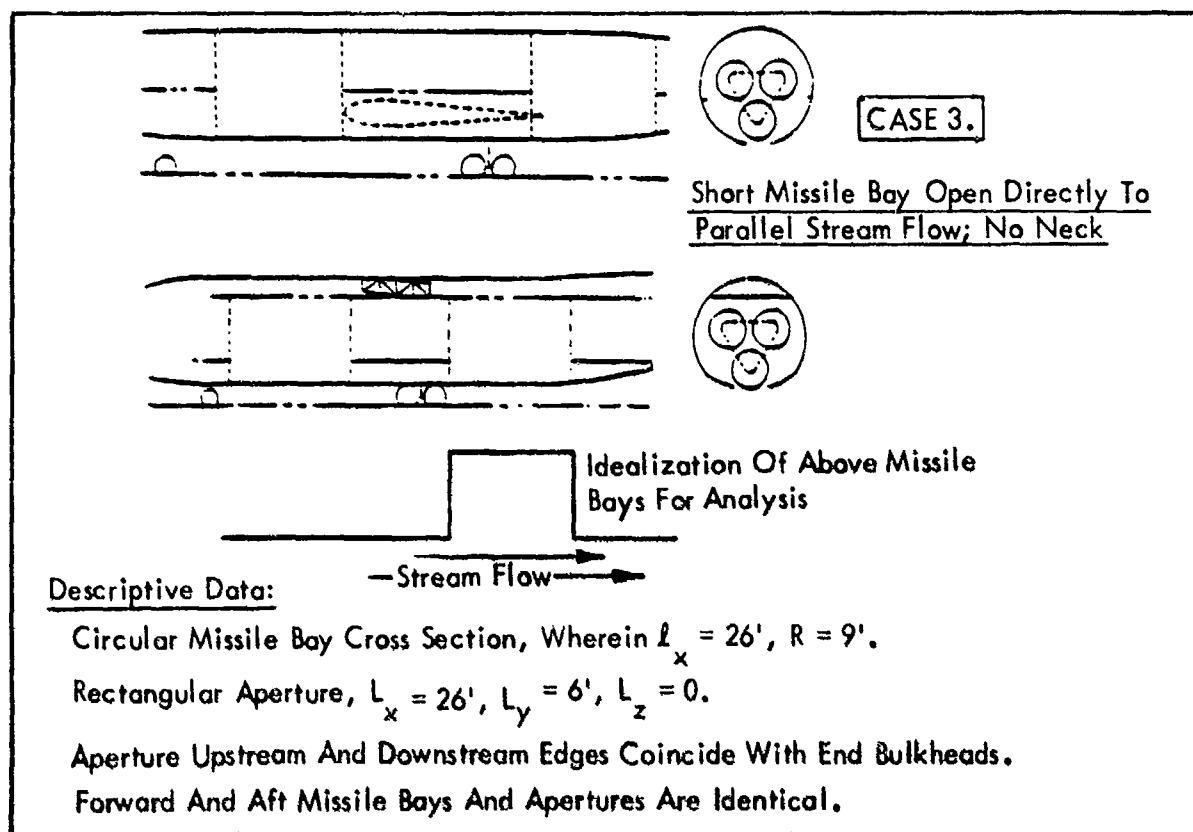


Figure 3. Short CMCA Missile Bays Selected For Analysis.

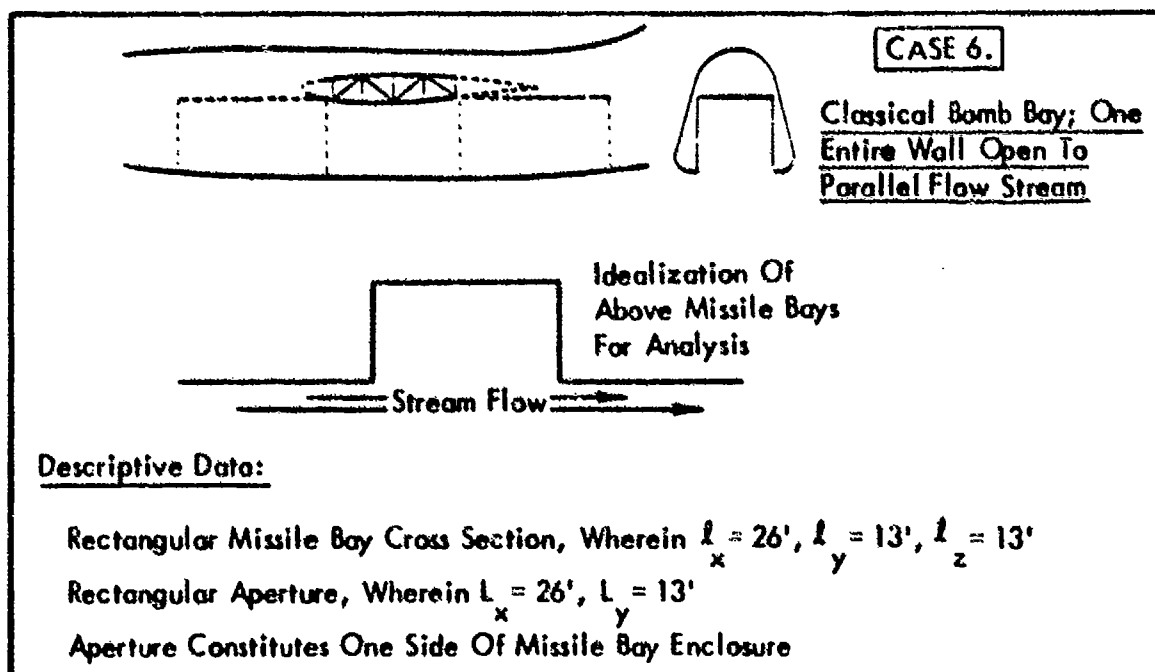
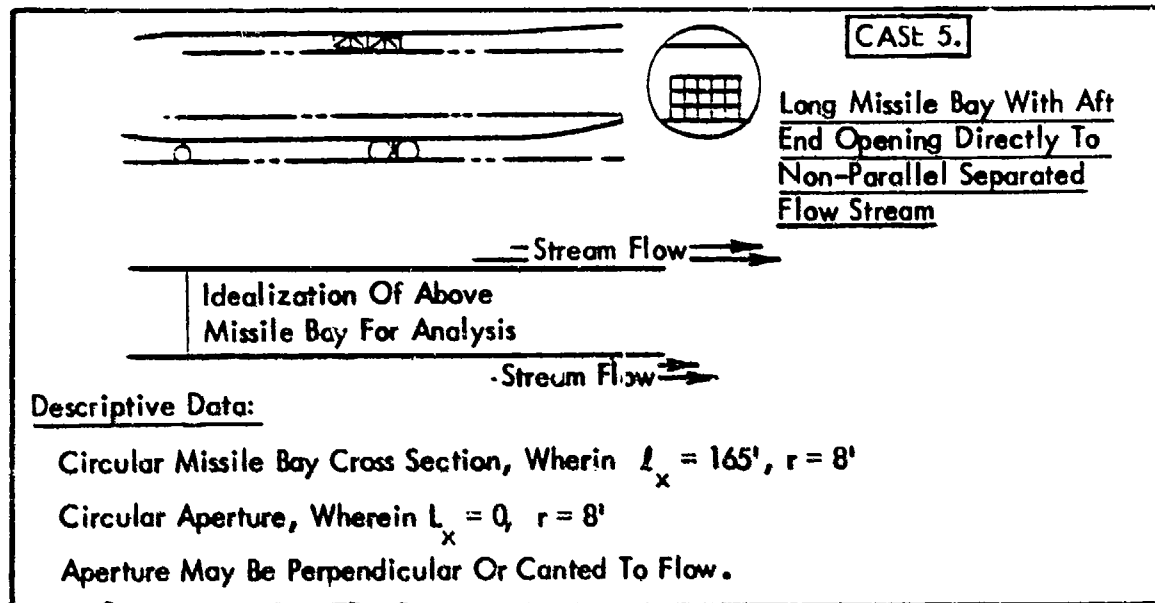


Figure 4. Aft Launch And Conventional CMCA Missile Bays Selected For Analysis

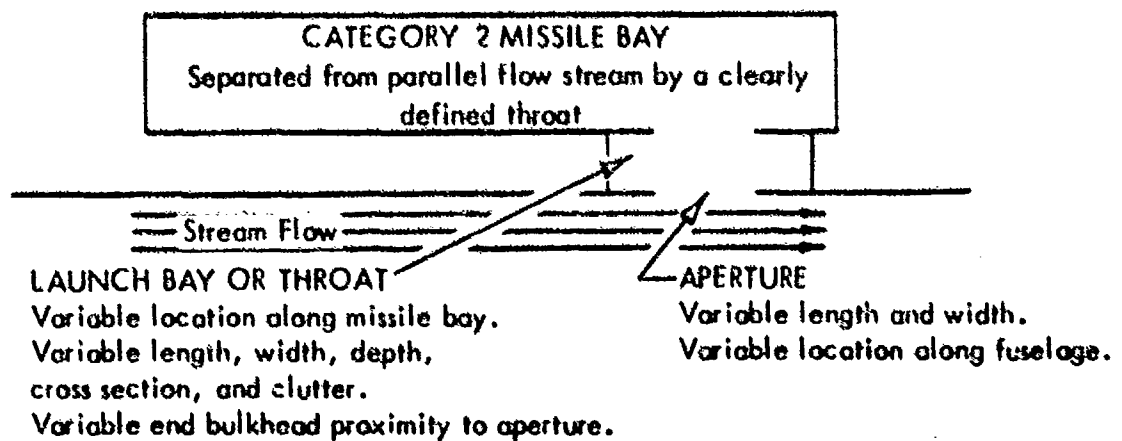
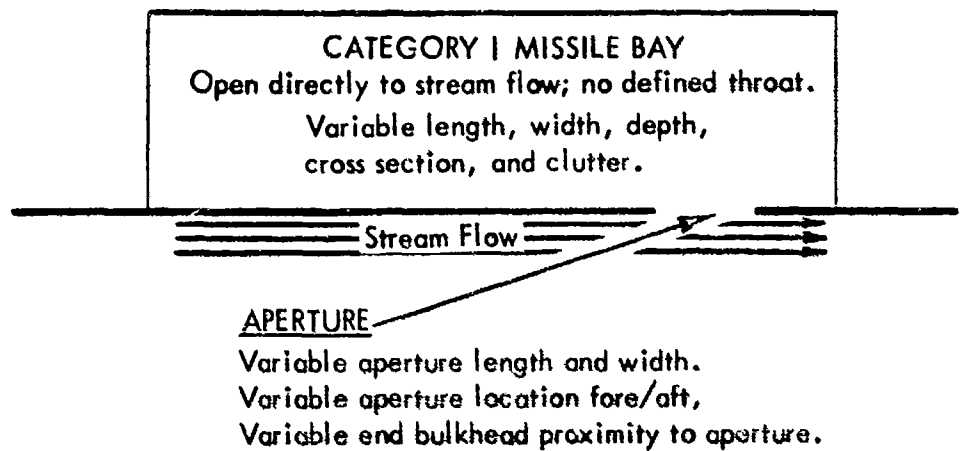
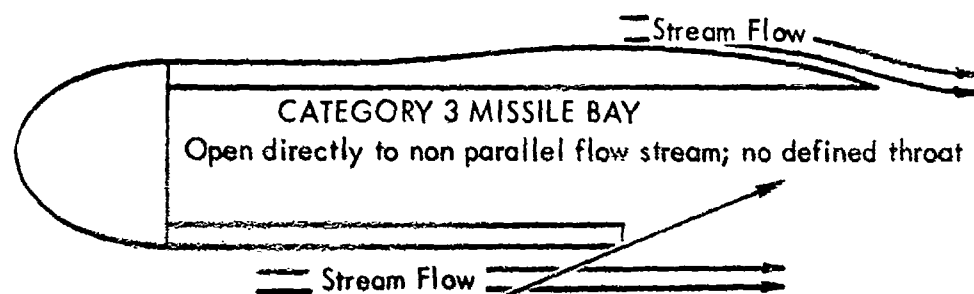
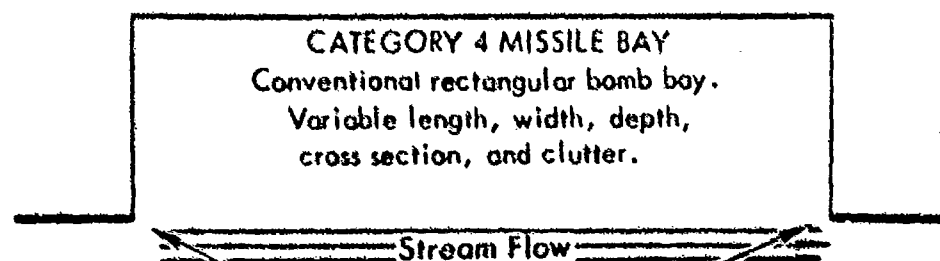


Figure 5. Generic Representation of CMCA Missile Bays



APERTURE:

Variable aperture location fore/aft.  
 Variable length, width, and cross section.  
 Variable wall thickness.  
 Variable air flow angle of incidence  
 relative to plane of opening.



APERTURE

Length and width same as missile bay.

Figure 6. Generic Representation of CMCA Missile Bays



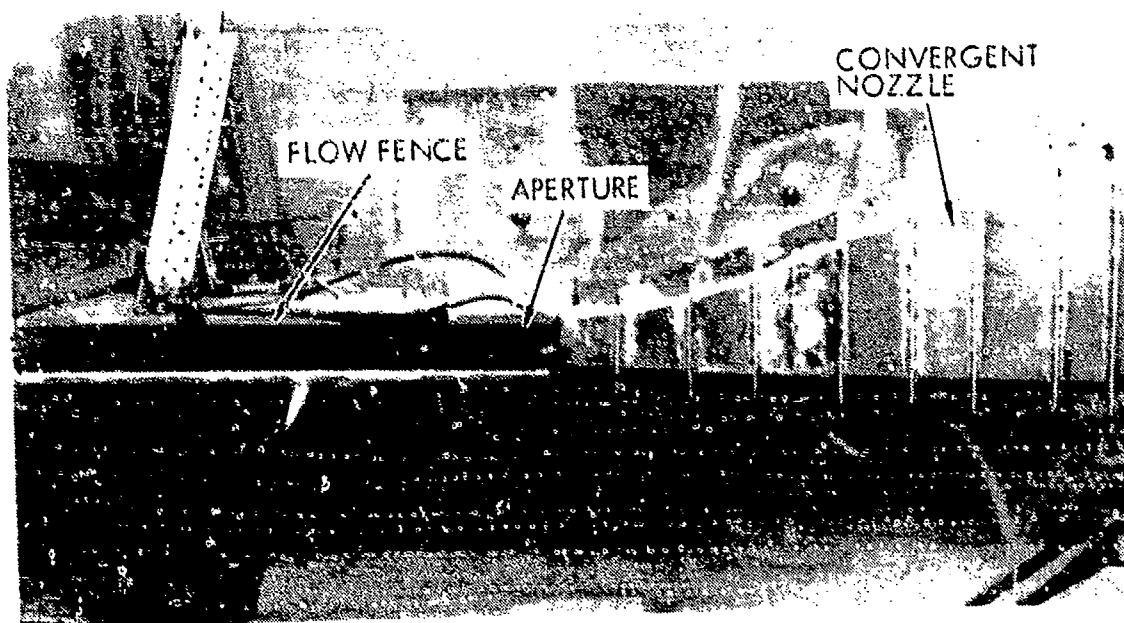
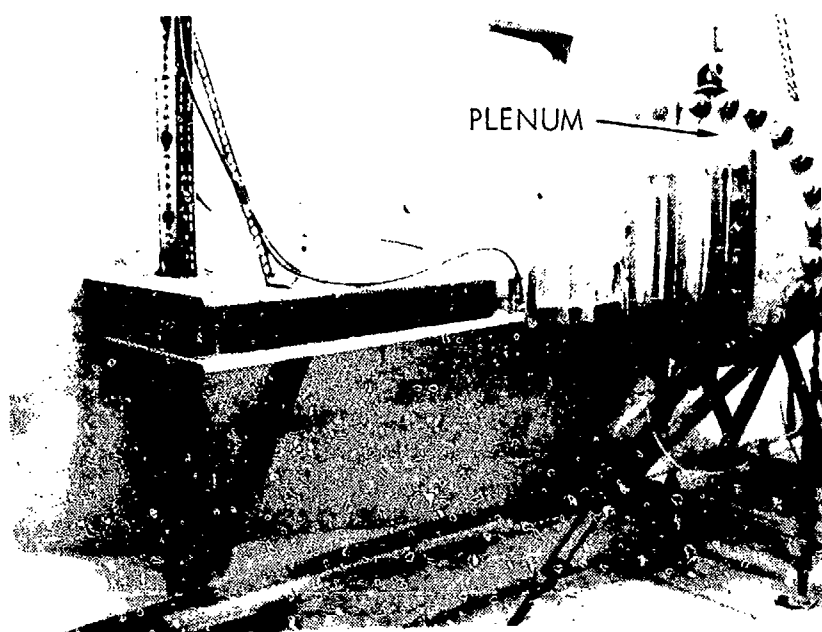


Figure 7. Wall Jet Flow Facility

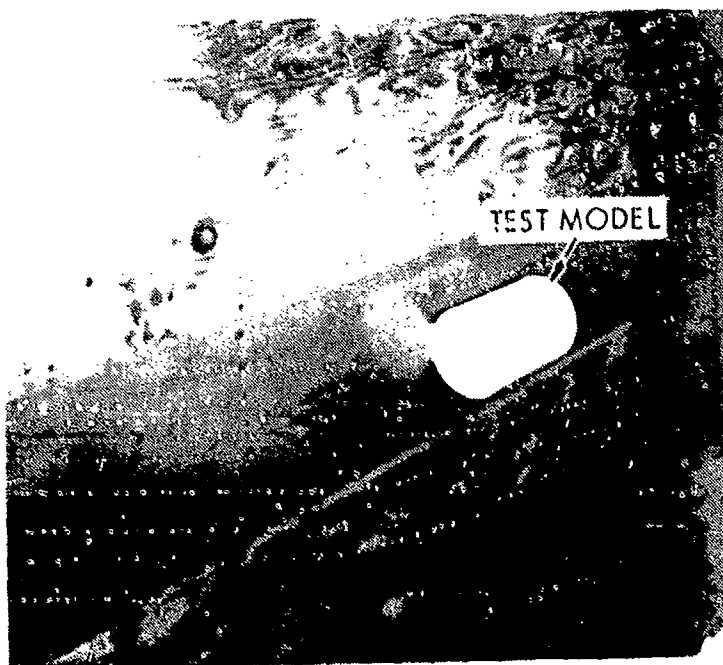
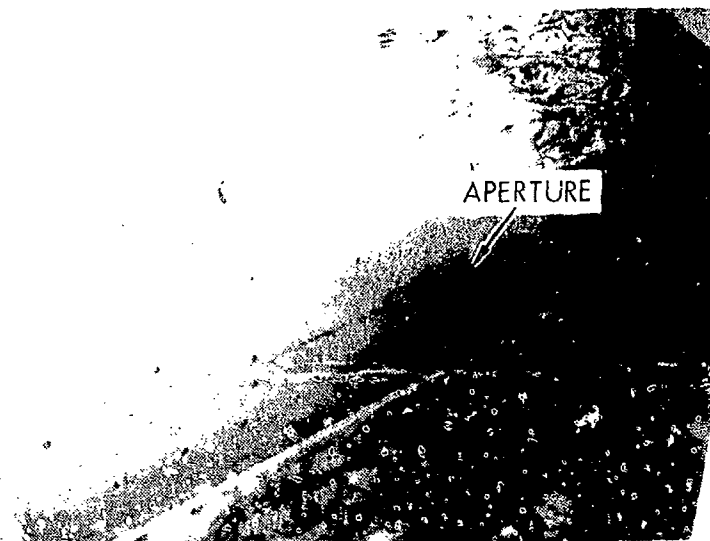


Figure 8. Aperture Viewed From Back Side of Flow Plane, and Test Model in Position.

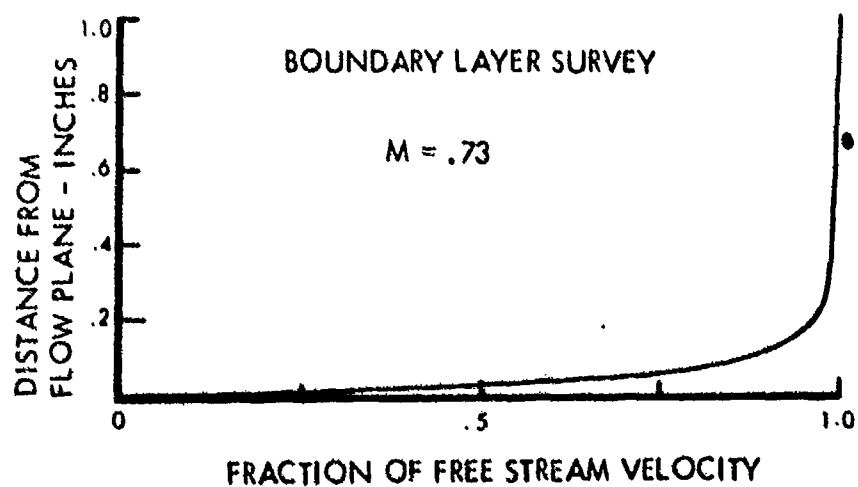
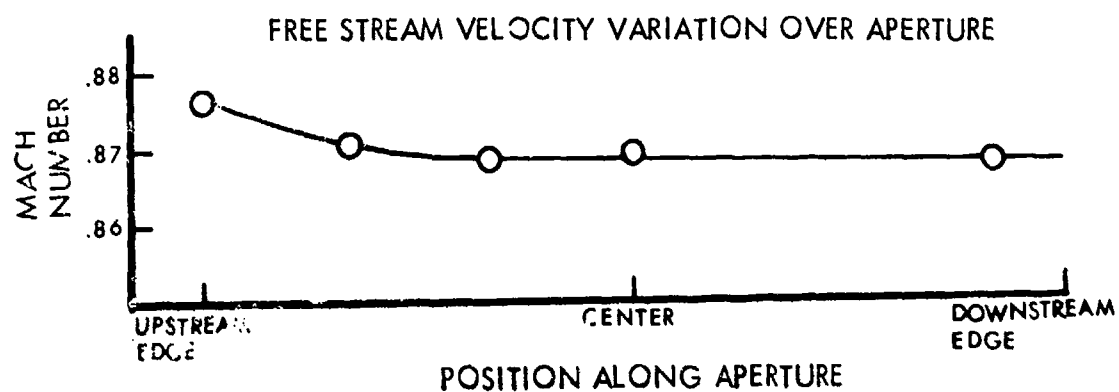


Figure 9. Test Facility Flow Conditions At The Aperture

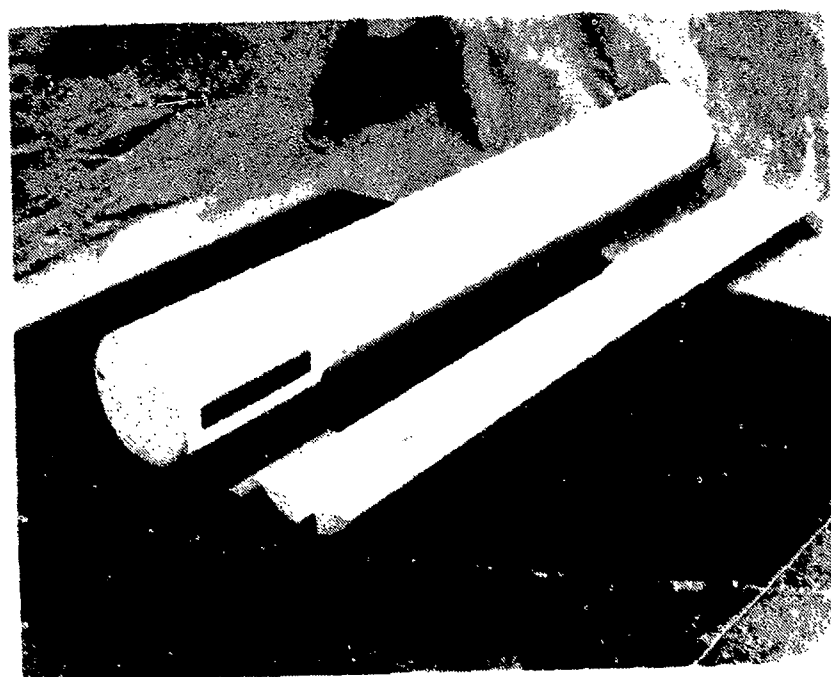
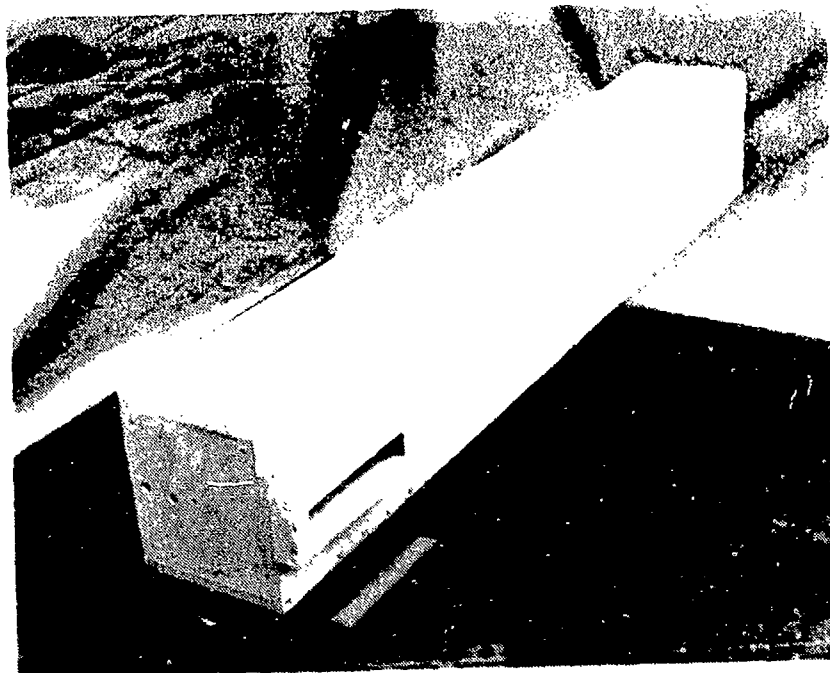


Figure 10. Representative Category 1 and Category 2 Models.

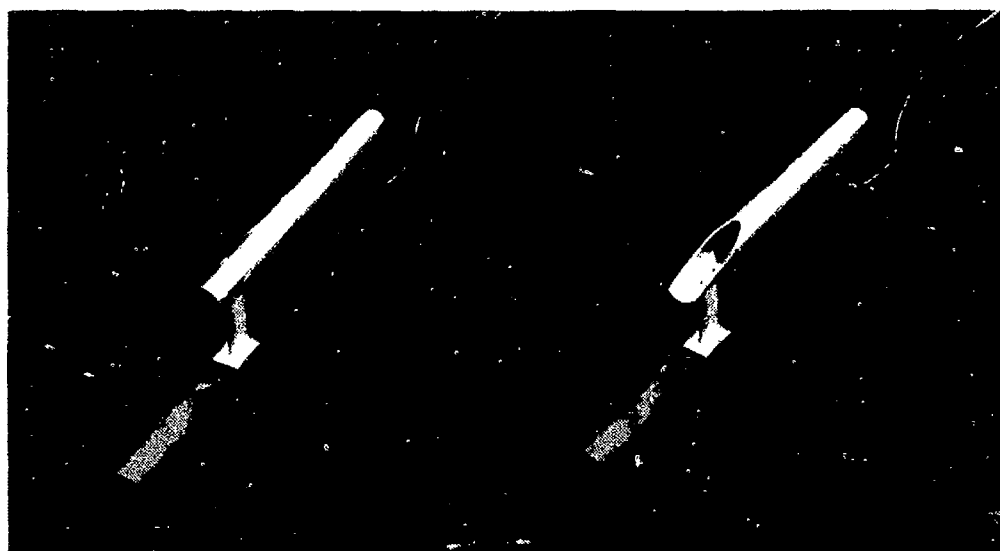


Figure 11. Category 3 Model With Two Aperture Configurations, and Installation In Flow Stream.

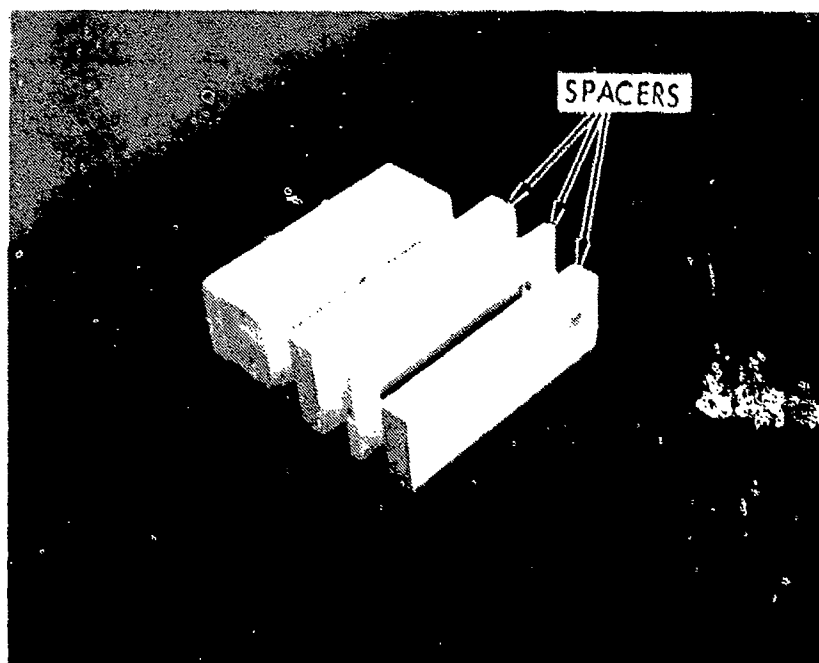


Figure 12. Category 4 Models with Spacers to Vary L/D.

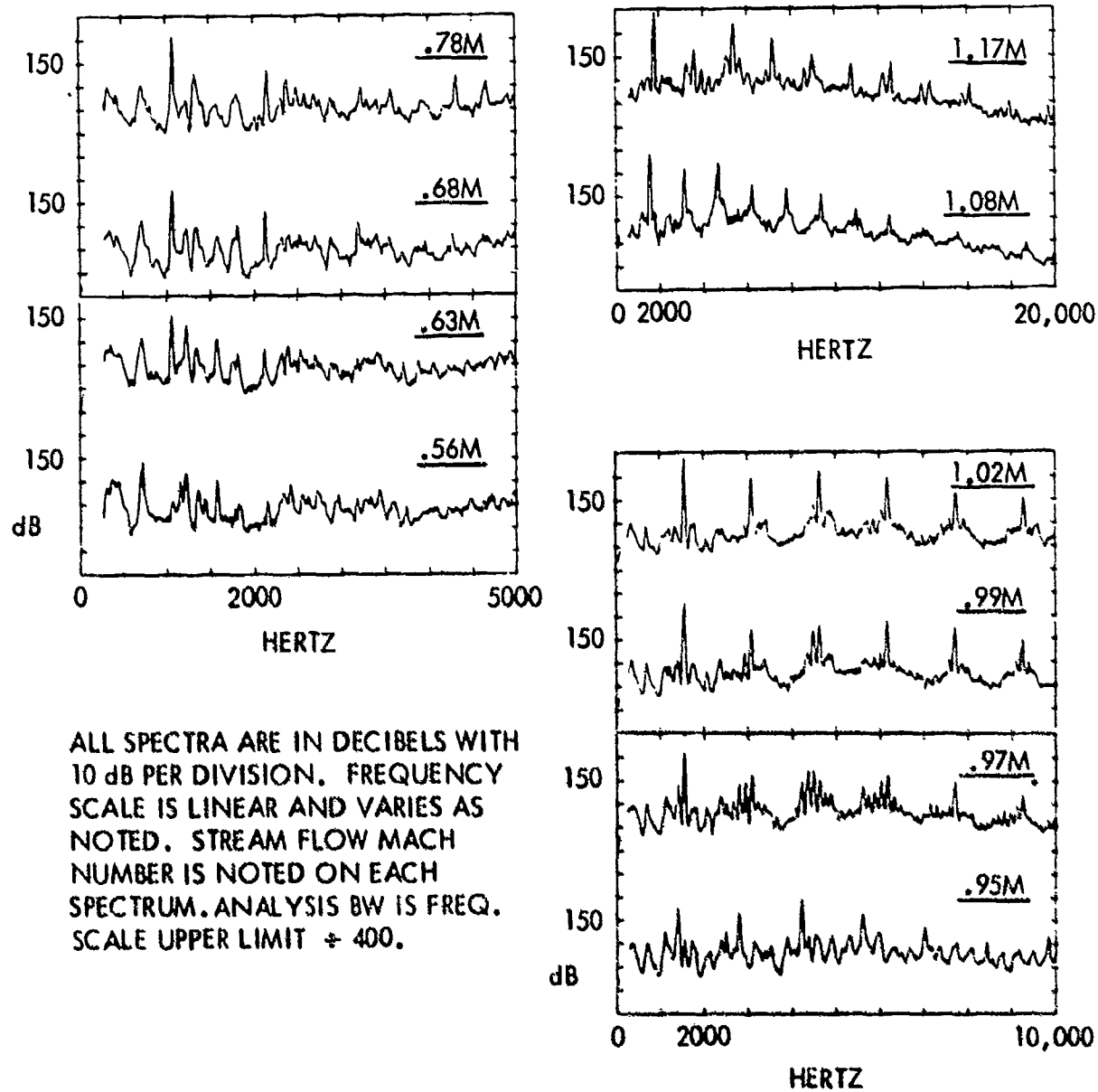


Figure 13. Response Spectra Measured at Various Flow Velocities.  
Rectangular Cavity, 18" X 5.75" X 5.75" with 0.5"  
Neck, Aperture Located at Downstream End.

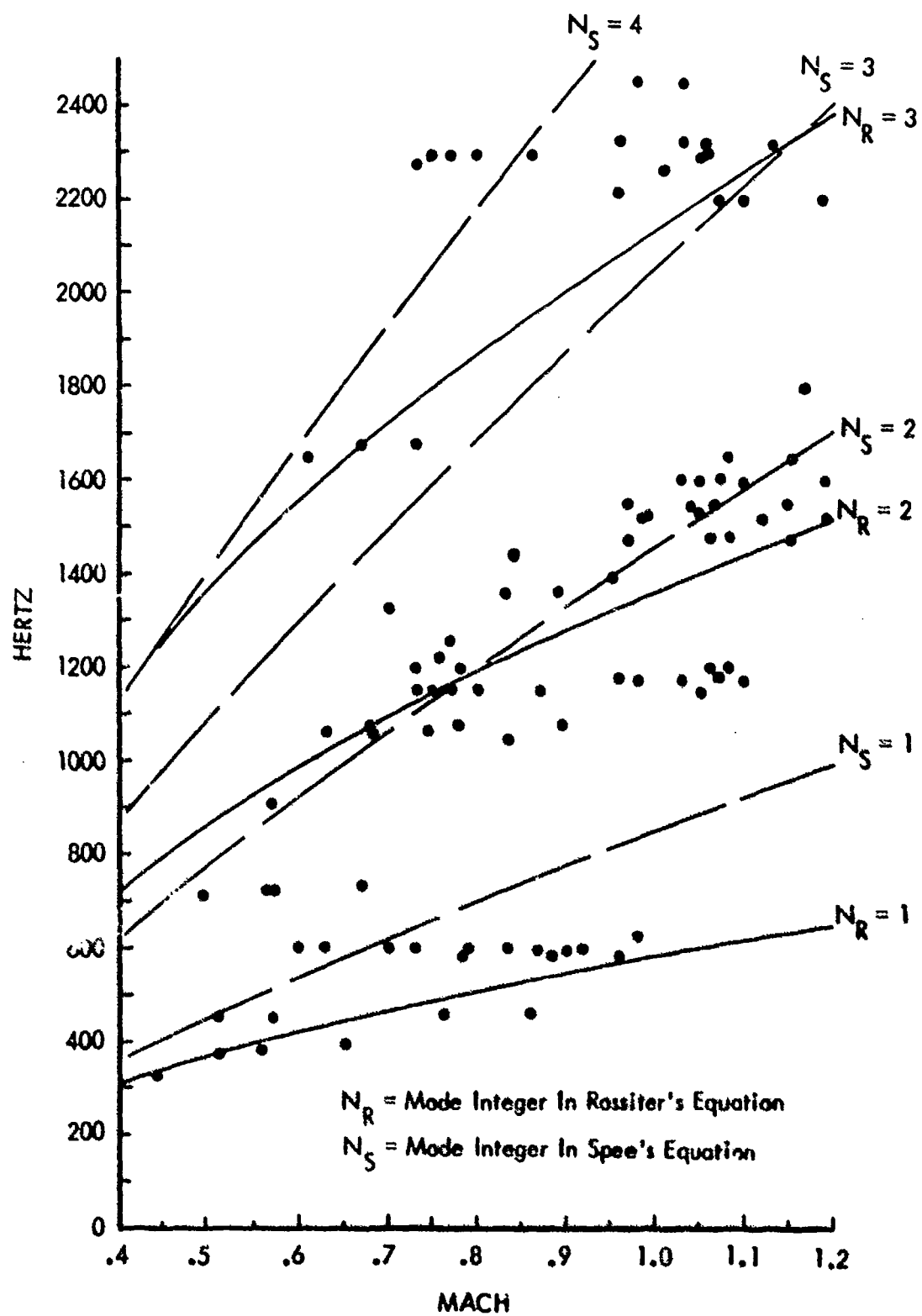


Figure 14. Frequency and Mach Number of Oscillatory Responses Exceeding 150 dB, in Six Variations of Rectangular Missile Bays.



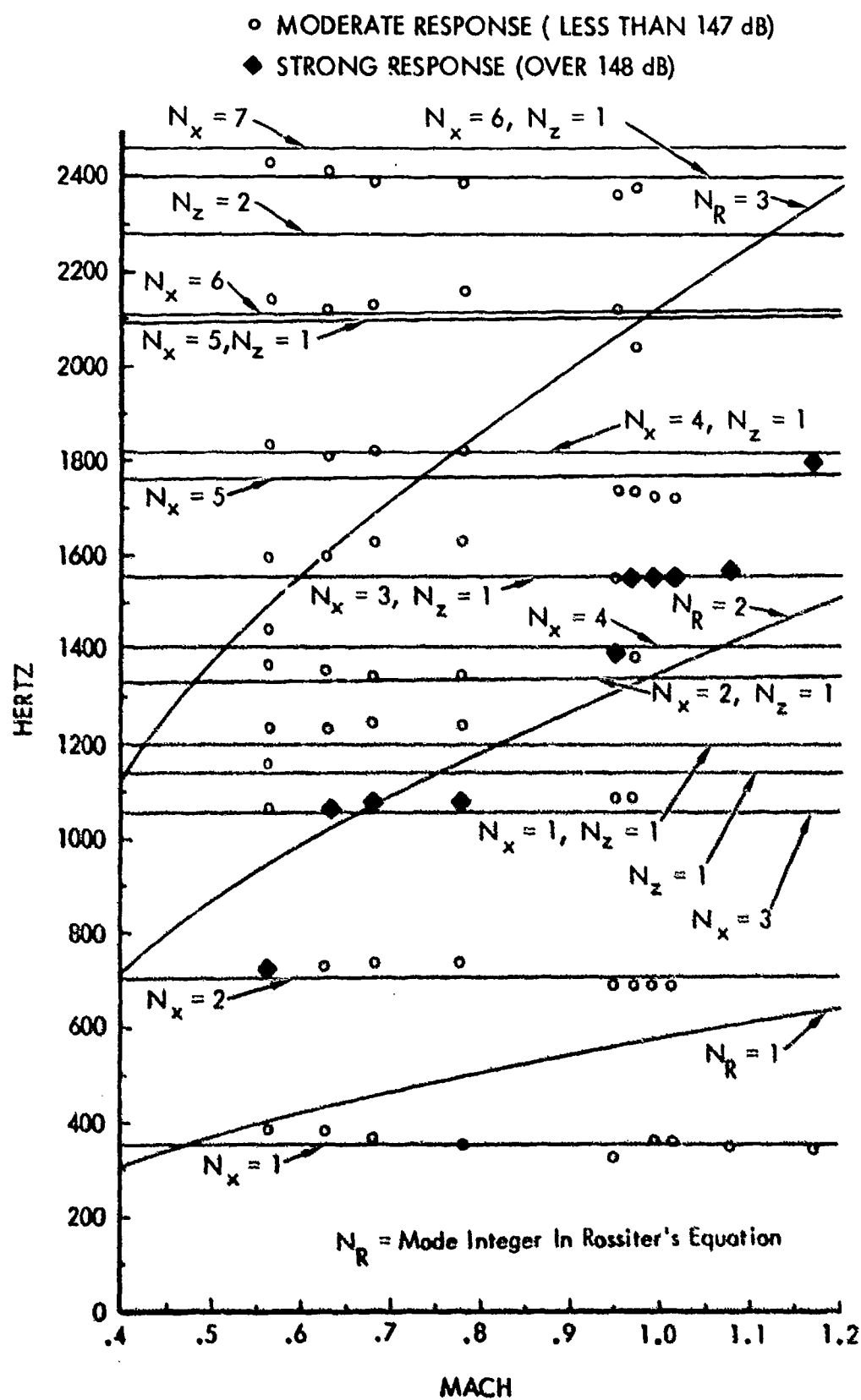


Figure 15. Frequency and Mach Number of Responses in a Rectangular  
 18" X 5.75" X 5.75" Missile Bay with a 6" Aperture And 1/2" Neck.

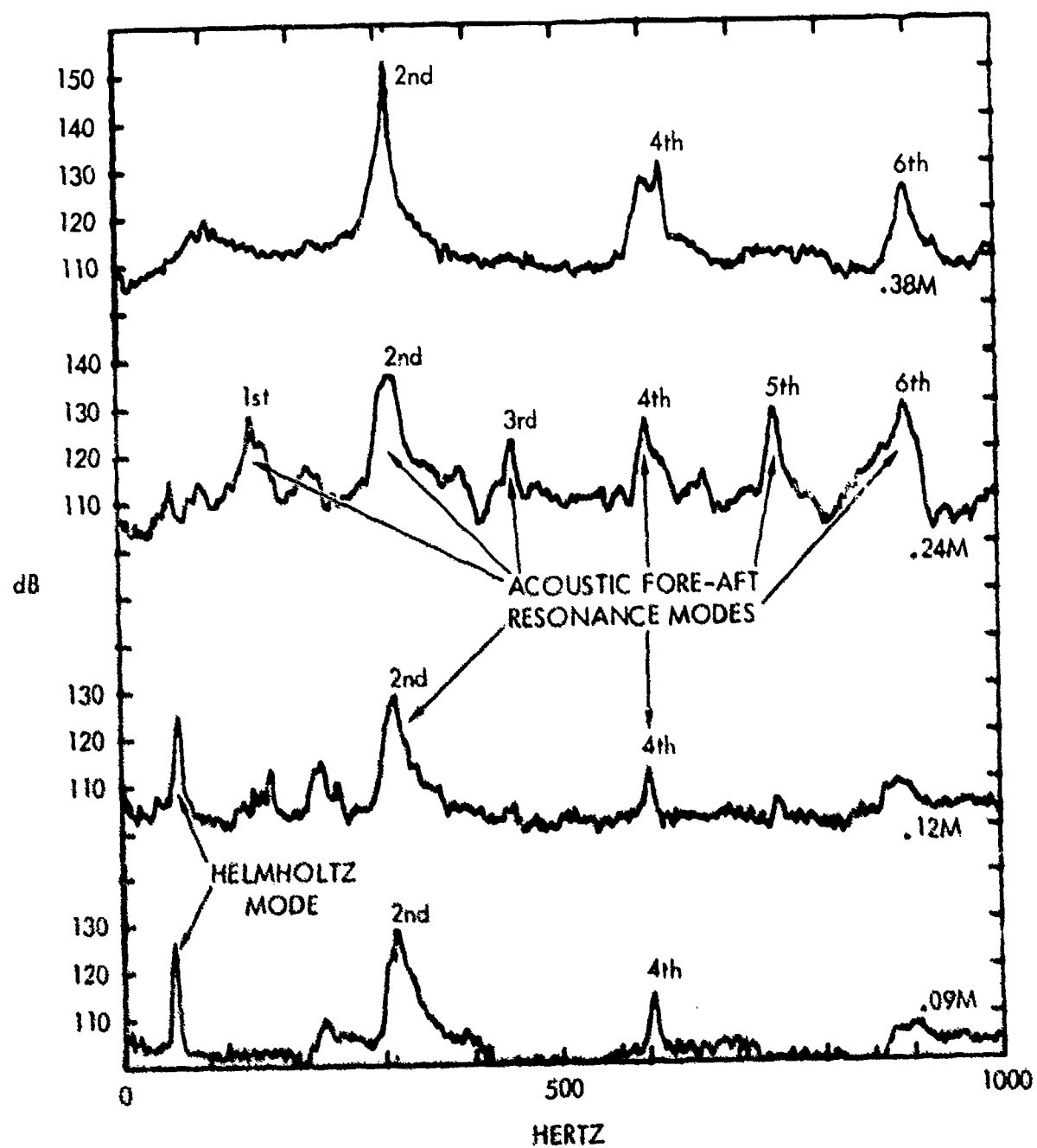


Figure 16. Helmholtz Response in a Large Missile Bay Equipped with a Neck.

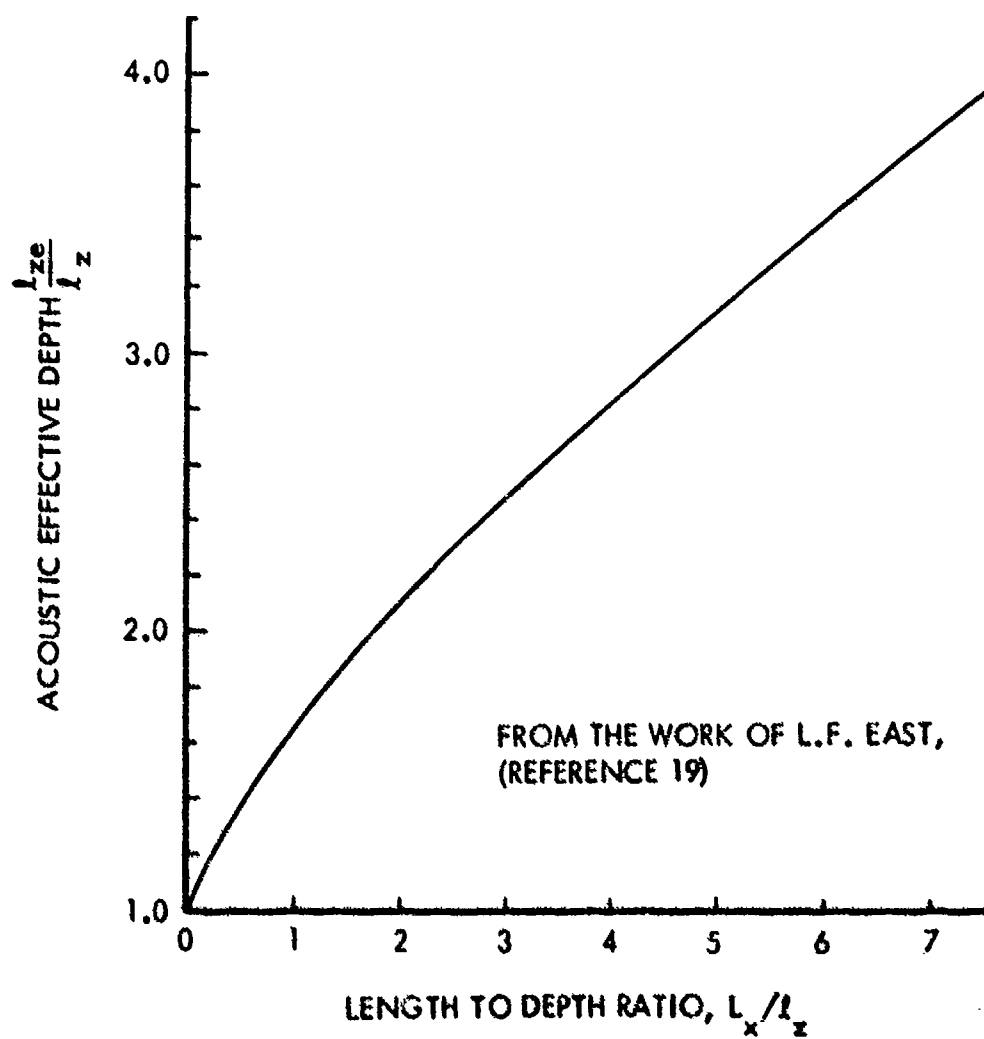


Figure 17. Cavity Depth Correction for Depthwise Acoustic Models in Conventional Bomb Bays.

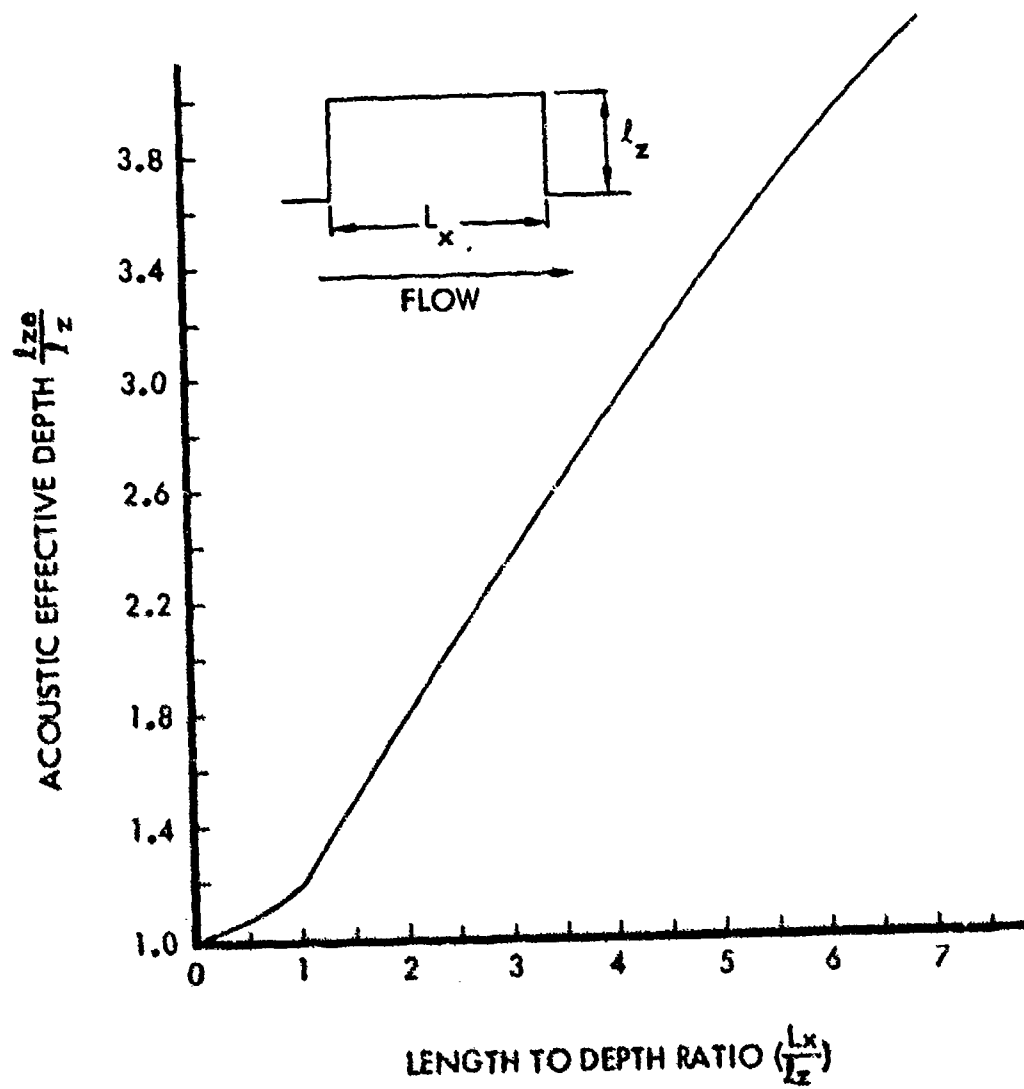
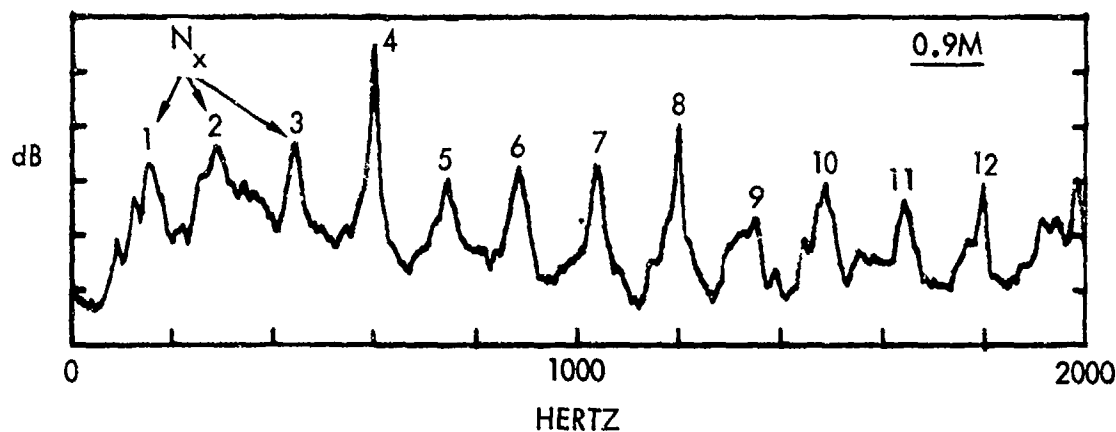


Figure 18. Cavity Depth Correction for Depthwise Acoustic Modes in Category 4 Missile Bays.

# EXPERIMENTALLY



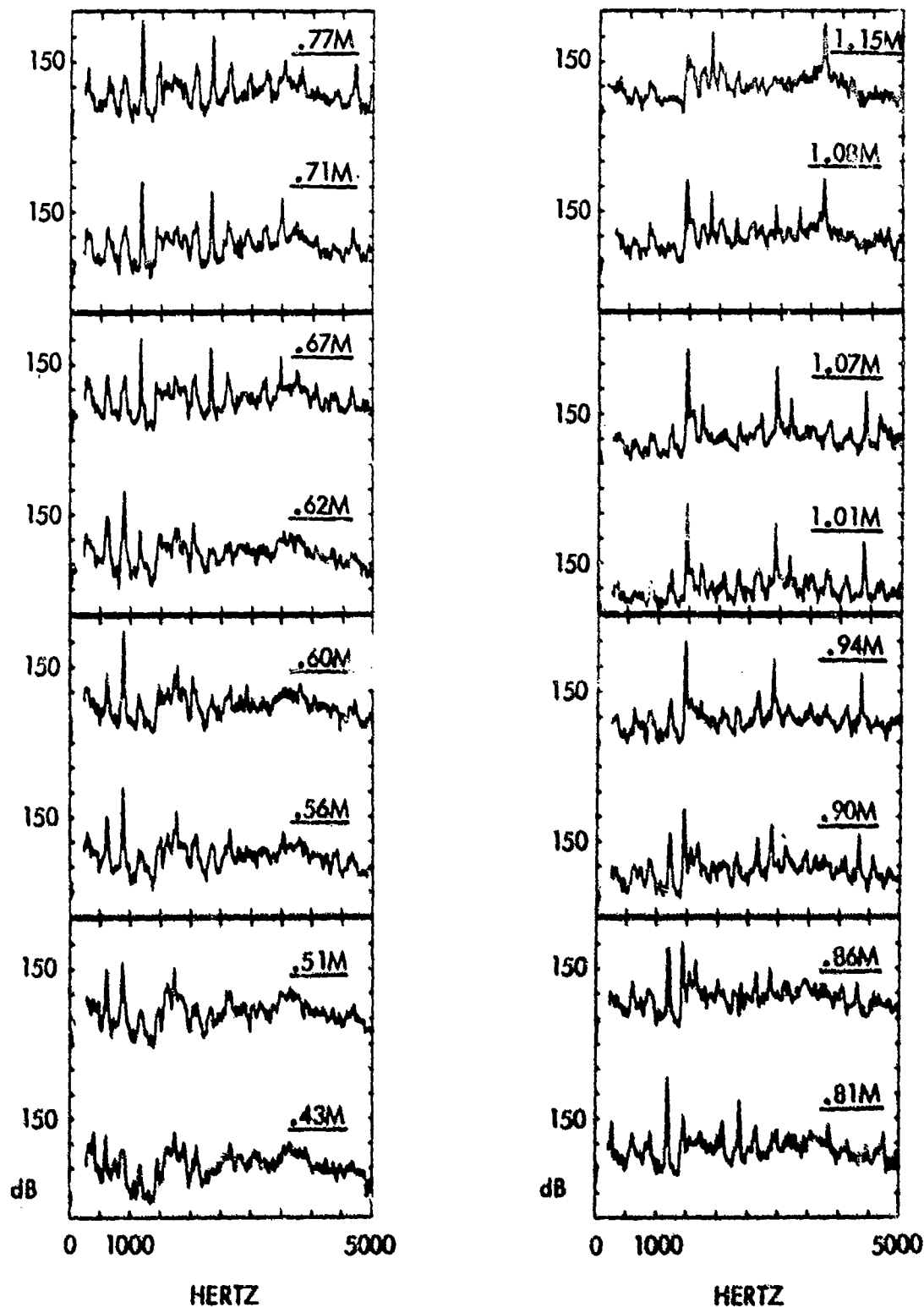
# ANALYTICALLY

$$f_x = \frac{N_x C_\infty (1 + .2M^2)^{1/2}}{2l_x}$$

# COMPARISON

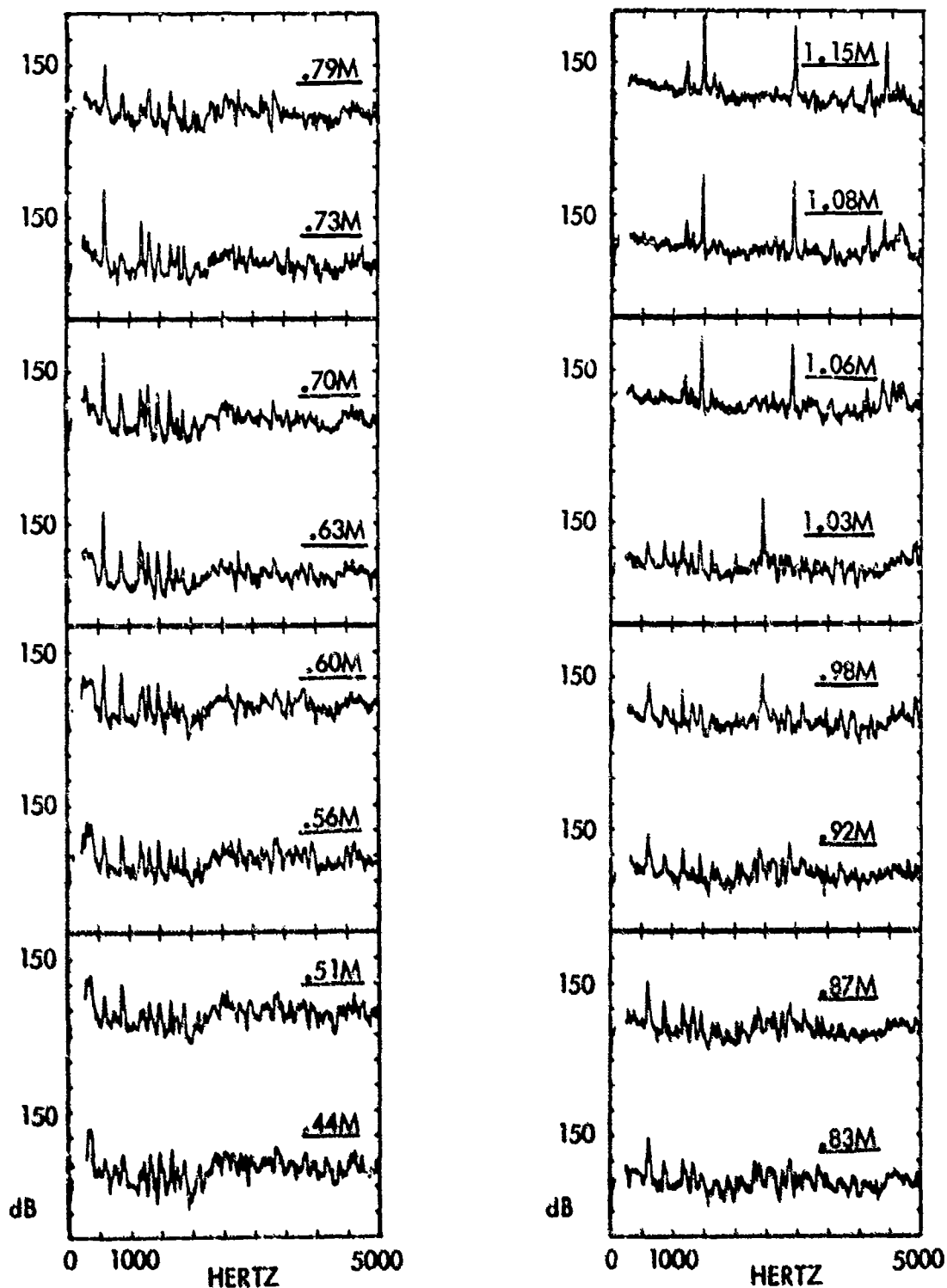
MODE ORDER ~ $N_x$	FREQUENCY HERTZ	
	EXPERIMENTAL	CALCULATED
1	154	150
2	293	299
3	440	449
4	597	598
5	747	748
6	887	898
7	1049	1047
8	1202	1197
9	1352	1346
10	1492	1496
11	1646	1646
12	1800	1795

Figure 19. Fore-Aft Acoustic Resonance Frequencies  
Calculated and Measured in a 44" Missile Bay.



NOTE: ANALYSIS BW = 12.5 HERTZ  
 ALL SPECTRA ARE IN DECIBELS, 10dB PER DIVISION. THE FREQUENCY SCALE IS LINEAR, 0 TO 5000 HERTZ IN ALL CASES. FLOW MACH NUMBER IS NOTED ON EACH SPECTRUM.

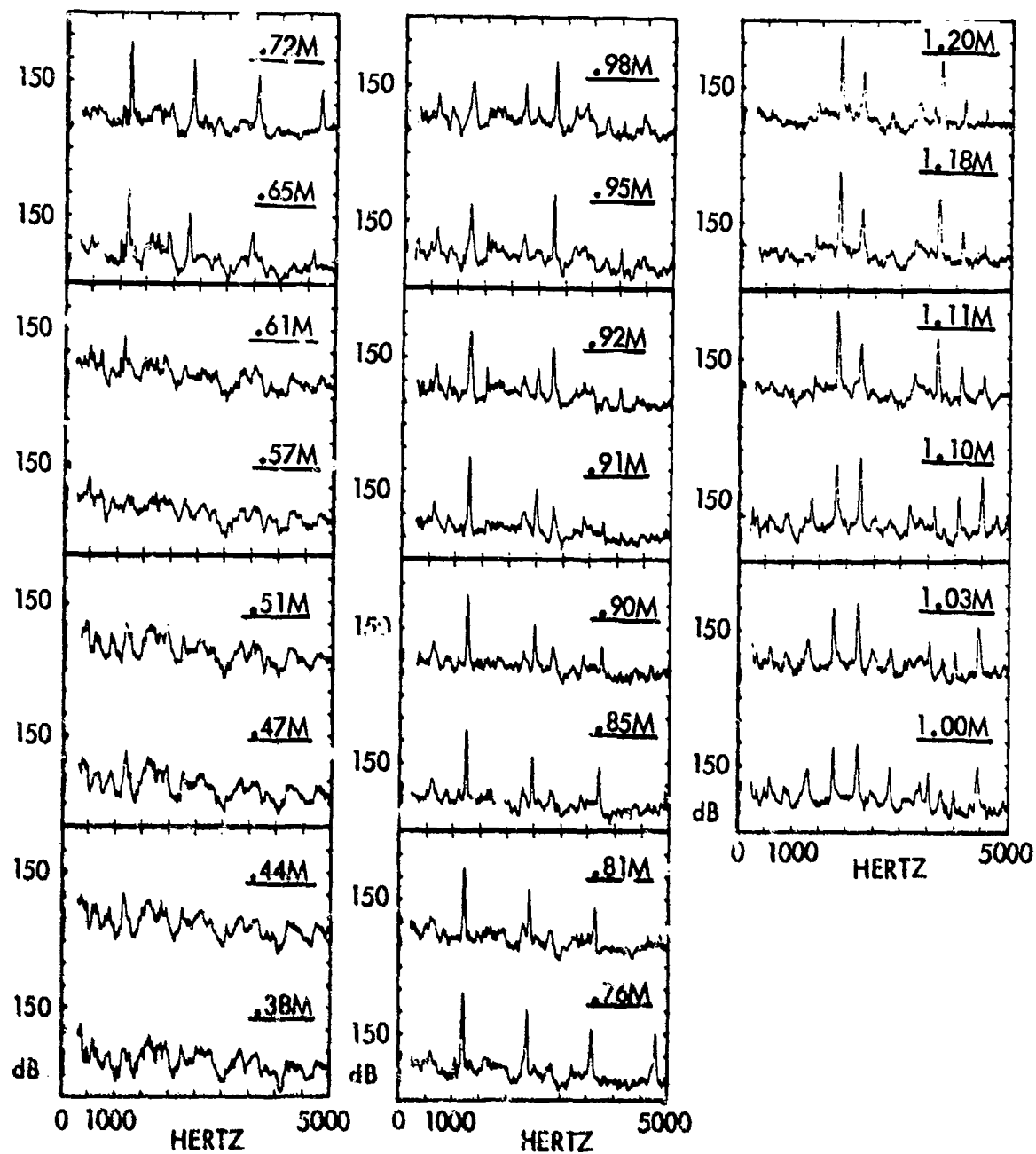
Figure 20. CMCA Case 1 Response Test Spectra, Cylindrical Missile Bay 23.2" X 5.4" D.



**NOTE:**

ALL SPECTRA ARE IN DECIBELS, 10 dB PER DIVISION. THE FREQUENCY SCALE IS LINEAR, 0 TO 5000 HERTZ IN ALL CASES. FLOW MACH NUMBER IS NOTED ON EACH SPECTRUM. BW = 12.5 HERTZ

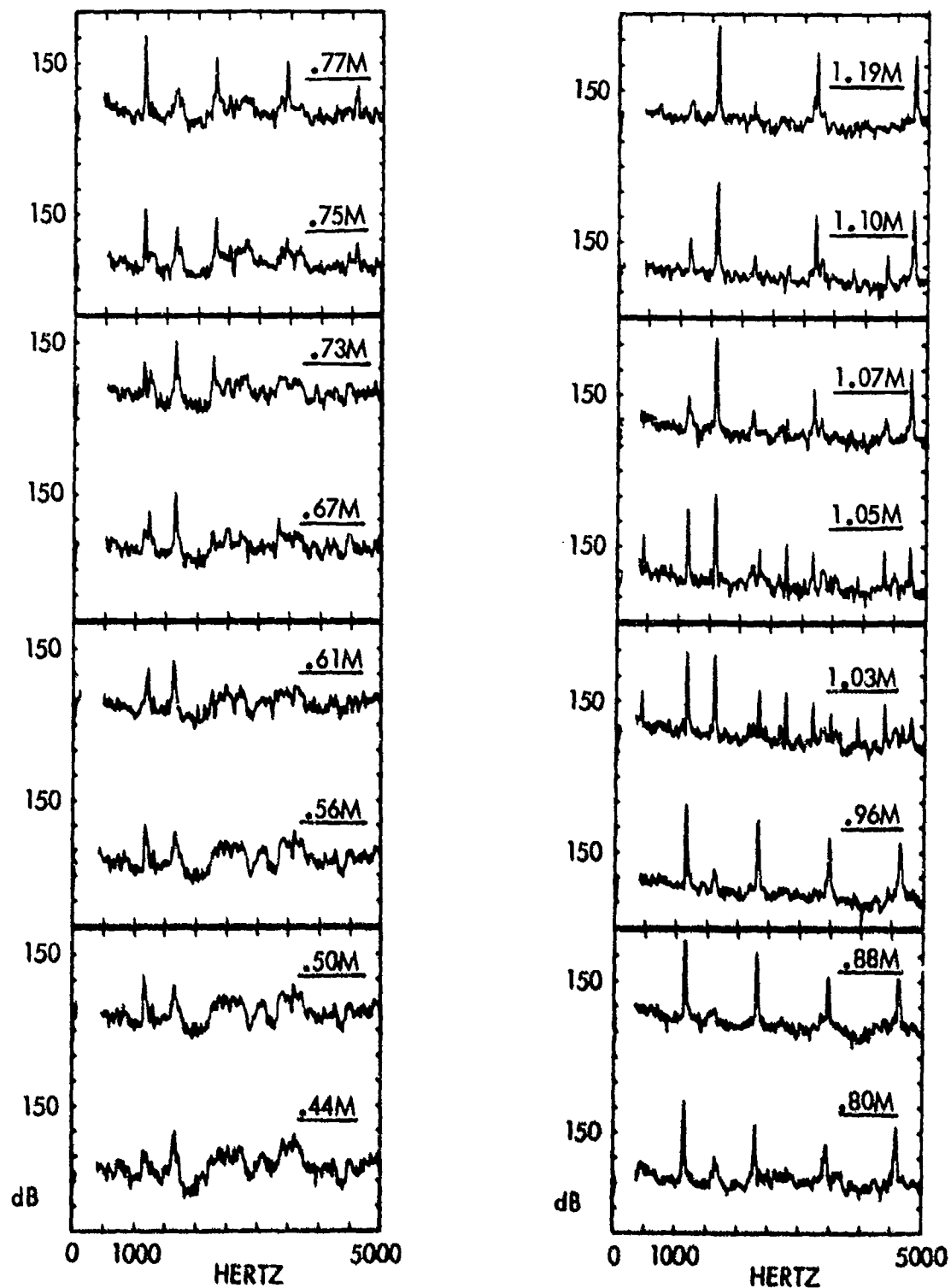
Figure 21. CMCA Case 2 Response Test Spectra Rectangular Missile Bay 23.2 X 5.75" X 5.75".



NOTE: ANALYSIS BANDWIDTH IS 12.5 HERTZ  
 ALL SPECTRA ARE IN DECIBELS, 10 dB PER DIVISION. THE  
 FREQUENCY SCALE IS LINEAR, 0 TO 5000 HERTZ IN ALL  
 CASES. FLOW MACH NUMBER IS NOTED ON EACH SPECTRUM.

Figure 22. CMCA Case 3 Response Test Spectra.  
 Cylindrical Missile Bay 6" X 5.4" D.





NOTE: ANALYSIS BANDWIDTH IS 12.5 HERTZ  
 ALL SPECTRA ARE IN DECIBELS, 10 dB PER DIVISION. THE  
 FREQUENCY SCALE IS LINEAR, 0 TO 5000 HERTZ IN ALL  
 CASES. FLOW MACH NUMBER IS NOTED ON EACH SPECTRUM.

Figure 23. CMCA Case 4 Response Test Spectra.  
 Rectangular Missile Bay 6" X 5.75" X 5.75".

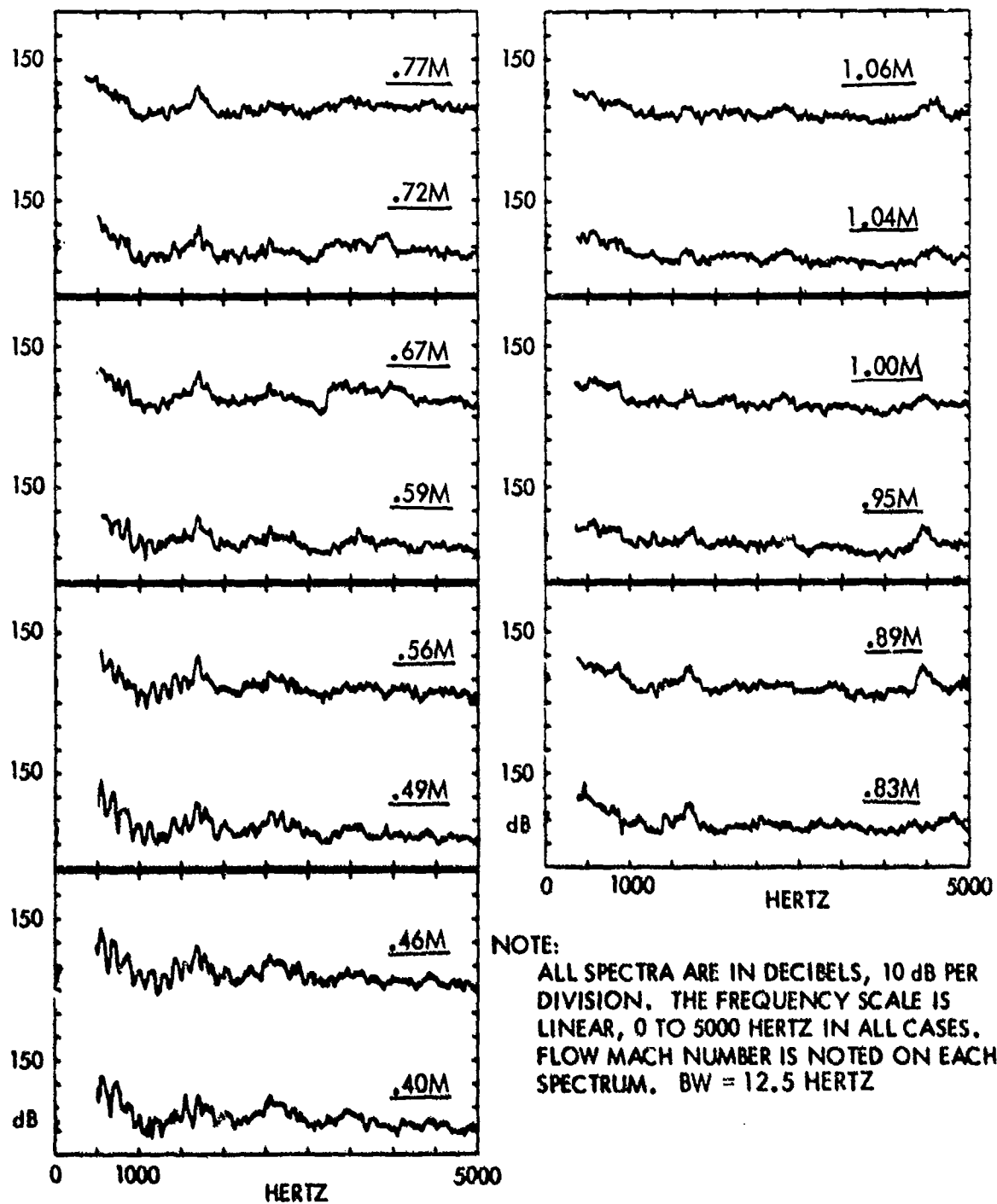
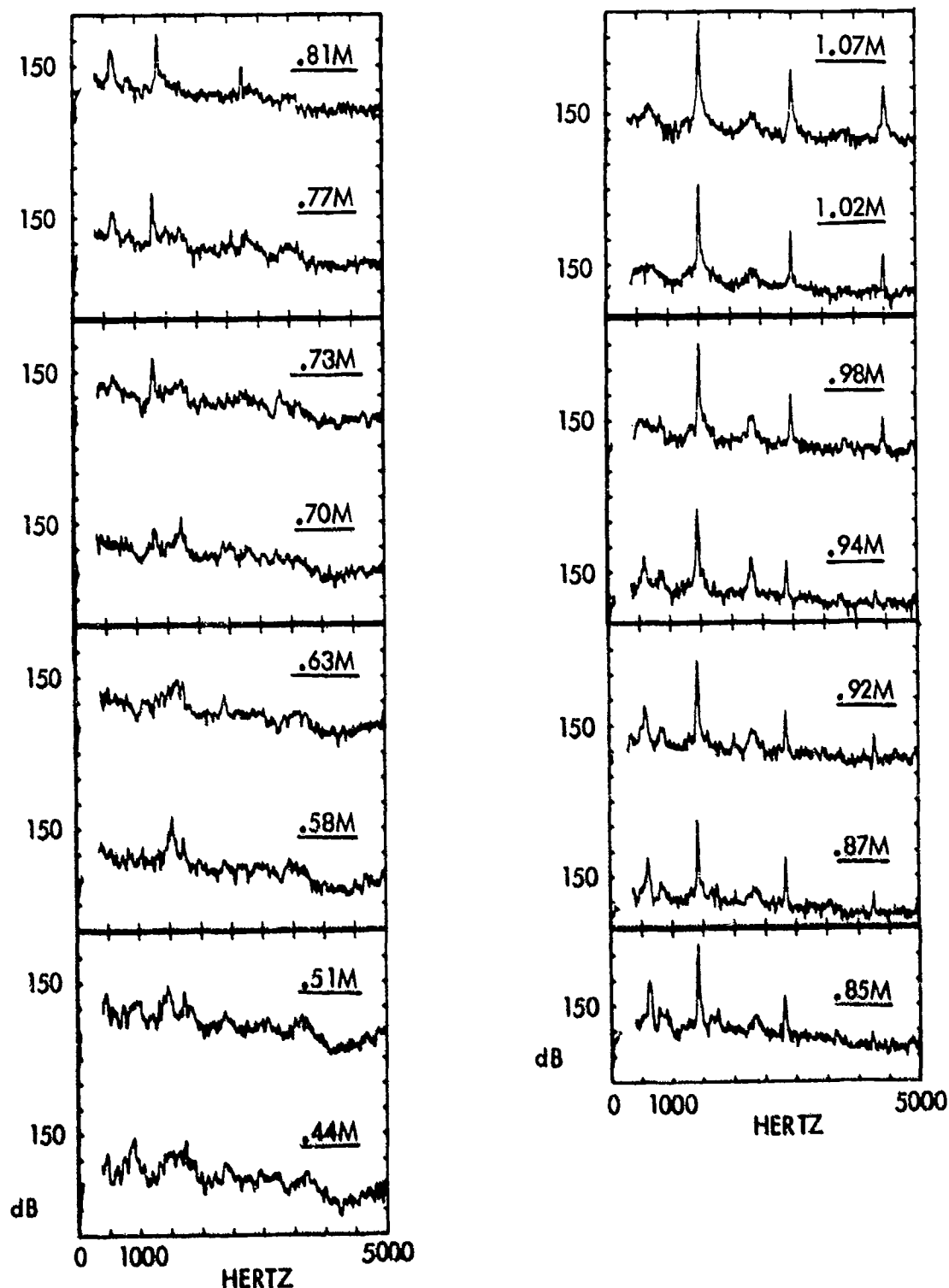


Figure 24. CMCA Case 5 Response Test Spectra.  
Cylindrical Missile Bay, 7" X .85" D. Aft Launch.



**NOTE.**

ALL SPECTRA ARE IN DECIBELS, 10 dB PER DIVISION. THE FREQUENCY SCALE IS LINEAR, 0 TO 5000 HERTZ IN ALL CASES. FLOW MACH NUMBER IS NOTED ON EACH SPECTRUM. ANALYSIS BANDWIDTH IS 12.5 HERTZ

Figure 25. CMCA Case 6 Response Test Spectra.  
Conventional Bomb Bay, 6" Aperture, 3" Depth.

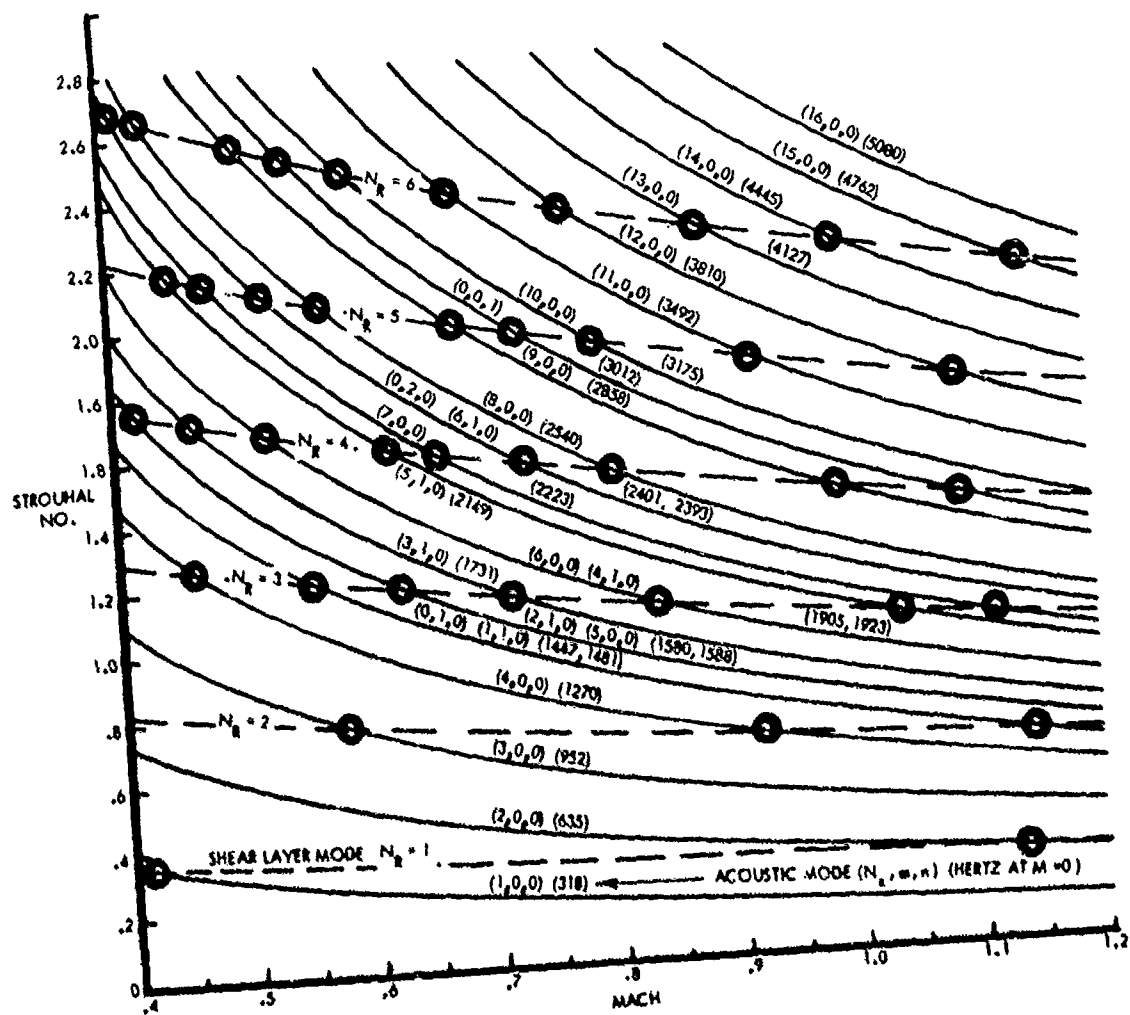


Figure 26. Computed Shear Layer and Acoustic Modes. Cylindrical Missile Bay, 21" x 5.4"D, With 6" Aperture.

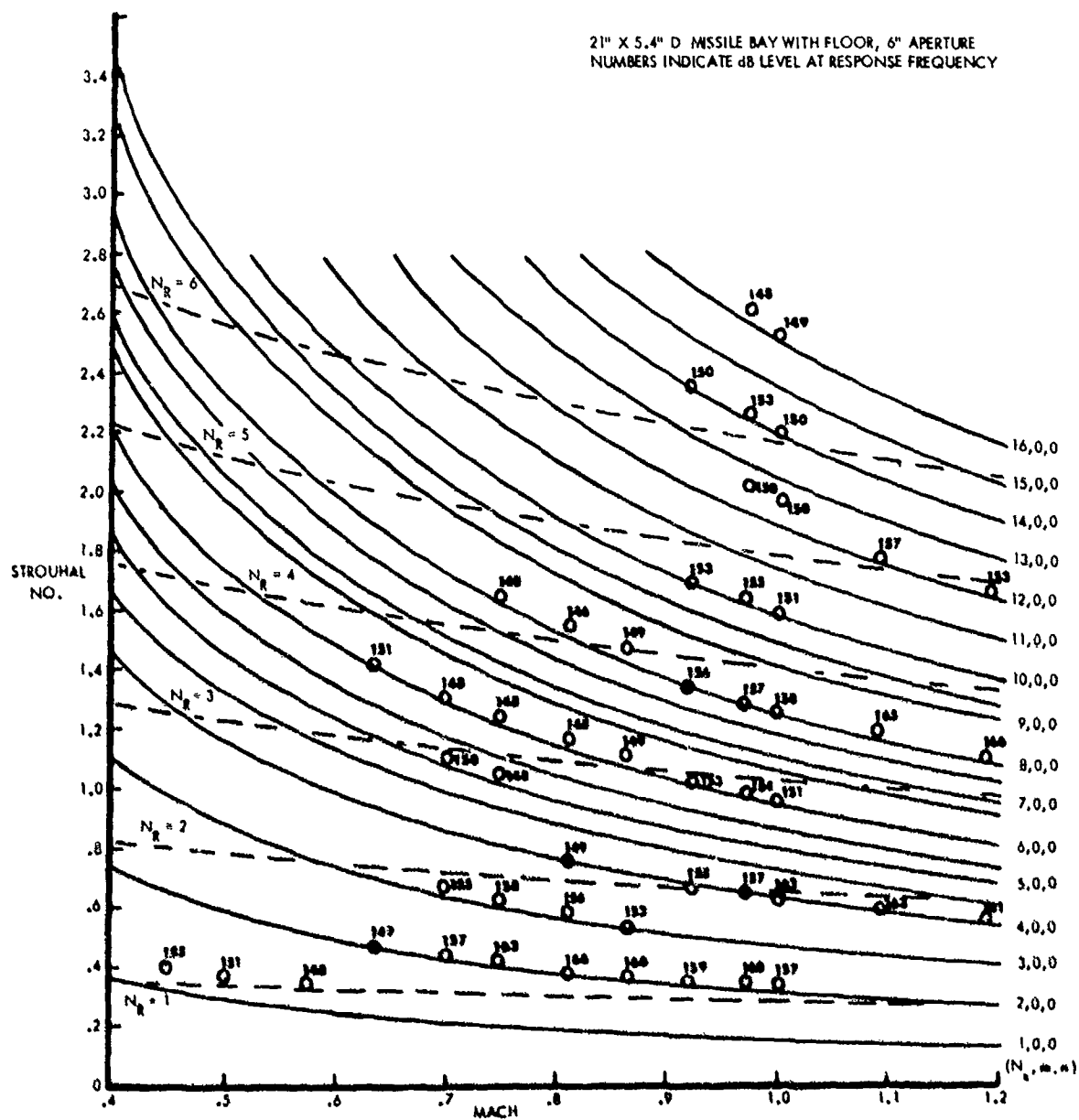


Figure 27. Cavity Oscillations Measured in a Cylindrical Missile Bay with Floor.

21" X 5.4" D MISSILE BAY WITHOUT FLOOR, 6" APERTURE  
NUMBERS INDICATE dB LEVEL AT RESPONSE FREQUENCY.

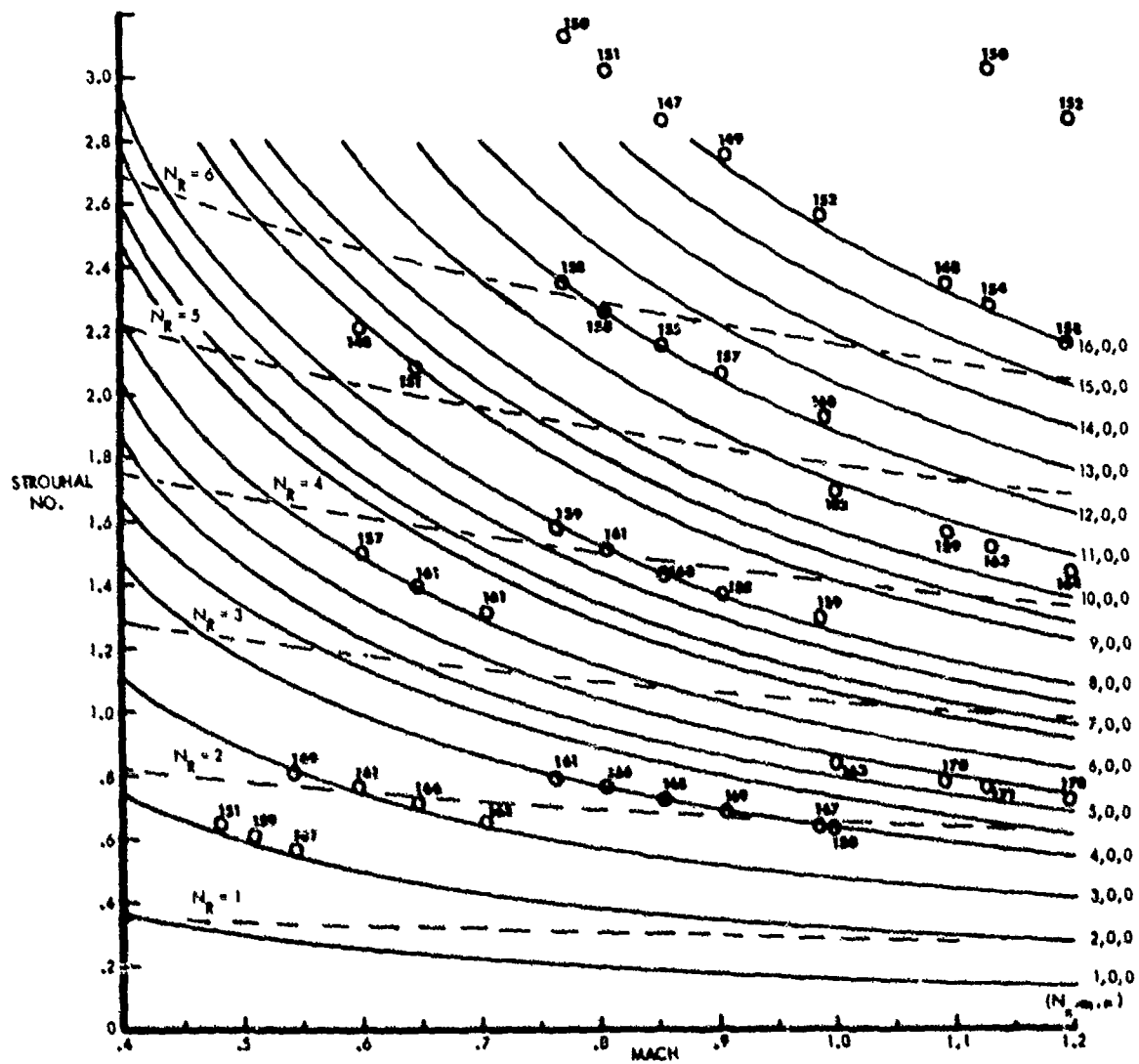


Figure 28. Cavity Oscillations Measured in a Cylindrical Missile Bay, No Floor.

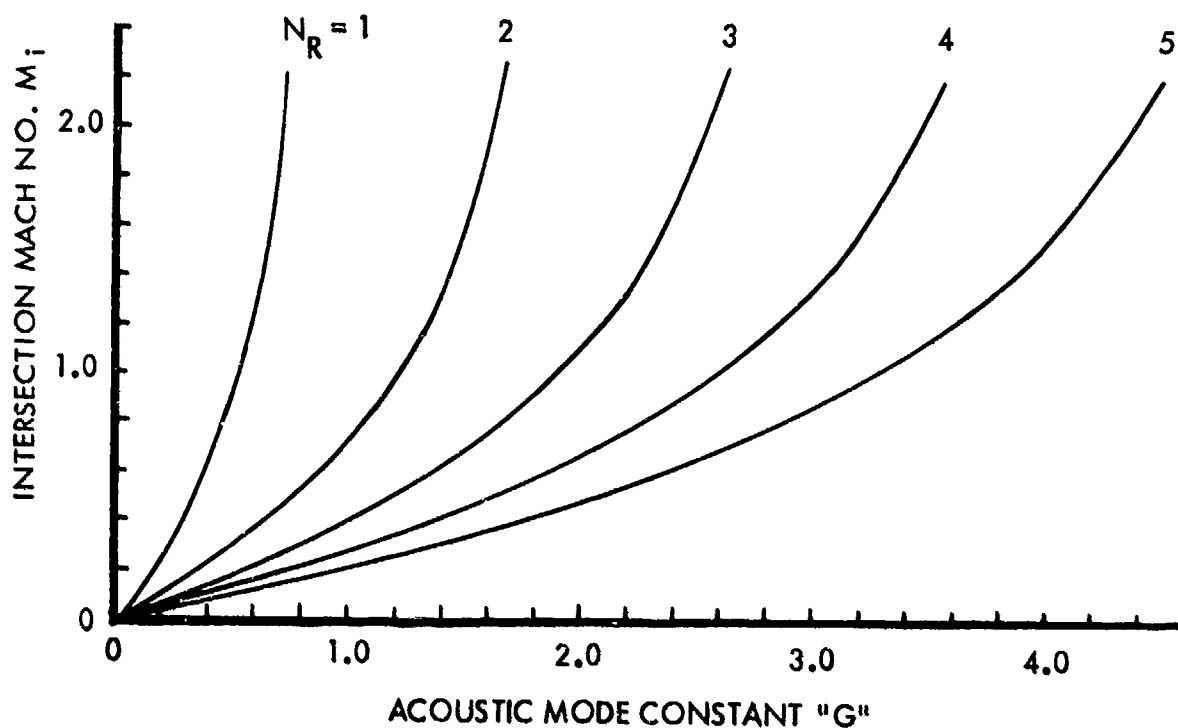


Figure 29. Mach Number ( $M_i$ ) at Which the Strouhal Curves for Acoustic Modes and Shear Layer Modes Intersect.

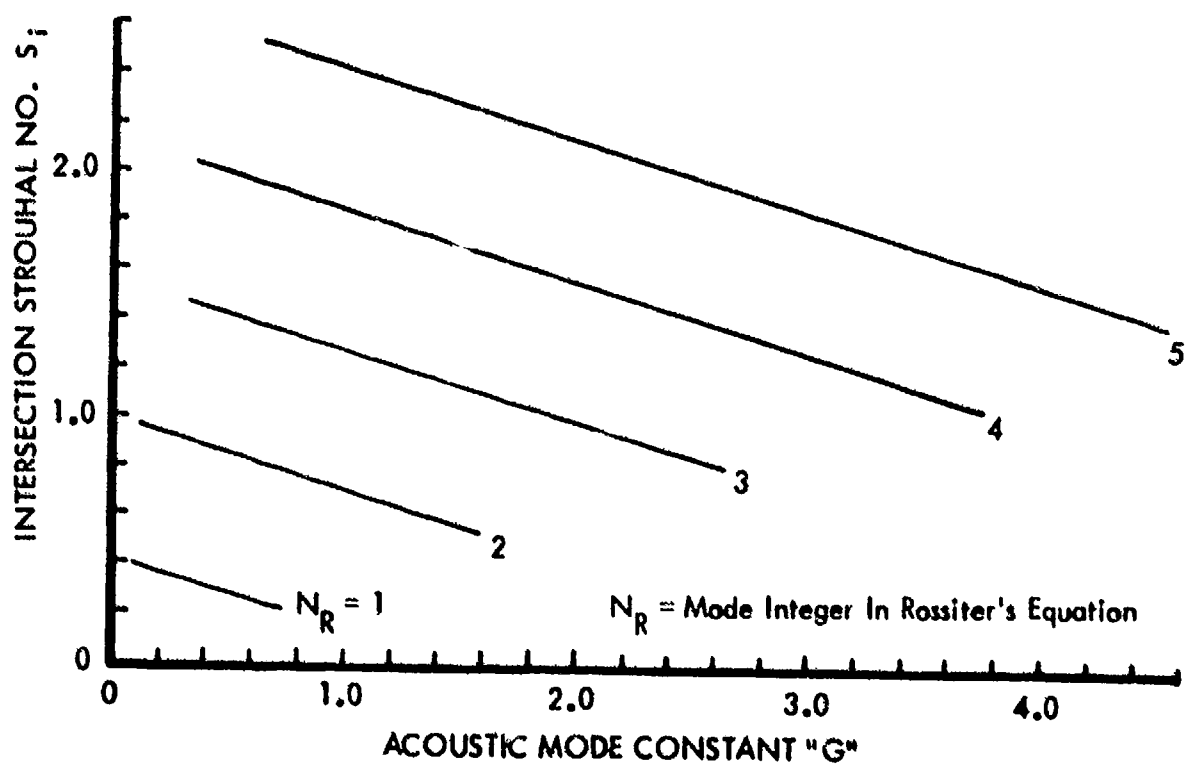


Figure 30. Strouhal Number ( $S_i$ ) at Which the Strouhal Curves For Acoustic Modes and Shear Layer Modes Intersect.

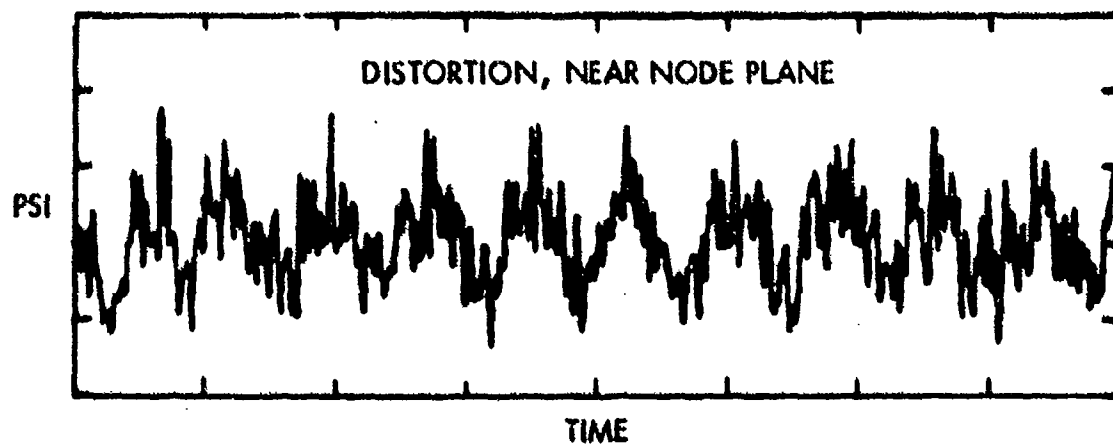
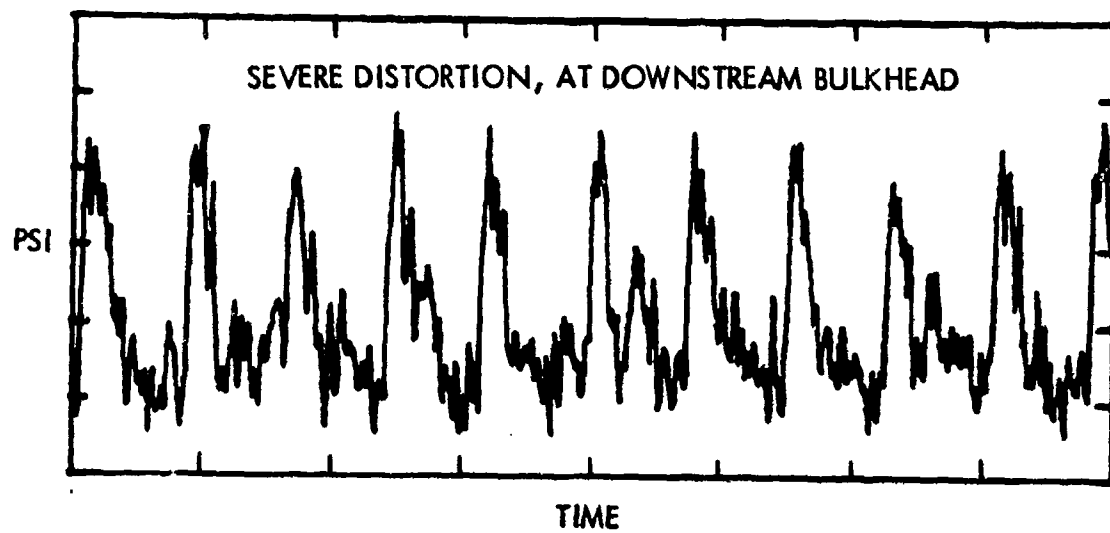
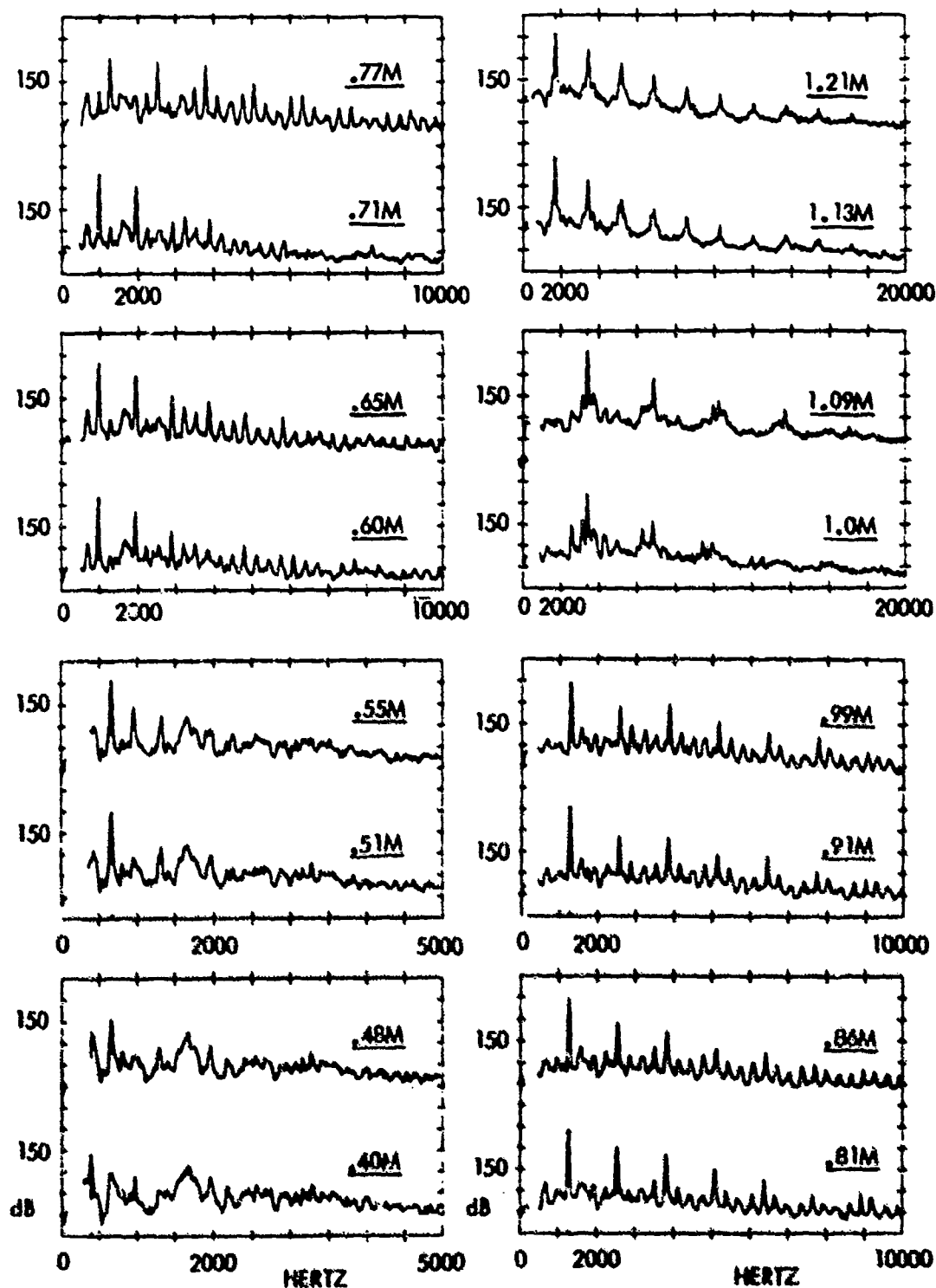


Figure 31. Example of Oscillatory Sound Pressure Wave Distortion.





NOTE: ANALYSIS BW IS FREQUENCY SCALE UPPER LIMIT  $\div$  400.  
 ALL SPECTRA ARE IN DECIBELS, 10 dB PER DIVISION. FREQUENCY SCALE IS LINEAR  
 AND VARIES AS NOTED. FLOW MACH NUMBER IS NOTED ON EACH SPECTRUM.

Figure 32. Response Spectra Measured in a Cylindrical Missile Bay,  
 21" x 5.4" D, No Floor, 6" Aperture at Downstream End.

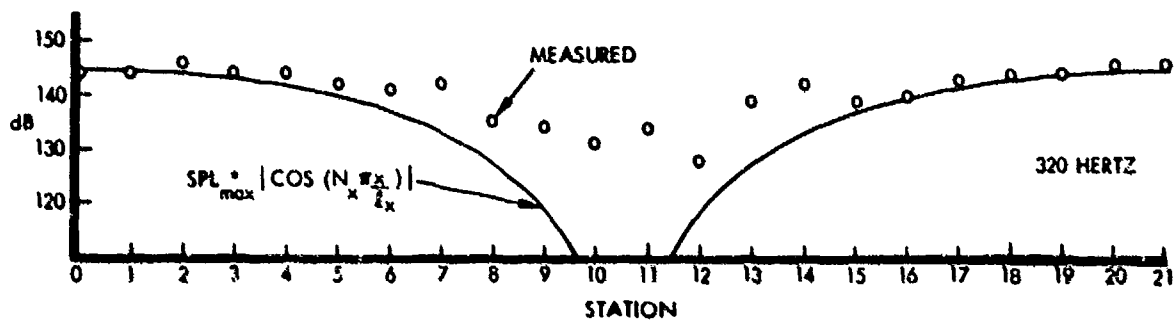
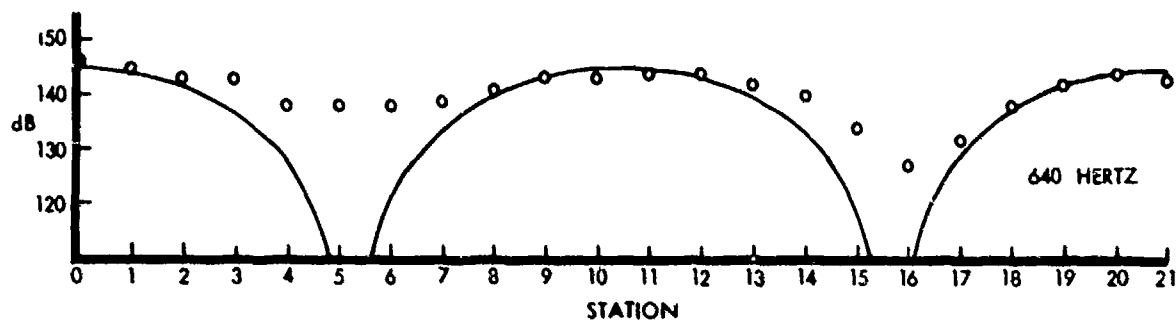


Figure 33. SPL Spatial Variation Fore-Aft in 21" x 5.4" D. Cylindrical Missile Bay, At Mach 0.81, 320 and 640 Hertz Modes

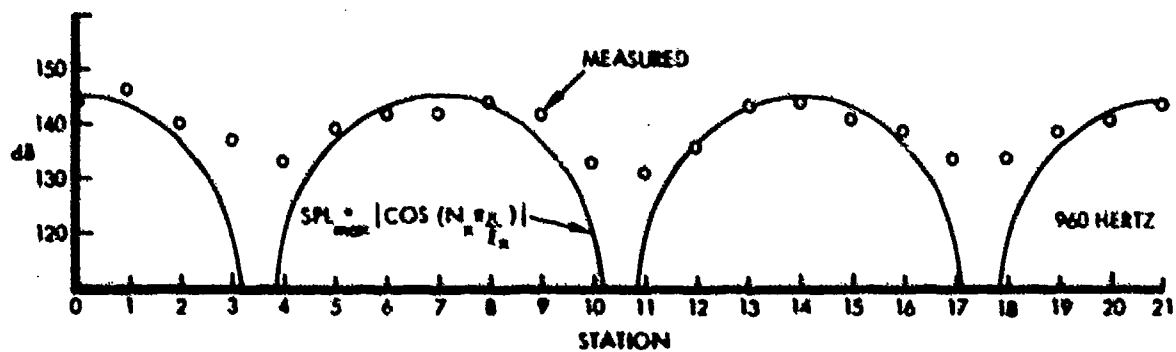
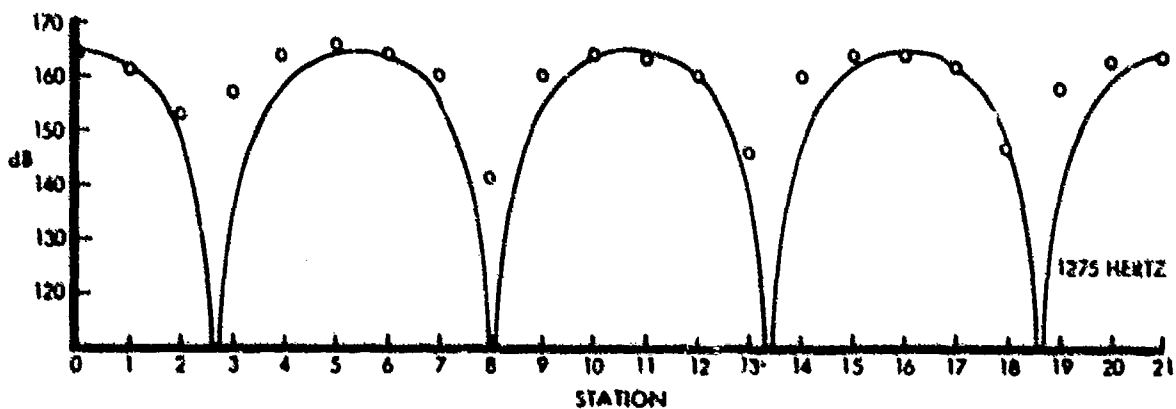


Figure 34. SPL Spatial Variation Fore-Aft in 21" x 5.4" D. Cylindrical Missile Bay, At Mach 0.81, 960 And 1275 Hertz Modes

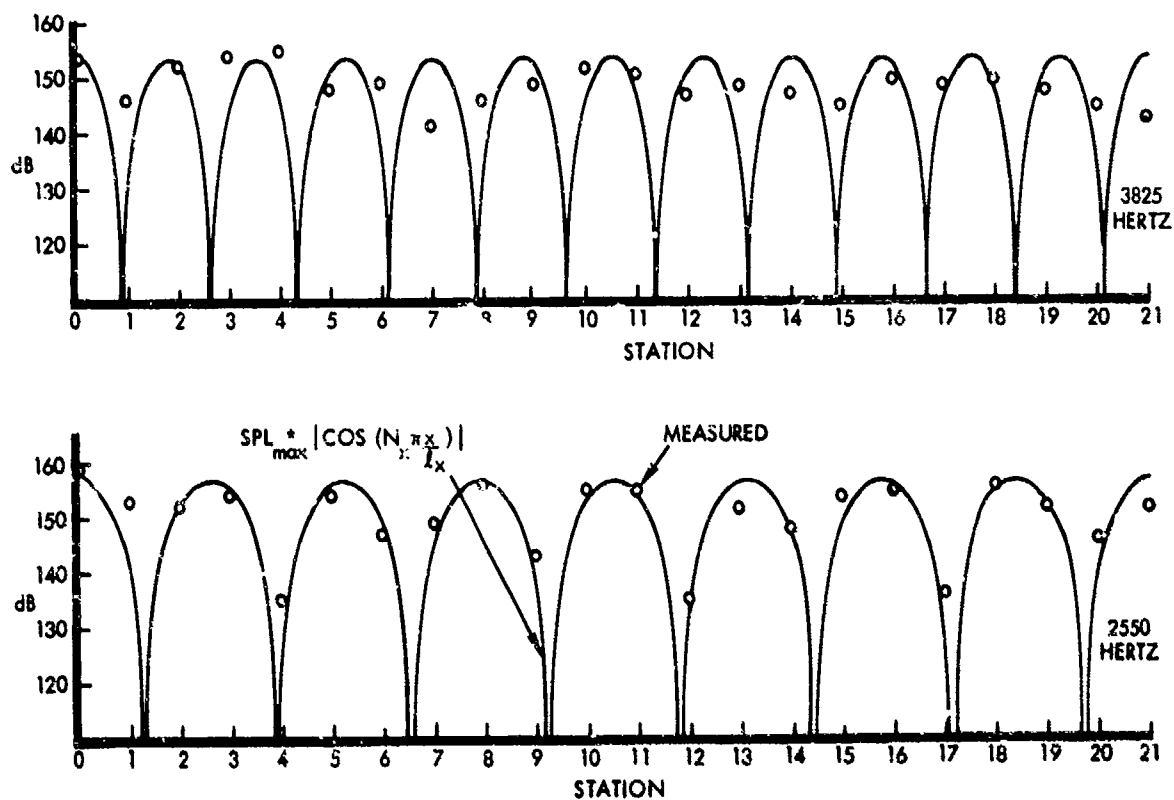


Figure 35. SPL Spatial Variation Fore-Aft In 21" x 5.4" D. Cylindrical Missile Bay, At Mach 0.81, 2550 And 3825 Hertz Modes

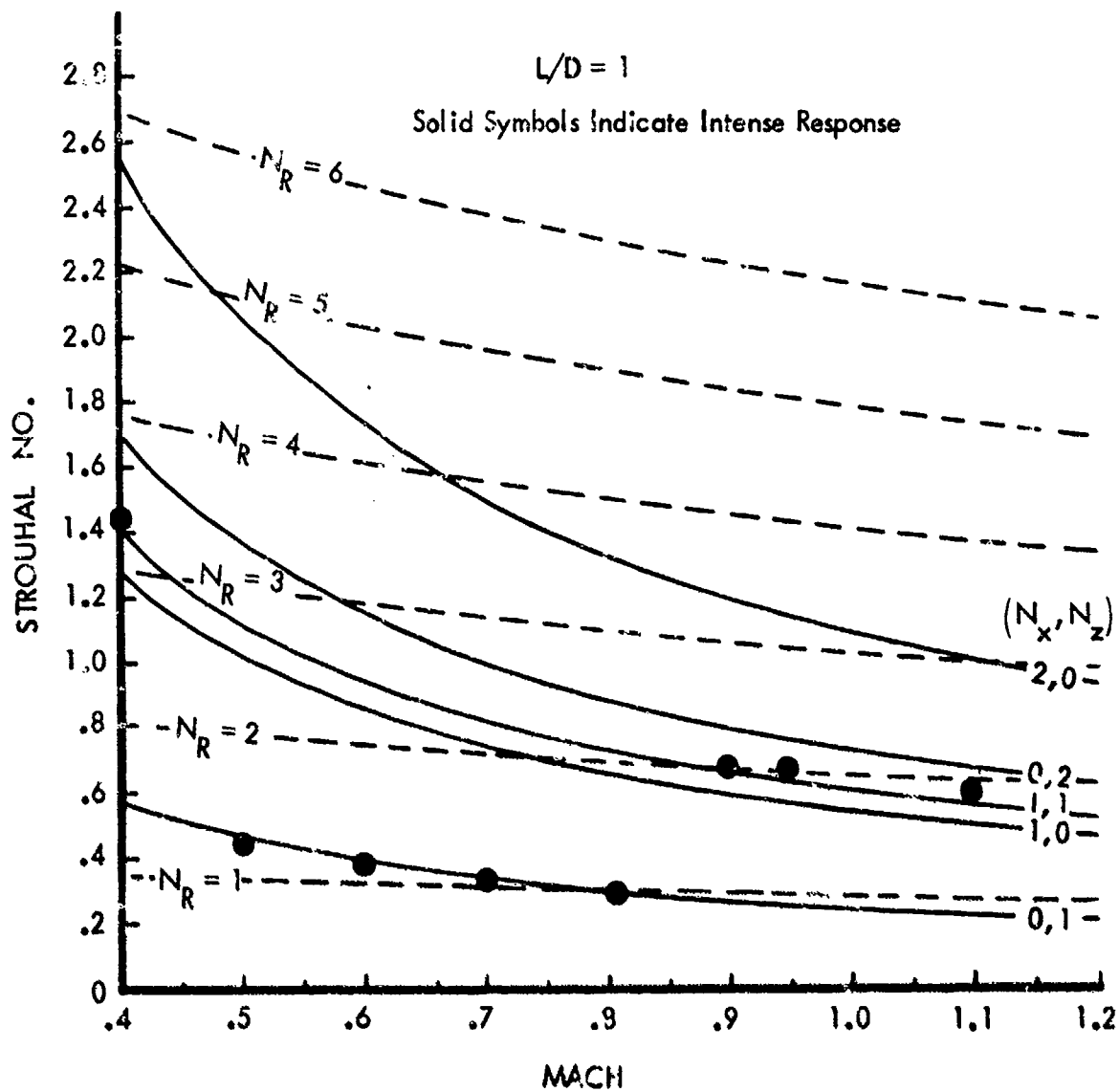


Figure 36. Rossiter's Measured Oscillatory Response (From Reference 2)  
Correlated with Predicted Acoustic Modes for  $L/D = 1$  Cavity,  $L_x = 8$ .

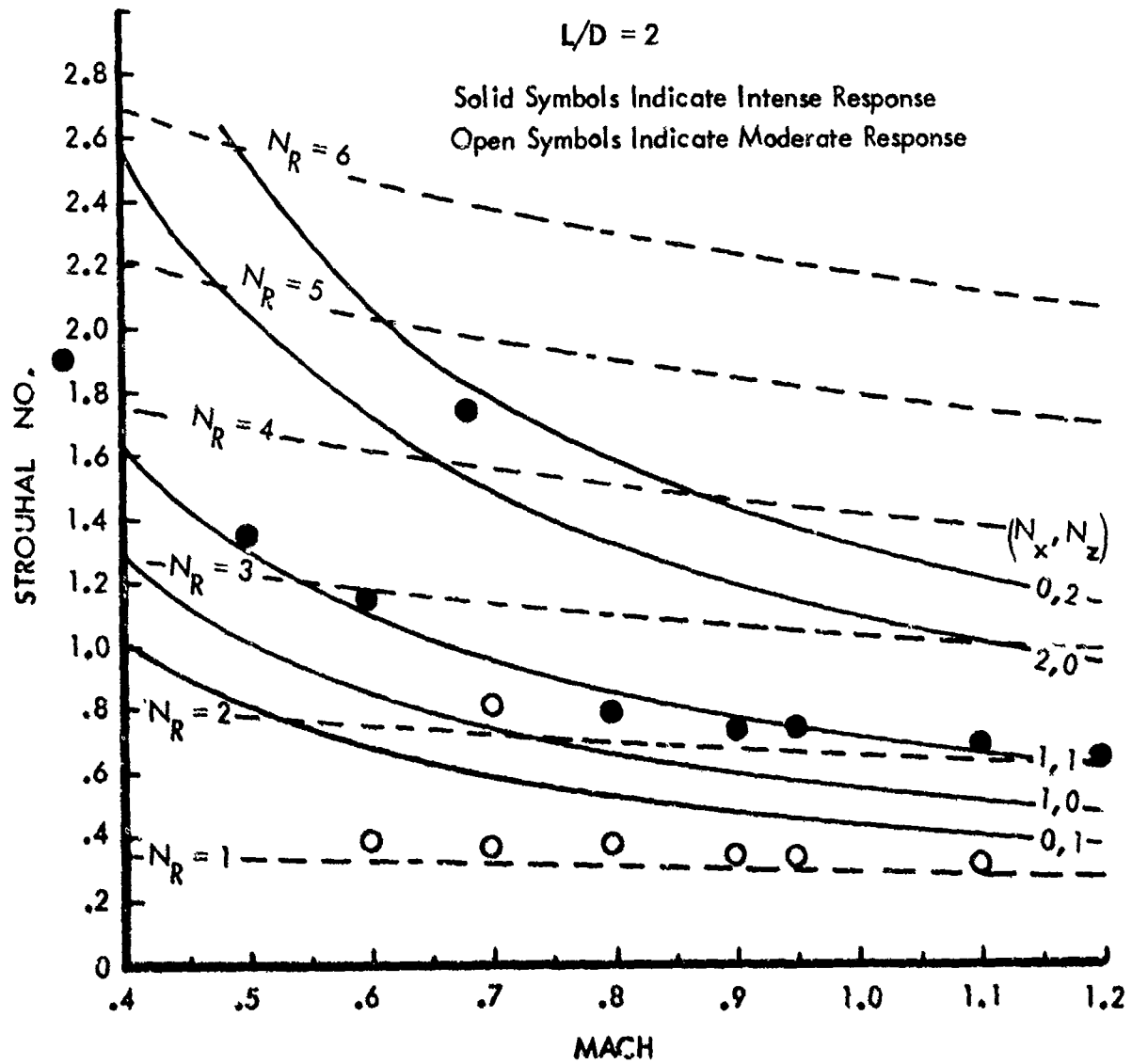


Figure 37. Rossiter's Measured Oscillatory Response (From Reference 2)  
Correlated With Predicted Acoustic Modes For  $L/D = 2$  Cavity,  $L_x = 8''$ .

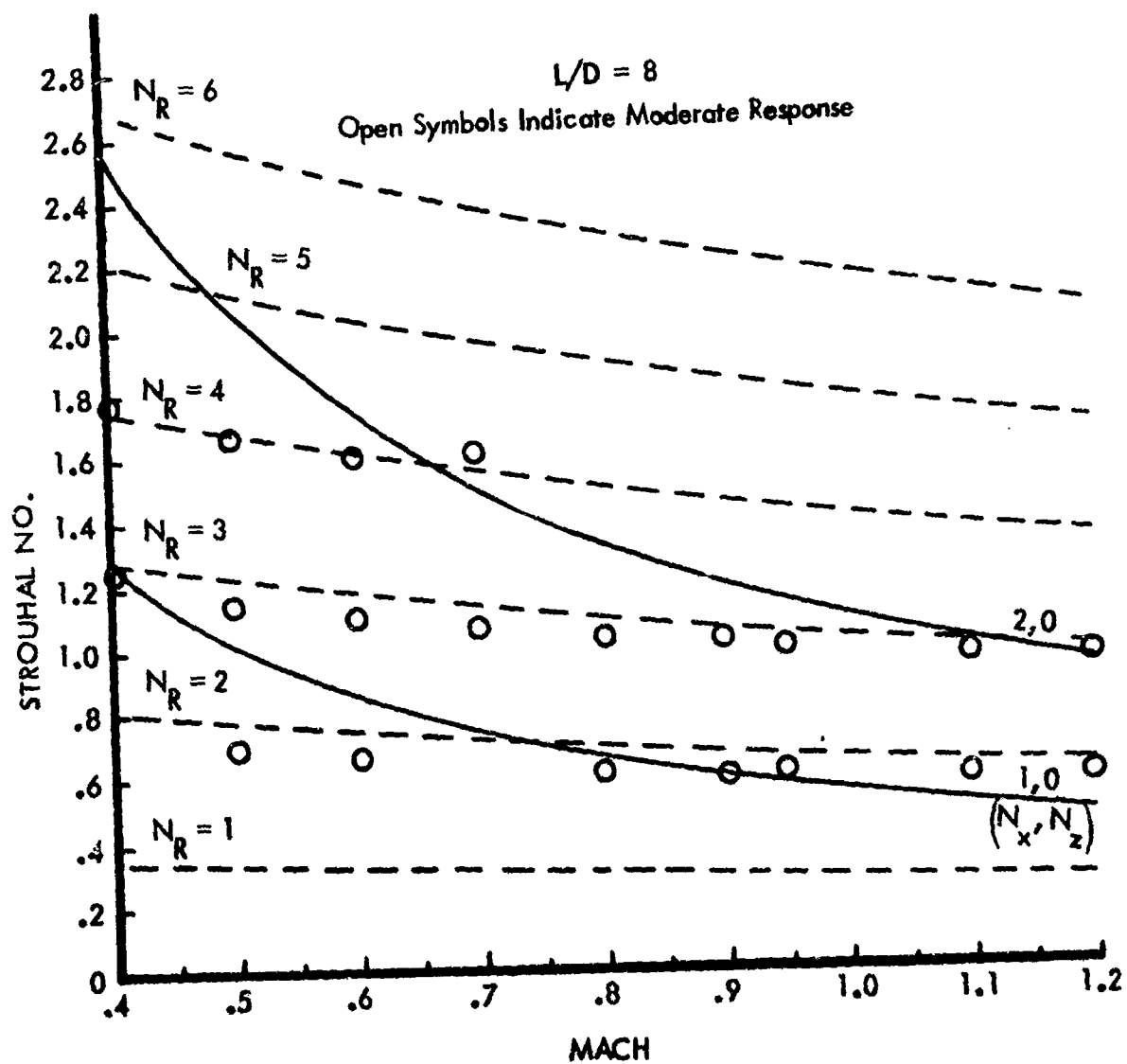


Figure 38. Rossiter's Measured Oscillatory Response (From Reference 2)  
Correlated With Predicted Acoustic Modes for  $L/D = 8$  Cavity,  $L_x = 8''$ .

COMPOSITE PLOT OF NORMALIZED MAXIMUM OSCILLATORY  
SOUND PRESSURE LEVELS FROM TEN VARIATIONS OF CYLINDRICAL  
MISSILE BAYS.

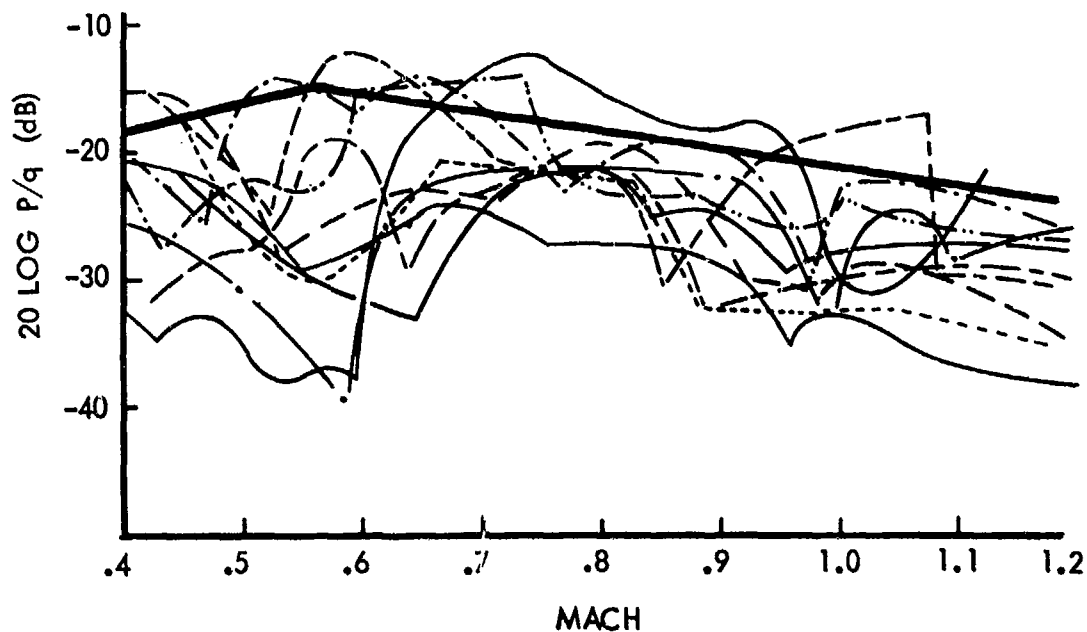


Figure 39. Development of Empirical Curve For Sound Pressure Level Predictions.

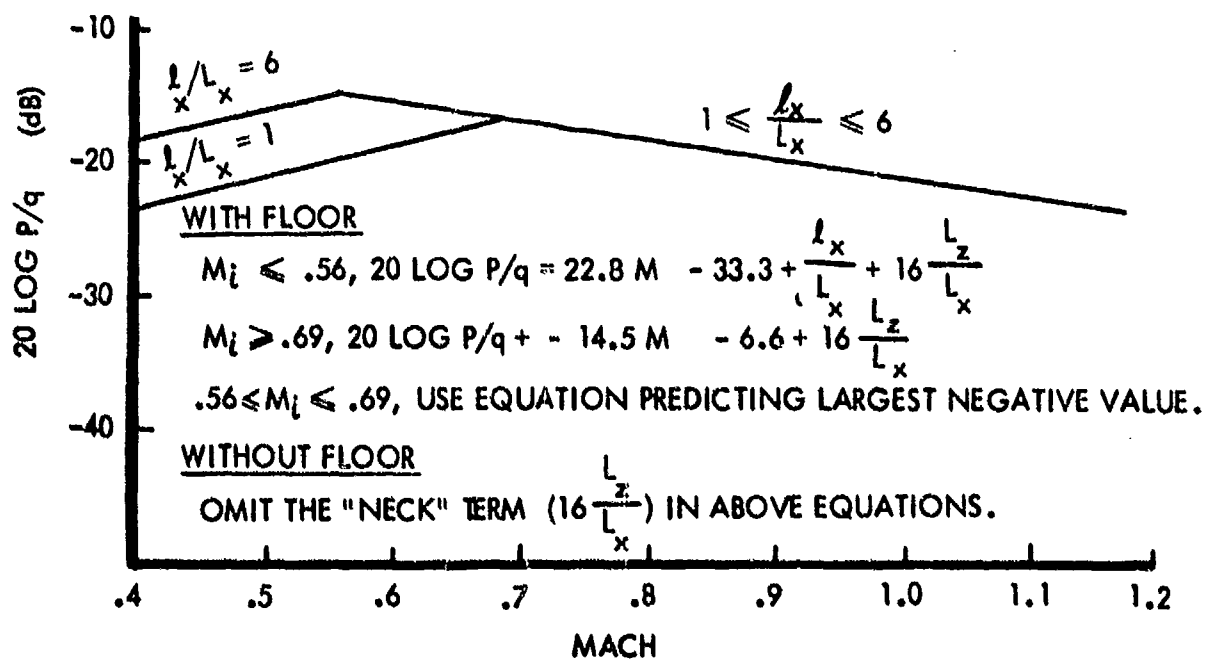


Figure 40. Normalized Maximum Oscillatory SPL in Cylindrical Missile Bays.

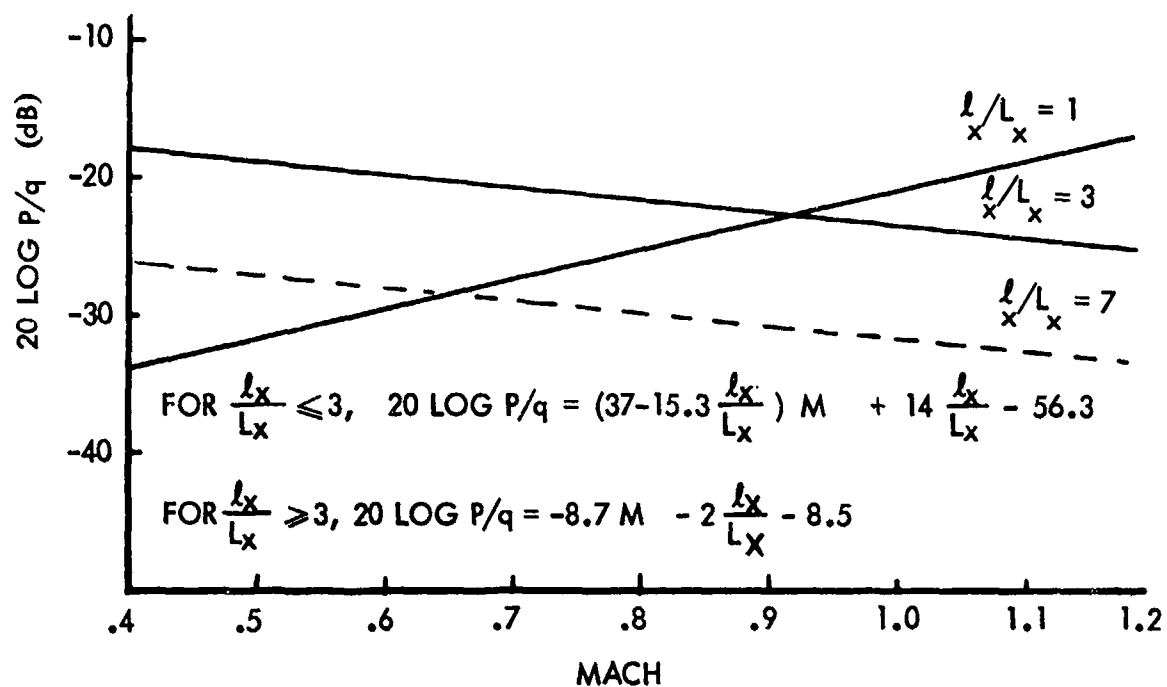


Figure 41. Normalized Maximum Oscillatory SPL in Rectangular Missile Bays.

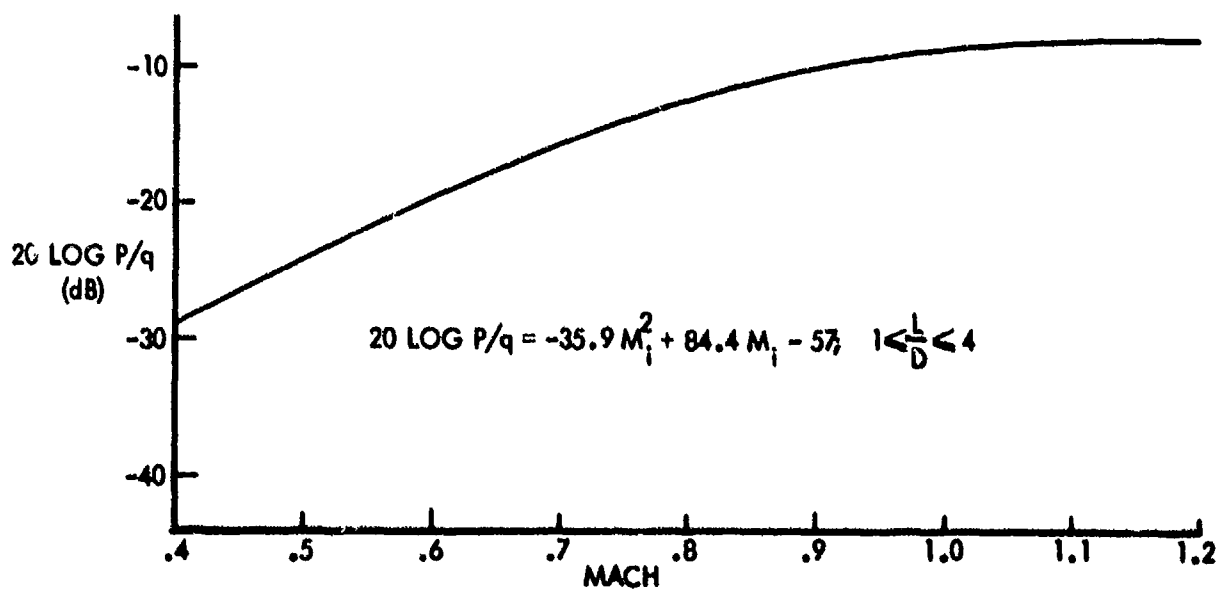


Figure 42. Normalized Maximum Oscillatory SPL In Conventional Bomb Bays



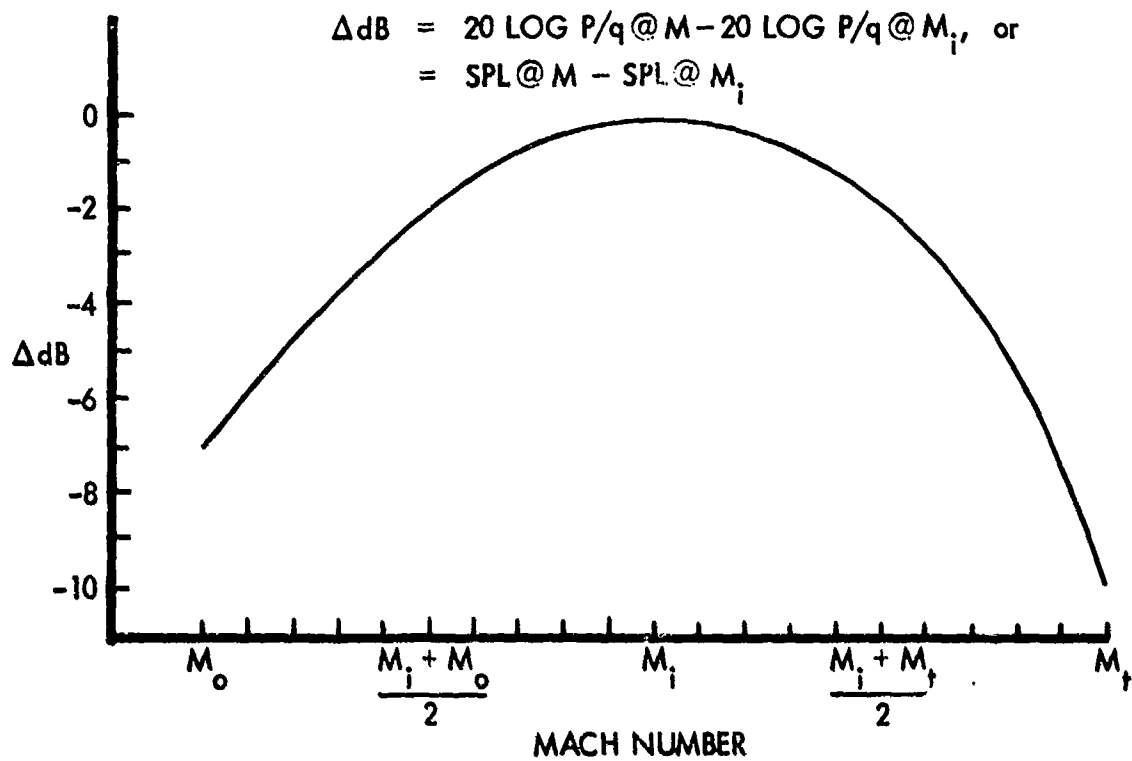


Figure 43. Oscillatory SPL Variation With Mach Number Between Onset and Termination

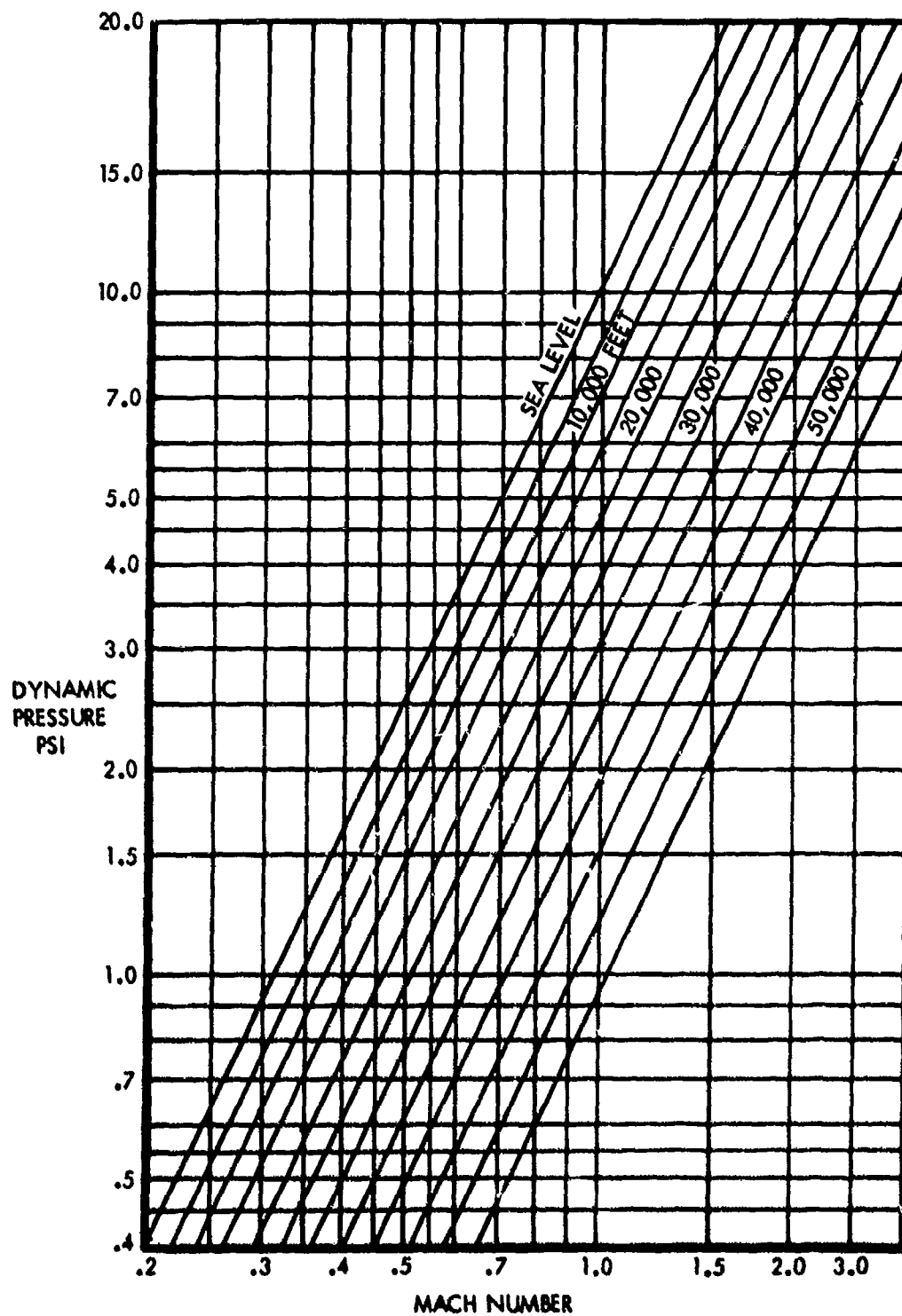


Figure 44. Free Stream Dynamic Pressure, Standard Atmosphere

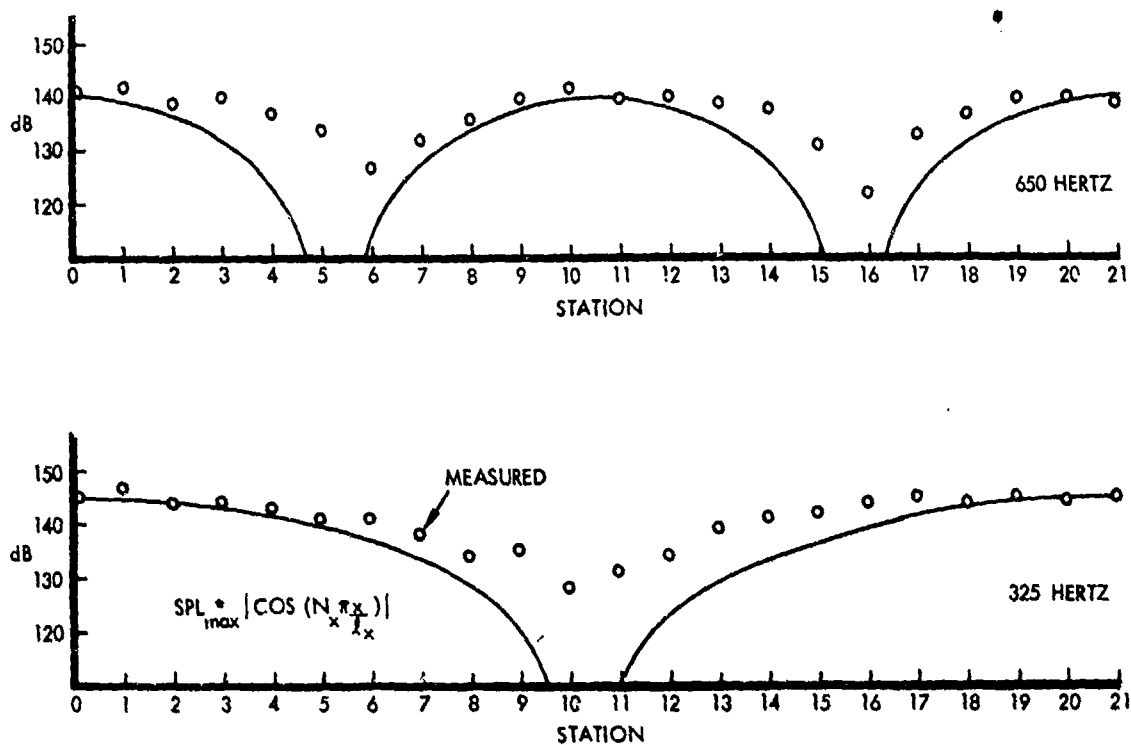


Figure 45. SPL Spatial Variation Fore-Aft in 21" x 5.4" D. Cylindrical Missile Bay, At Mach 0.7, 325 and 650 Hertz

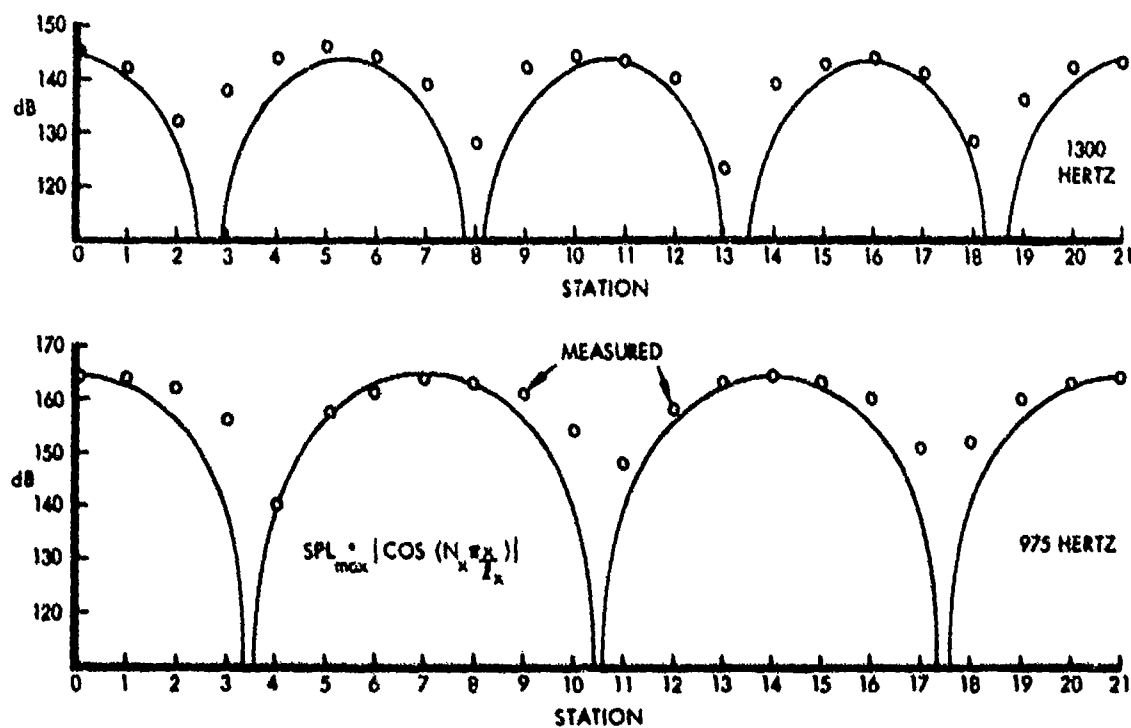


Figure 46. SPL Spatial Variation Fore-Aft in 21" x 5.4" D. Cylindrical Missile Bay, at Mach 0.71, 975 and 1300 Hertz

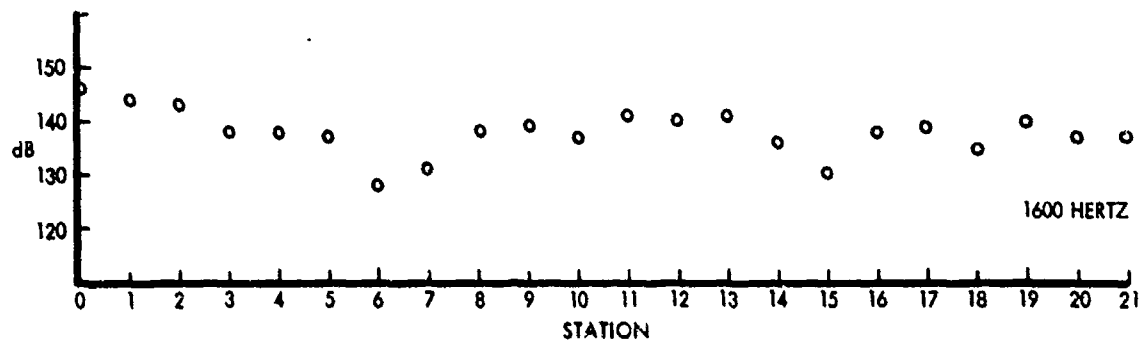
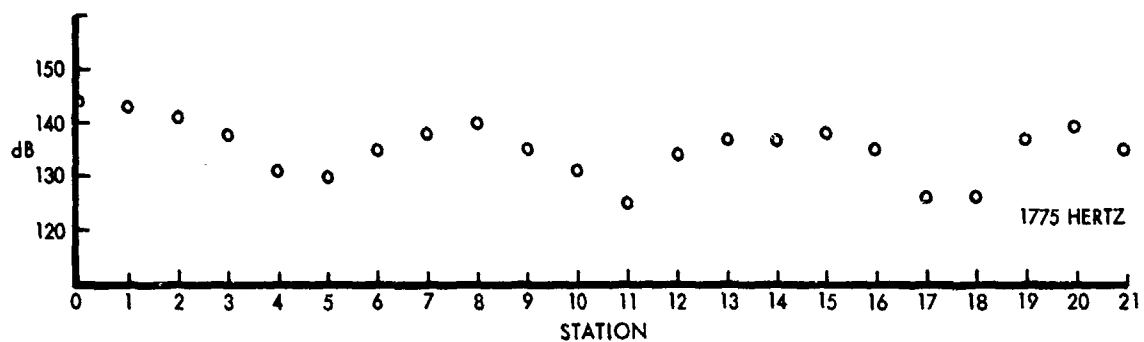


Figure 47. SPL Variation Measured Fore-Aft in 21" x 5.4" D. Cylindrical Missile Bay, at Mach 0.71, 1600 and 1775 Hertz

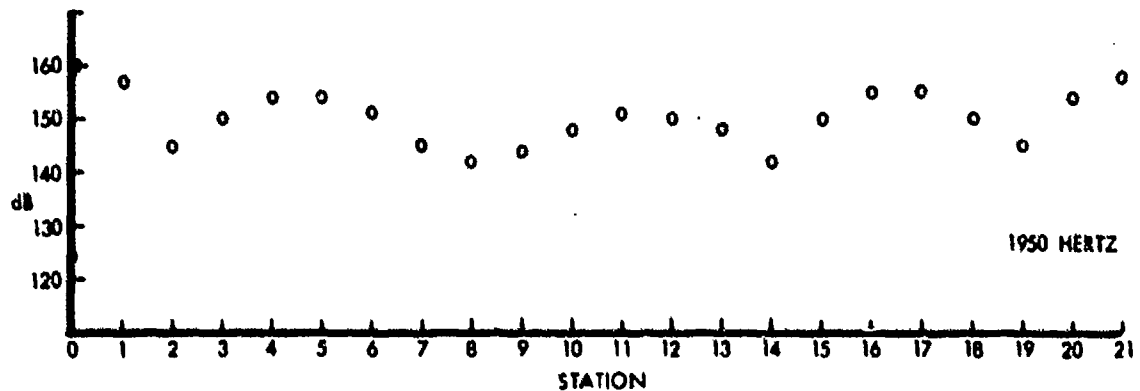
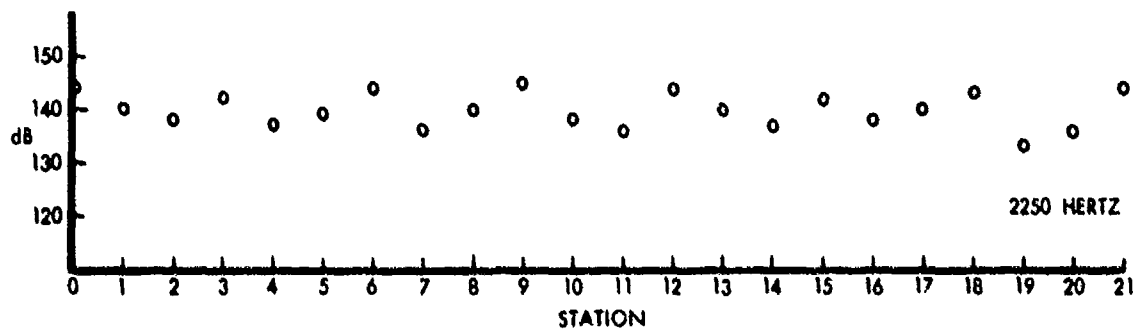


Figure 48. SPL Variation Measured Fore-Aft in 21" x 5.4" D. Cylindrical Missile Bay, at Mach 0.71, 1950 and 2250 Hertz

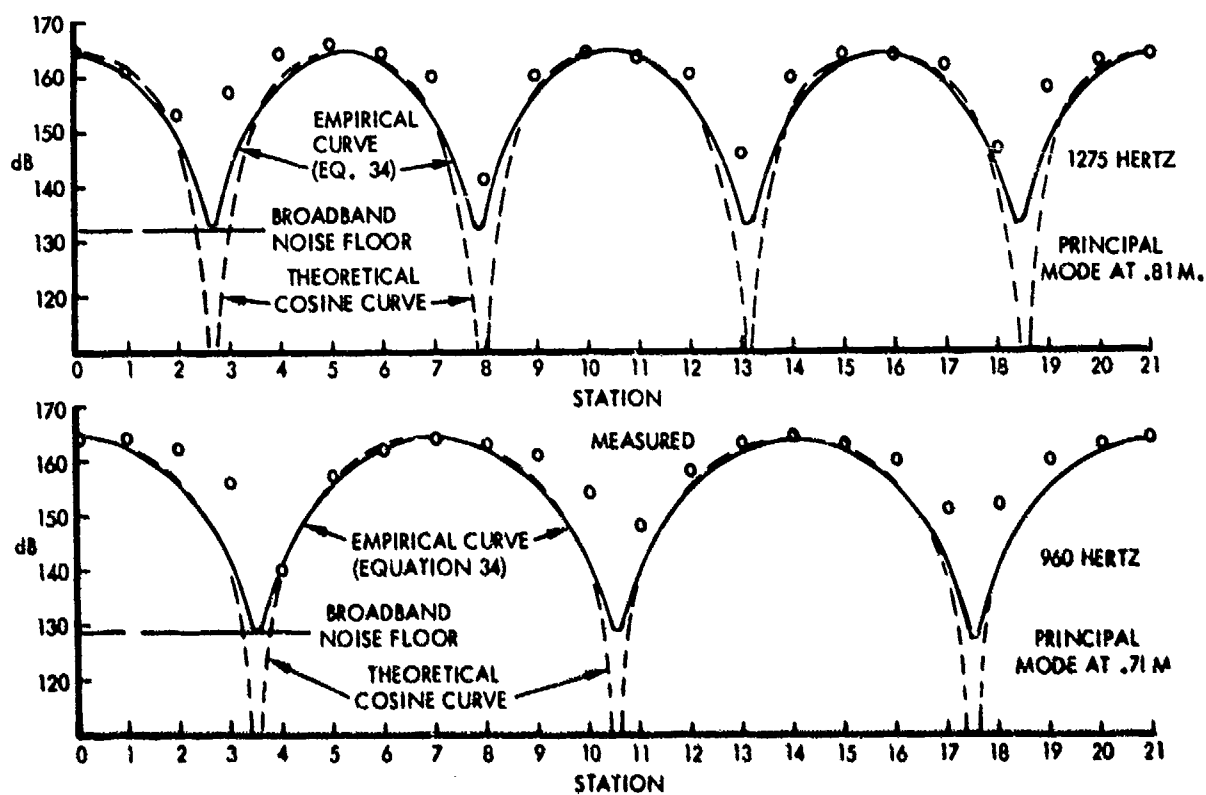


Figure 49. Fore-Aft SPL Variation Given by Equation 34 Which Accounts for Broadband Noise Level, 21" Cylindrical Missile Bay

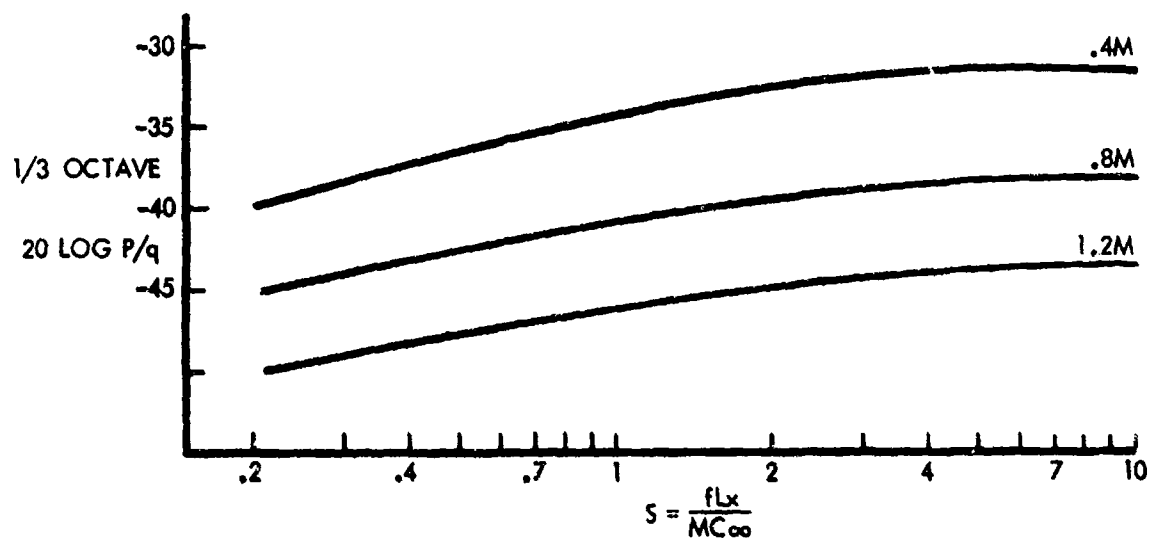


Figure 50. Broadband SPL at Downstream Wall Near Aperture

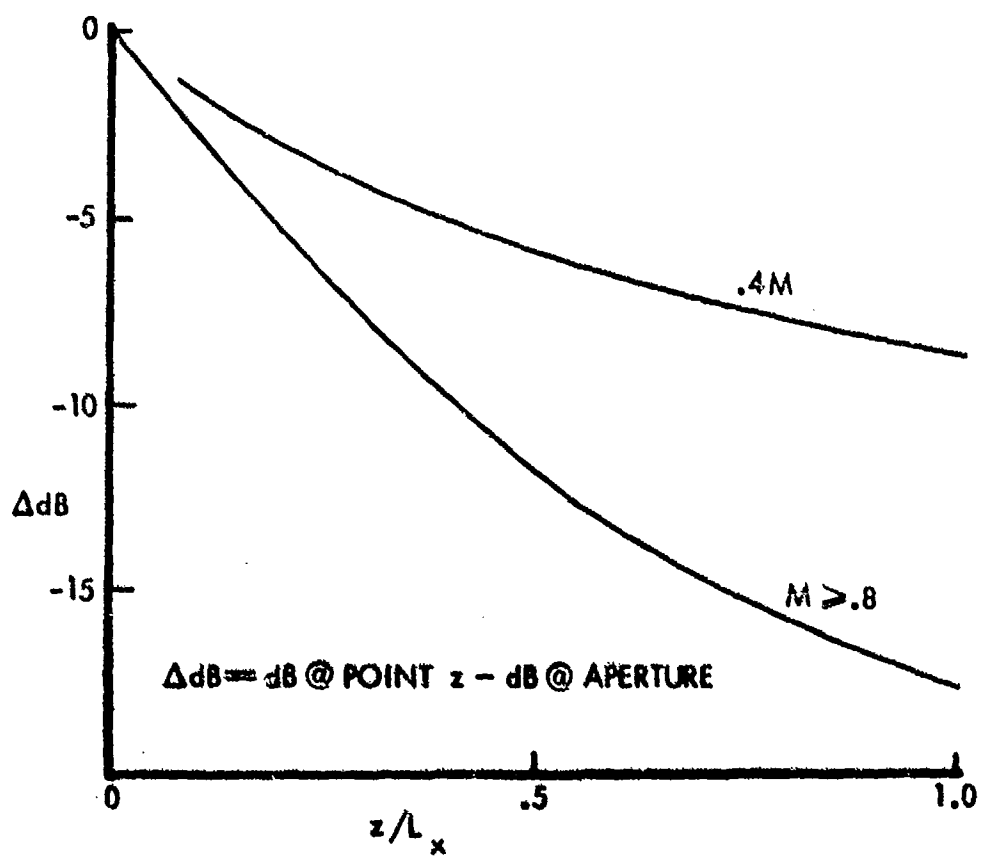
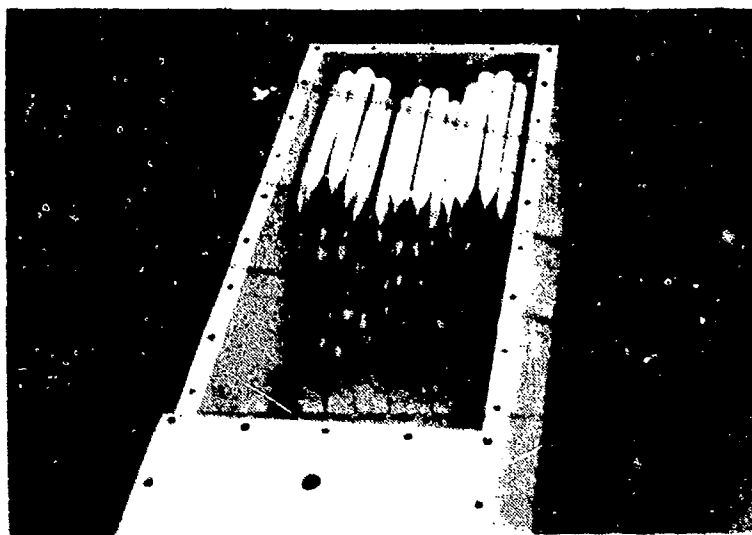


Figure 51. Depthwise Variation of Broadband SPL on Downstream End Wall



MAXIMUM CLUTTER IN SHORT MISSILE BAY (WALL REMOVED)

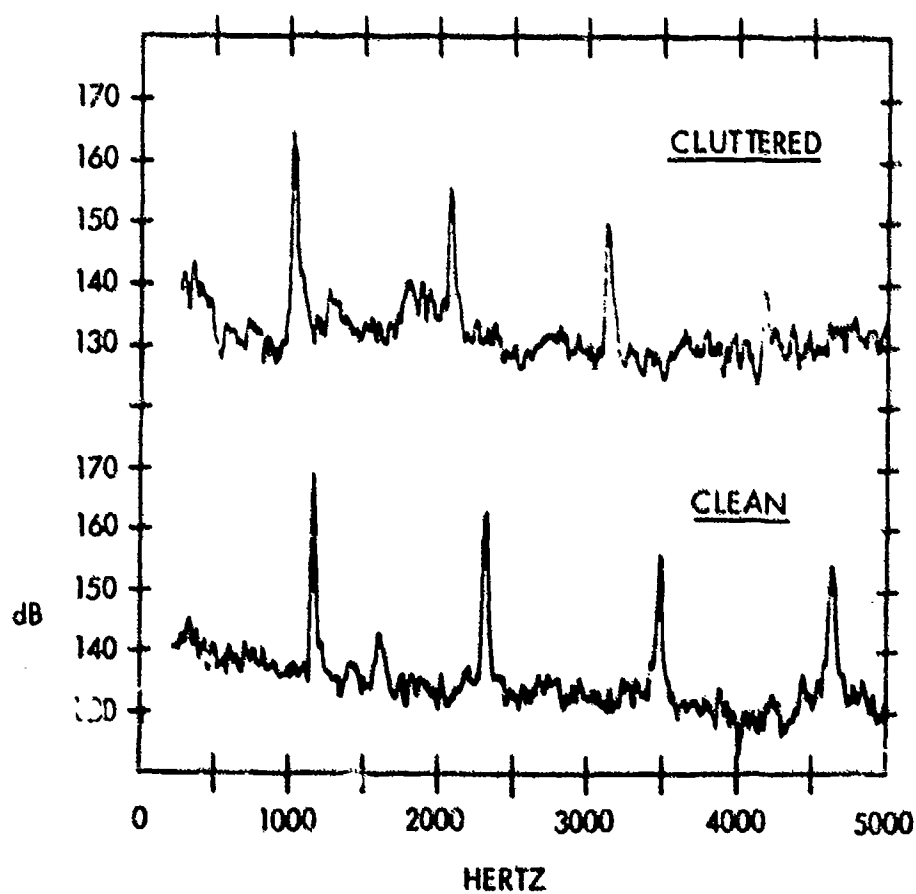


Figure 52. Effect of Clutter on Frequency and Level of Maximum Oscillation.



MAXIMUM CLUTTER AND BLOCKAGE IN CONVENTIONAL BOMB BAY

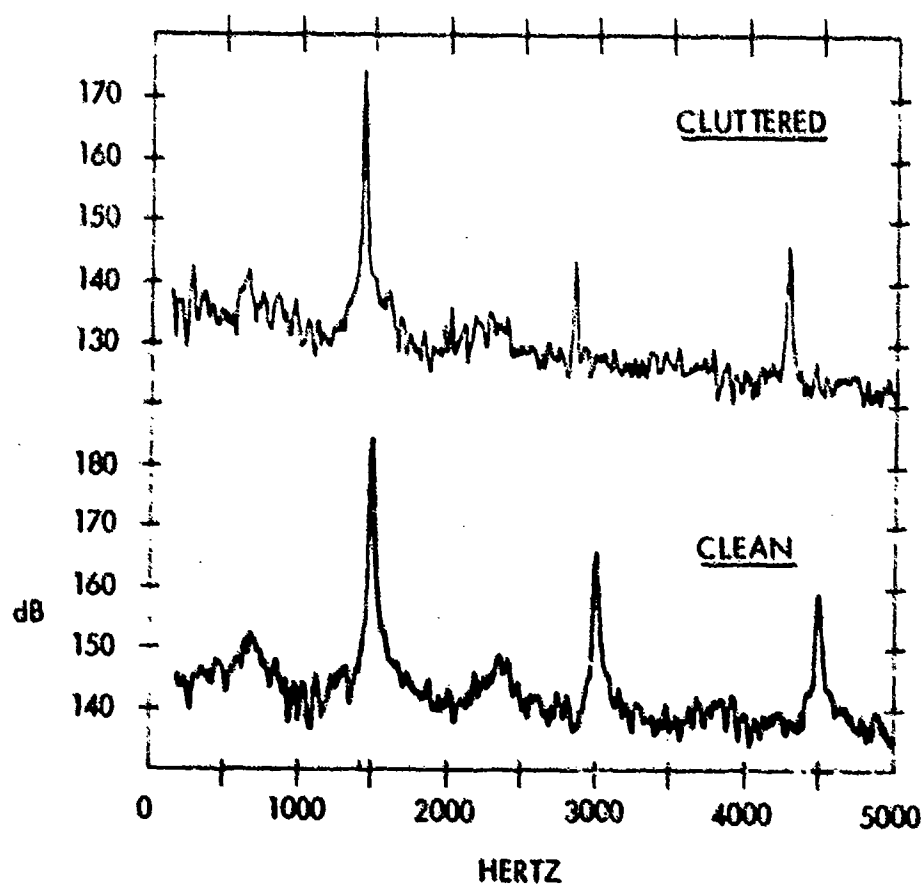


Figure 53. Effect of Clutter and Partial Blockage on Frequency and Level of Maximum Oscillation.



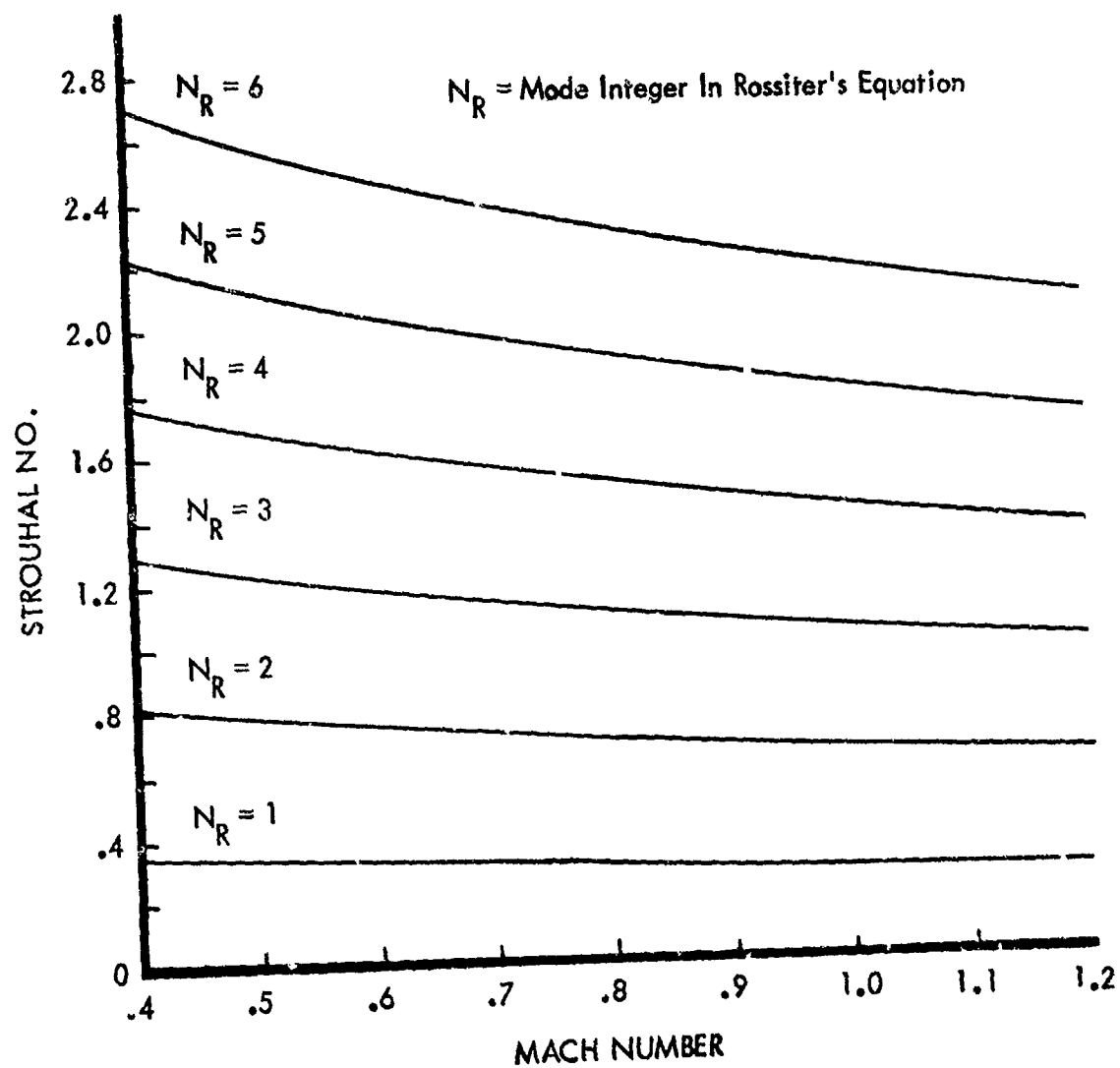


Figure 54. Shear Layer Oscillation Modes.

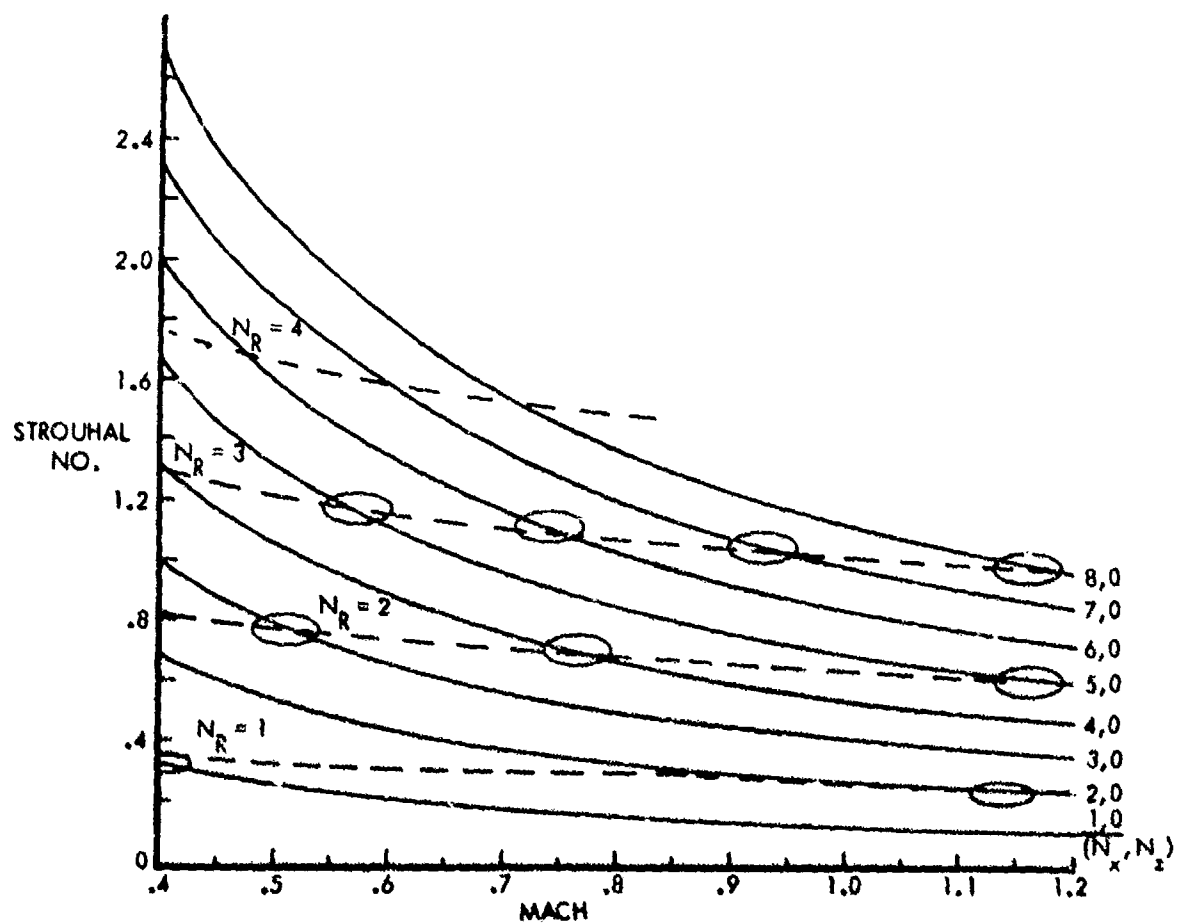


Figure 55. CMCA Case 2 Predicted Acoustic Modes Superimposed On Shear Layer Modes

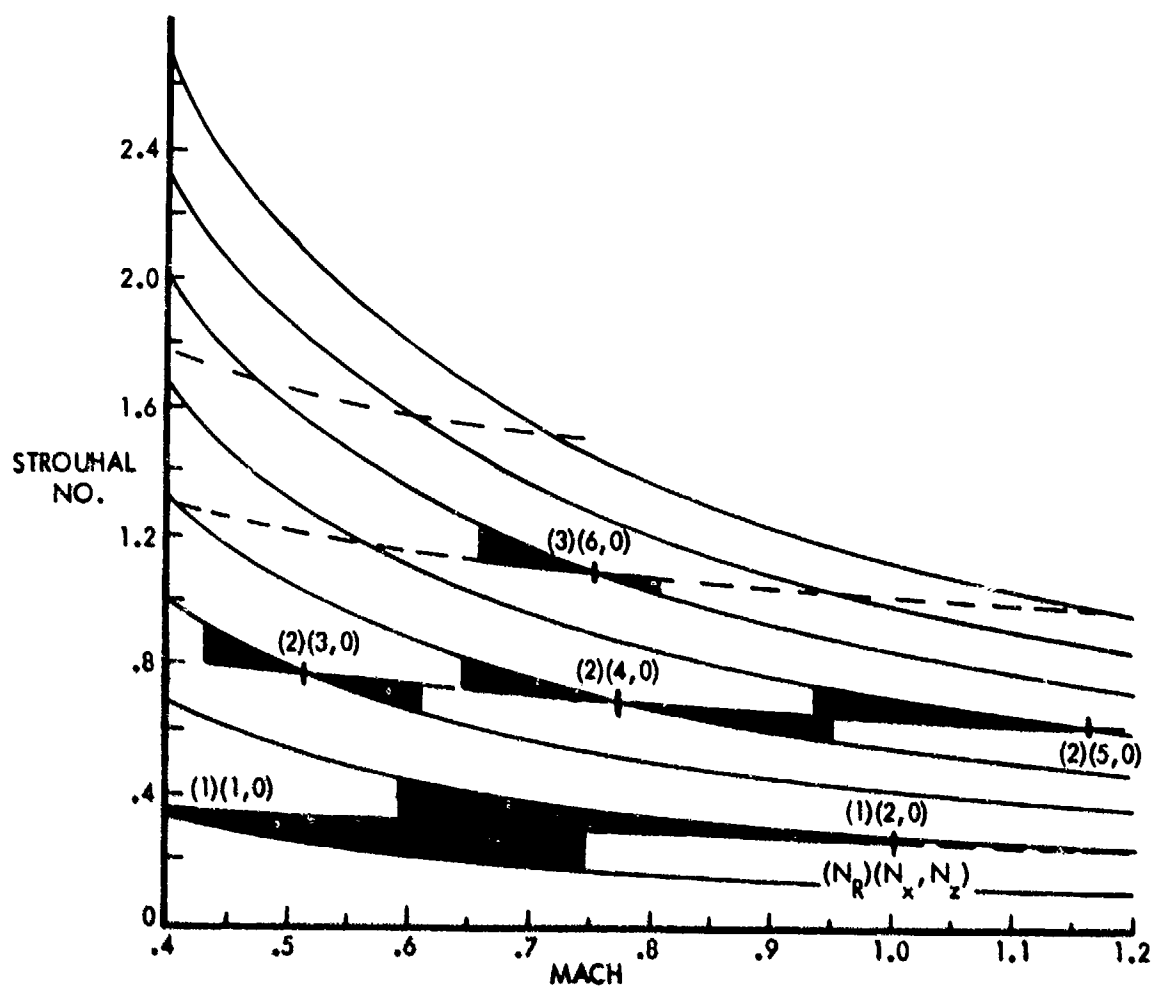


Figure 56. Speed Ranges Of Probable Modes Of Oscillation Predicted for CMCA Case 2

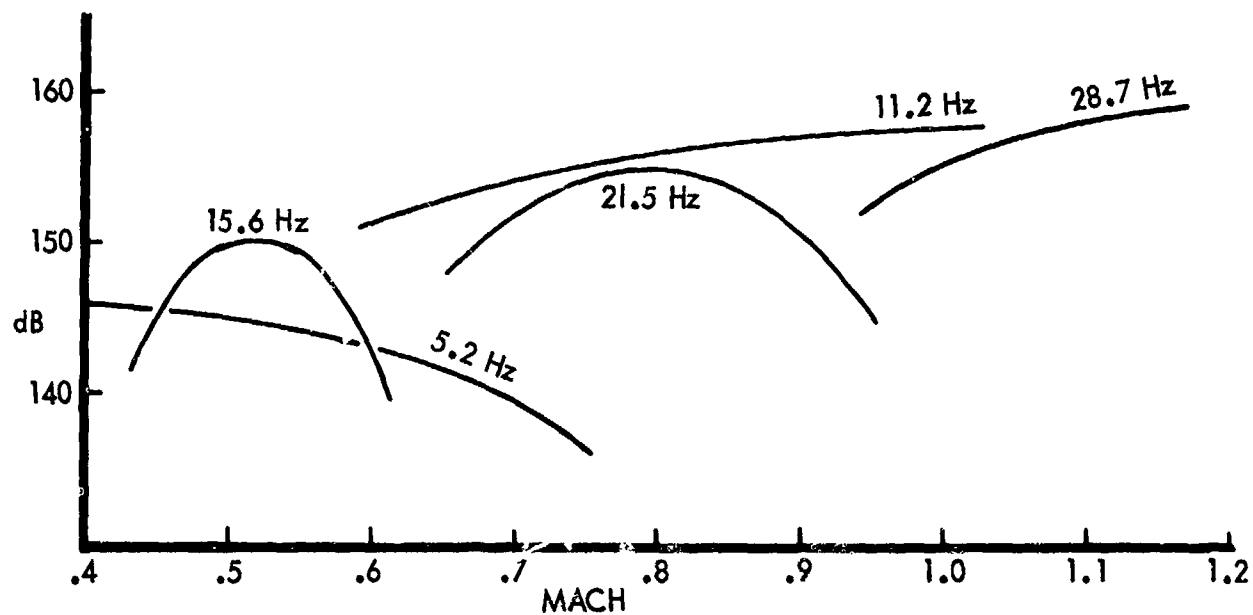


Figure 57. CMCA Case 2 Response Frequency and Maximum SPL Predicted for 25,000 Feet

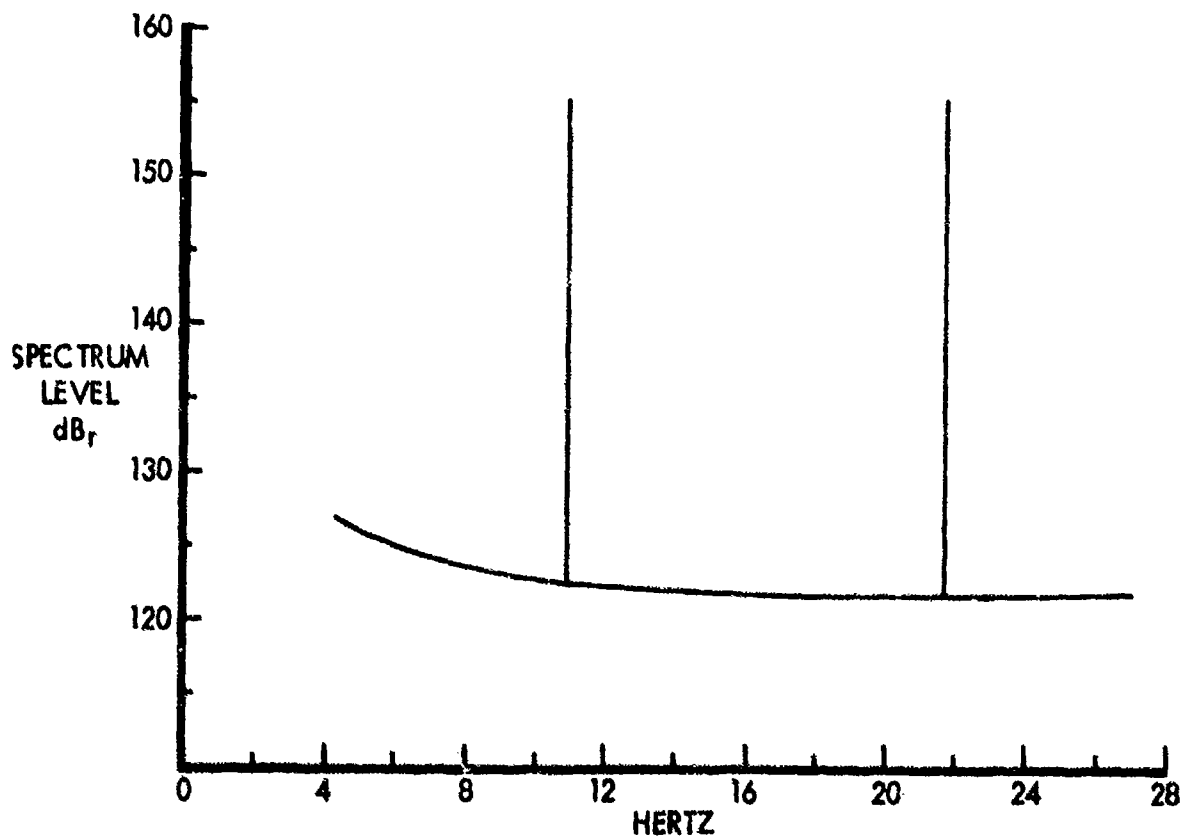


Figure 58. CMCA Case 2 Maximum Oscillatory Sound Pressure Spectrum Predicted For .8M, 25,000 Feet

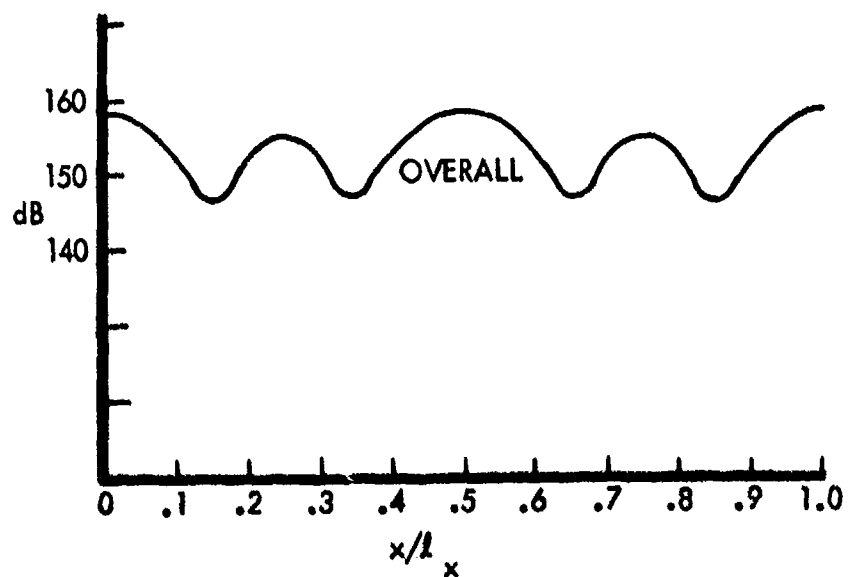
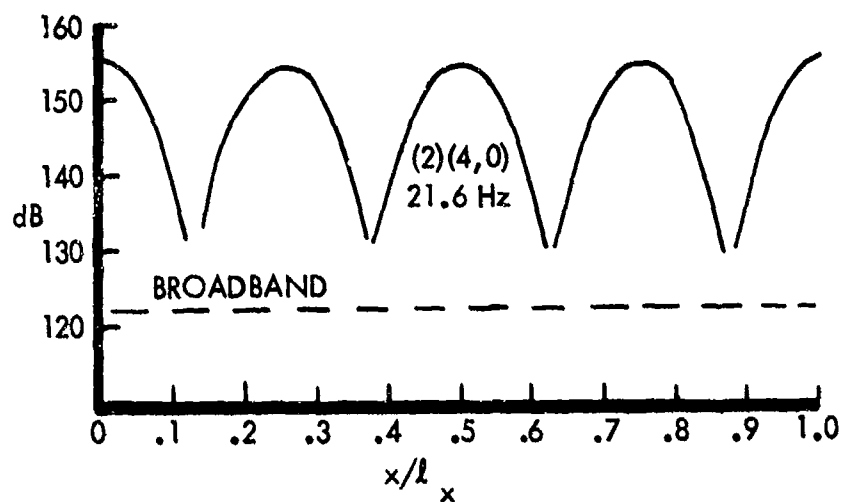
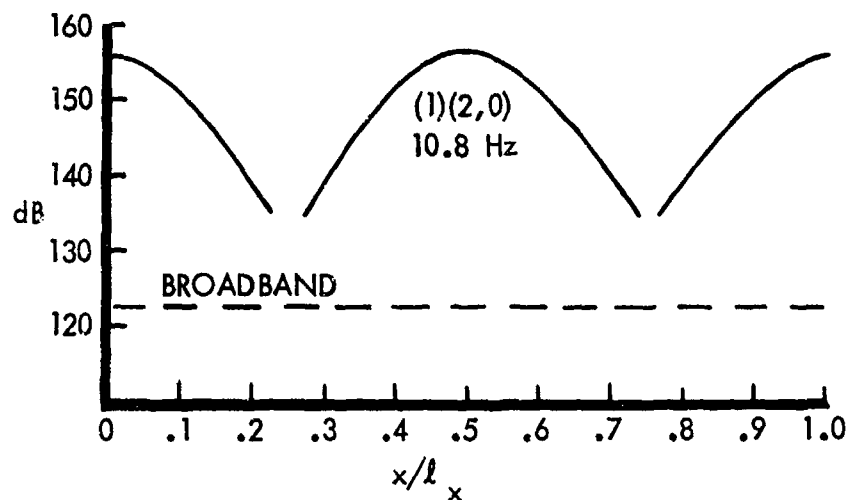


Figure 59. CMCA Case 2 Predicted Fore-Aft Variation in SPL On Wall Opposite Aperture, for .8M at 25,000 Feet

CMCA Case #	Oscillation Mode (N <sub>R</sub> )(N <sub>x</sub> , N <sub>F</sub> )	Mach No. Of			Oscillation Frequency Hertz	Maximum SPL dB
		On- Set	Inter- section	Termin- ation		
1	(1)(1,0)	-	.37	.75	5.2	153
	(1)(2,0)	.59	1.02	-	11.2	161
	(2)(3,0)	.43	.52	.61	15.6	157
	(2)(4,0)	.65	.78	.95	21.5	160
	(2)(5,0)	.94	1.17	-	28.7	162
2	(1)(1,0)	-	.37	.75	5.2	146
	(1)(2,0)	.59	1.02	-	11.2	158
	(2)(3,0)	.43	.52	.61	15.6	150
	(2)(4,0)	.65	.78	.95	21.5	155
	(2)(5,0)	.94	1.17	-	28.6	159
3	(2)(1,0)	.61	.74	.88	20.6	160
	(3)(1,0)	.36	.40	.43	19.8	154
	(3)(0,1)	.75	.83	.91	35.2	161
	(3)(1,1)	.96	1.08	-	42.7	161
4	(2)(1,0)	.46	.55	.65	16.4	143
	(3)(2,0)	.70	.78	.86	33.6	153
	(3)(0,1)	.78	.86	.95	36.3	156
5	None	-	-	-	None	-
6	(1)(0,1)	.68	1.2	-	12.6	178
	(2)(1,0)	.61	.74	.88	20.6	163
	(2)(1,1)	.76	.93	1.13	24.3	172
	(3)(0,2)	.76	.84	.92	35.5	168

Figure 60. Predicted CMCA Missile Bay Oscillation Within the Speed Range of .4M to 1.2M, at 25000 Feet

CMCA Case #	Oscillation Mode $(N_R)(N_x, N_P)$	Launch Altitude Feet	Oscillation Frequency Hertz	Maximum SPL dB	Broadband Spectrum Level dB
1	(1)(2,0)	25000	10.8	159	123
		37000	10.3	154	118
	(2)(4,0)	25000	21.6	160	122
		37000	20.6	155	117
2	(1)(2,0)	25000	10.8	156	121
		37000	10.3	149	118
	(2)(4,0)	25000	21.6	155	122
		37000	20.6	150	117
3	(2)(1,0)	25000	20.8	158	123
		37000	19.8	153	118
4	(3)(2,0)	25000	33.7	151	120
		37000	33.1	146	115
5	None	-	-	-	-
6	(1)(0,1)	25000	11.8	162	125
		37000	11.2	157	120
	(2)(1,1)	25000	23.9	162	122
		37000	22.7	157	117

Figure 61. Predicted CMCA Missile Bay Oscillation At Mach 0.8, Altitudes Of 25000 And 37000 Feet

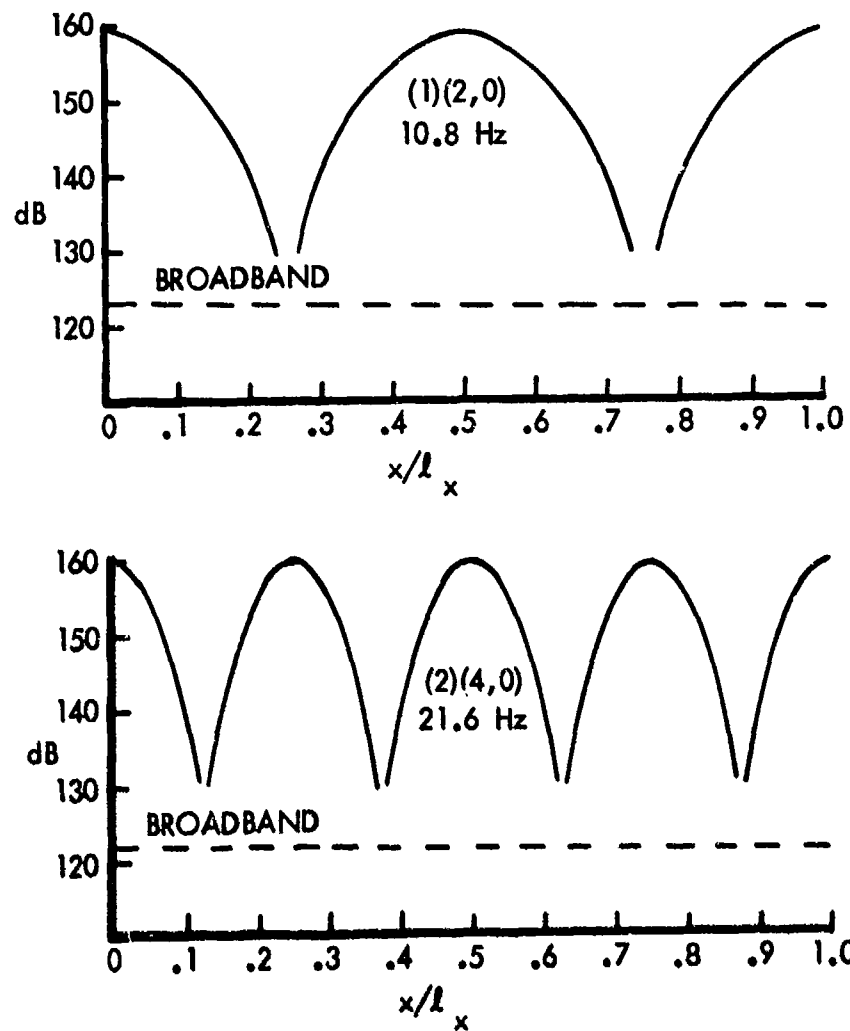


Figure 62. CMCA Case 1 Predicted Fore-Aft Variation in SPL on Wall Opposite Aperture, for .8M at 25,000 Feet



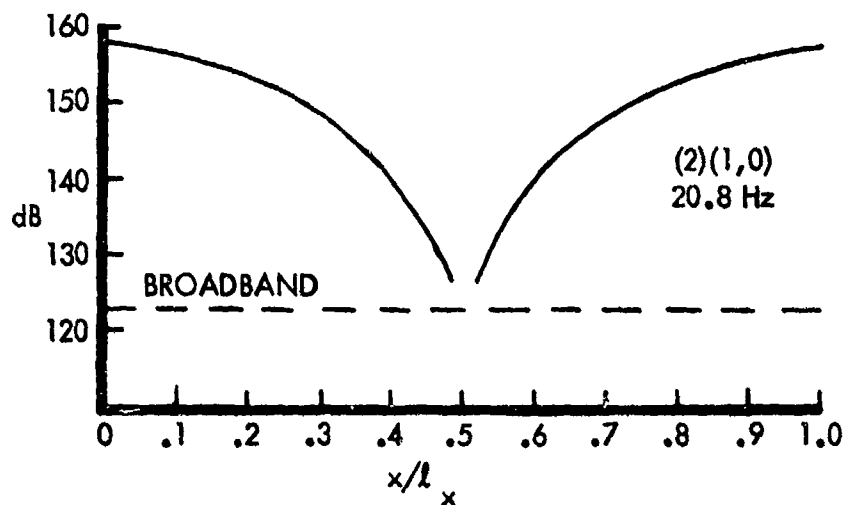


Figure 63. CMCA Case 3 Predicted Fore-Aft Variation in SPL On Wall Opposite Aperture, For .8M at 25,000 Feet

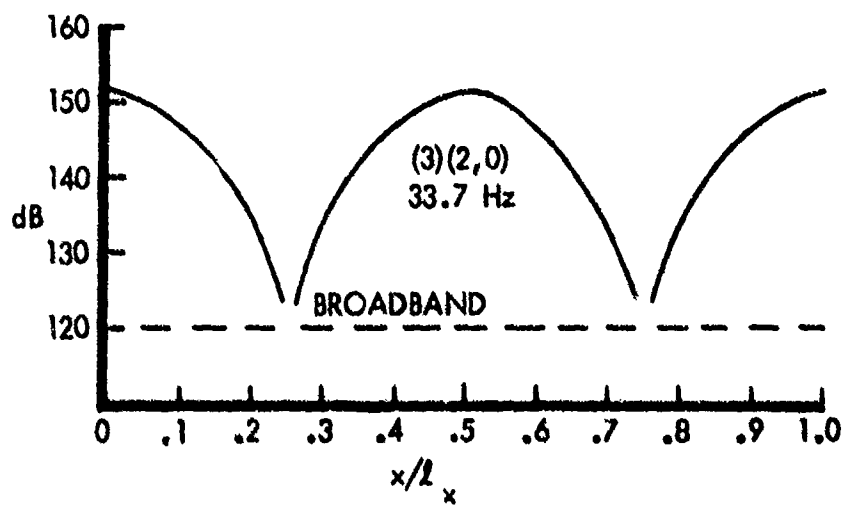


Figure 64. CMCA Case 4 Predicted Fore-Aft Variation in SPL On Wall Opposite Aperture, For .8M at 25,000 Feet

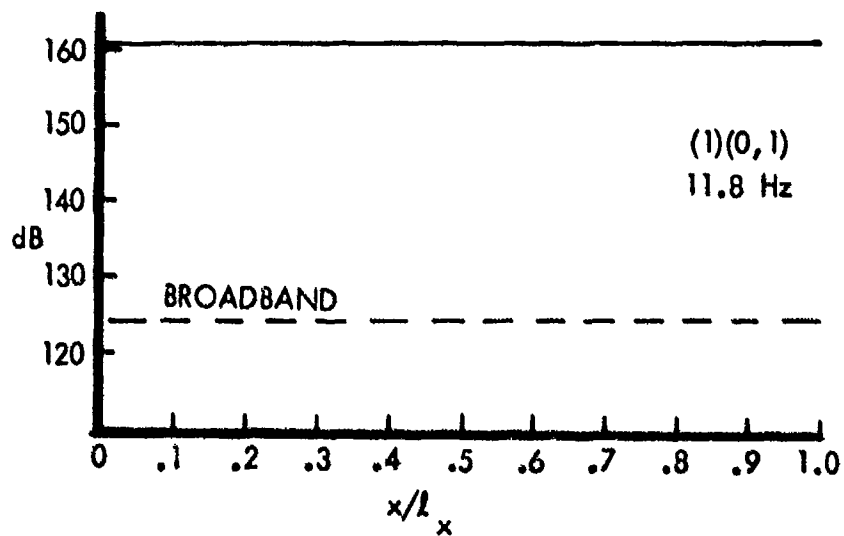
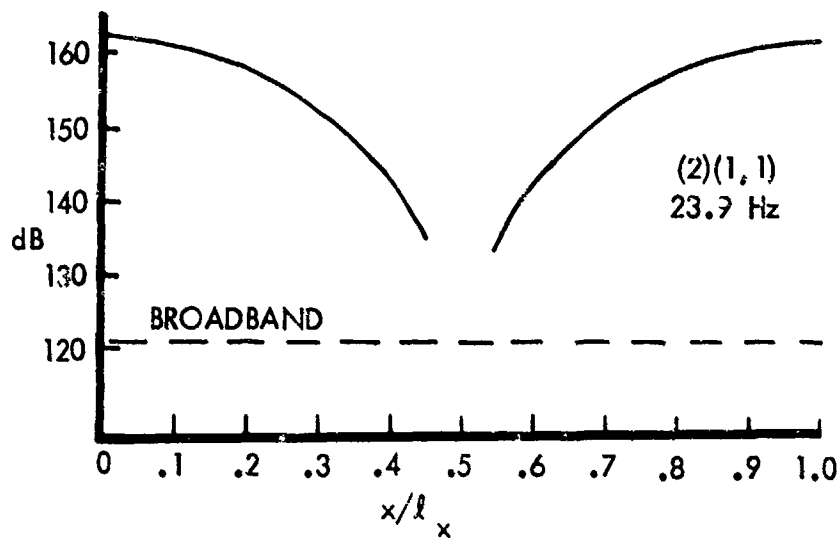


Figure 65. CMCA Case 6 Predicted Fore-Aft Variation in SPL on Wall Opposite Aperture, For .8M at 25,000 Feet

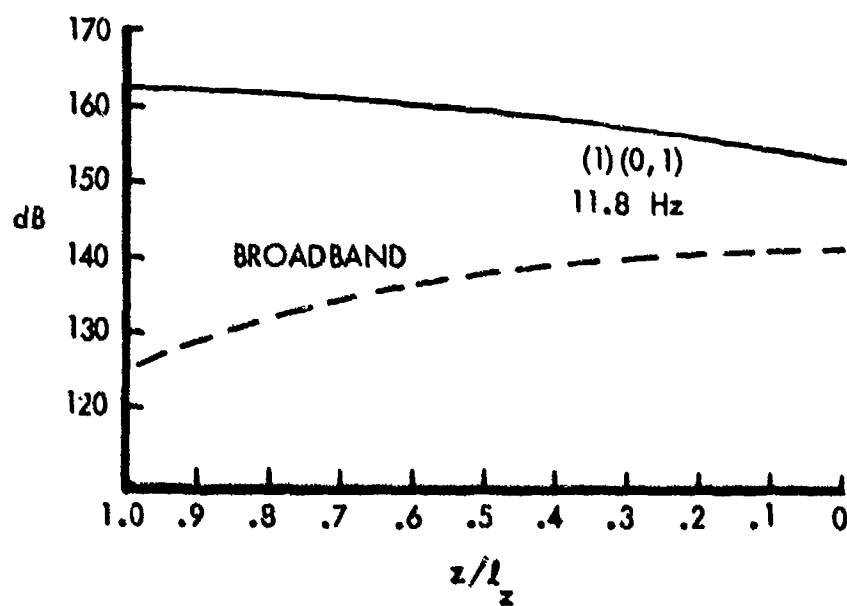
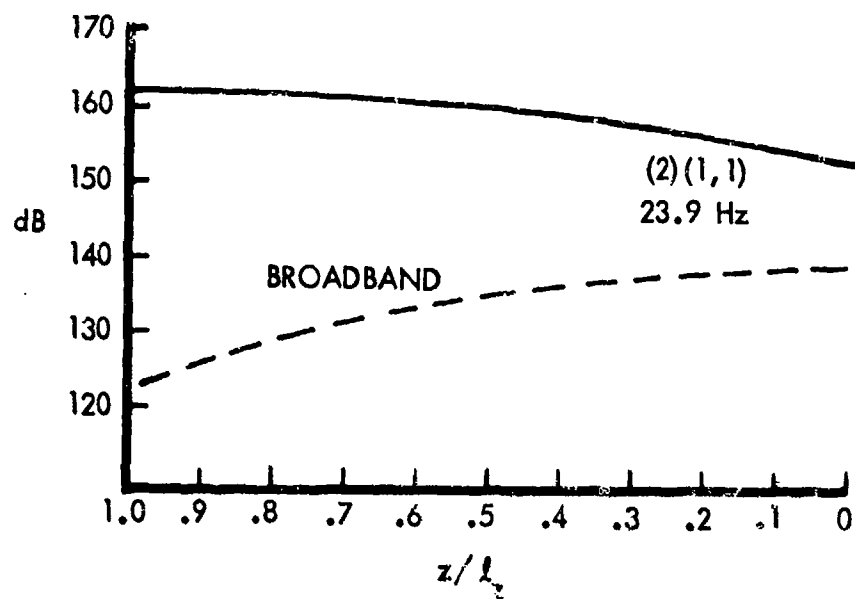


Figure 66. CMCA Case 3 Predicted Depthwise Variation in SPL on Downstream Wall, For .8M, at 25000 Feet.

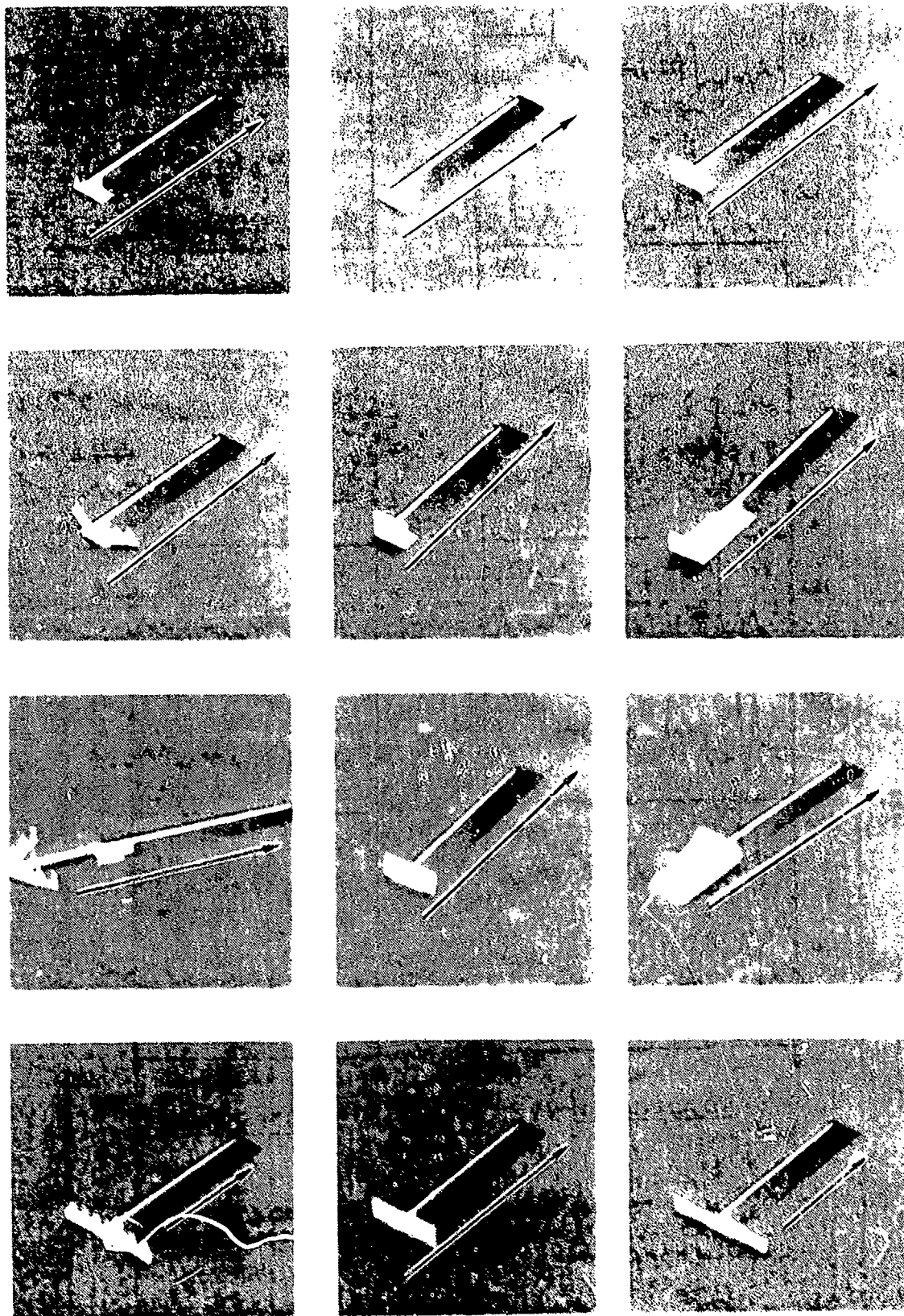
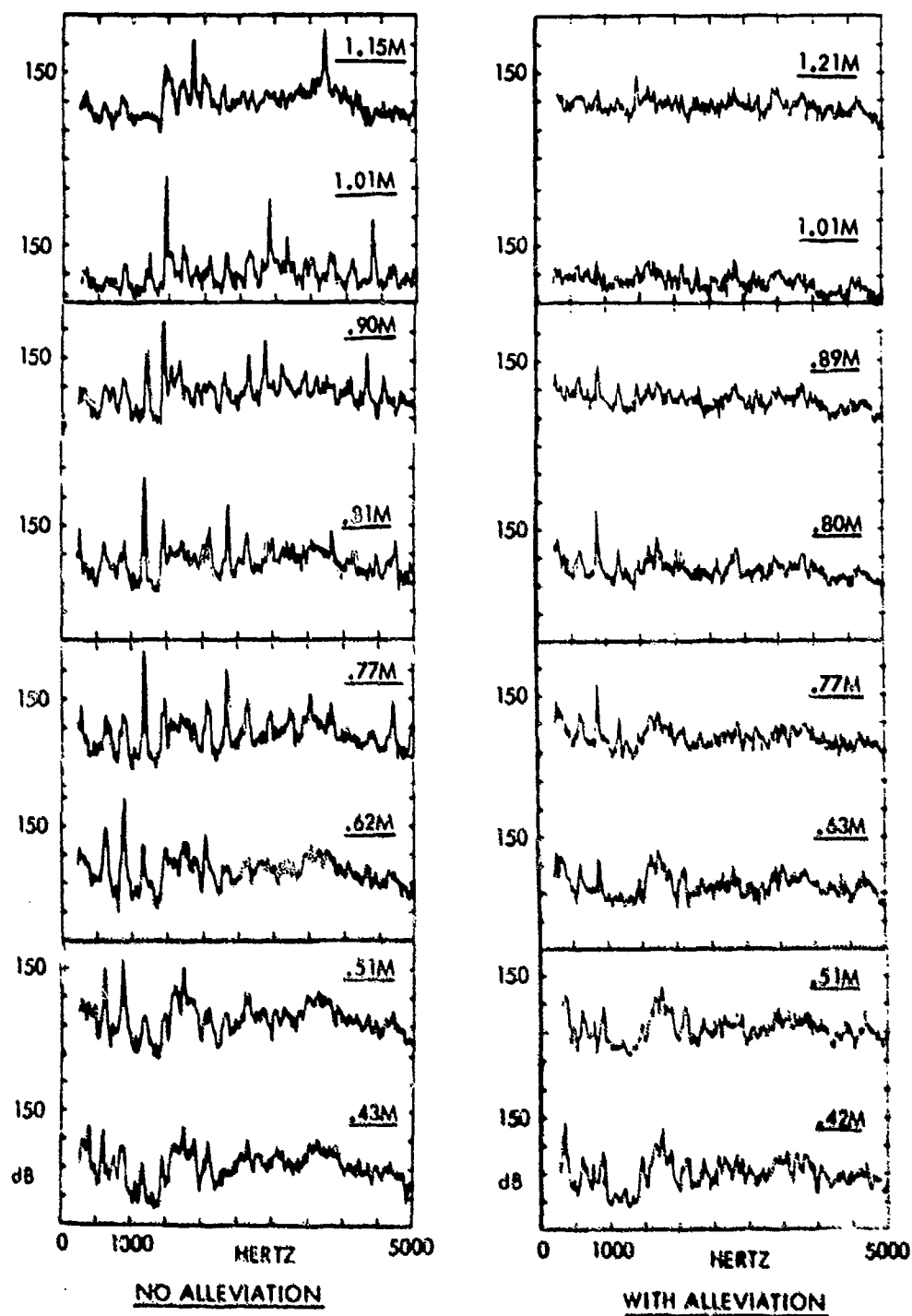


Figure 67. Illustration of Shear Layer Alteration Devices Examined.



NOTE:

ALL SPECTRA ARE 10 dB PER DIVISION, LINEAR FREQUENCY SCALE 0 TO 5000 HERTZ. STREAM FLOW MACH NUMBER IS NOTED ON EACH SPECTRUM.

Figure 68. CMCA Case 1 Response Spectra With and Without Spoiler/Ramp Alleviation Devices.

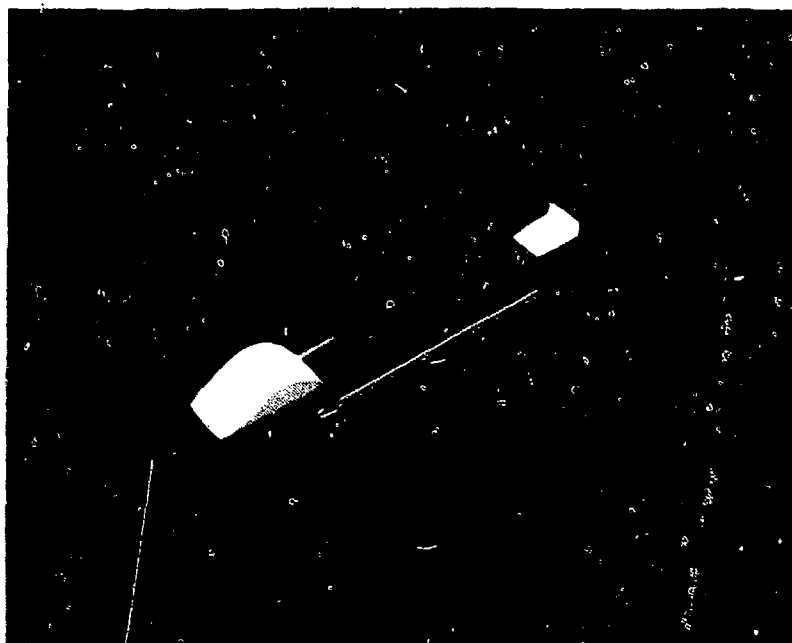


Figure 69. Illustration of Selected Alleviation Devices For Long Missile Bays

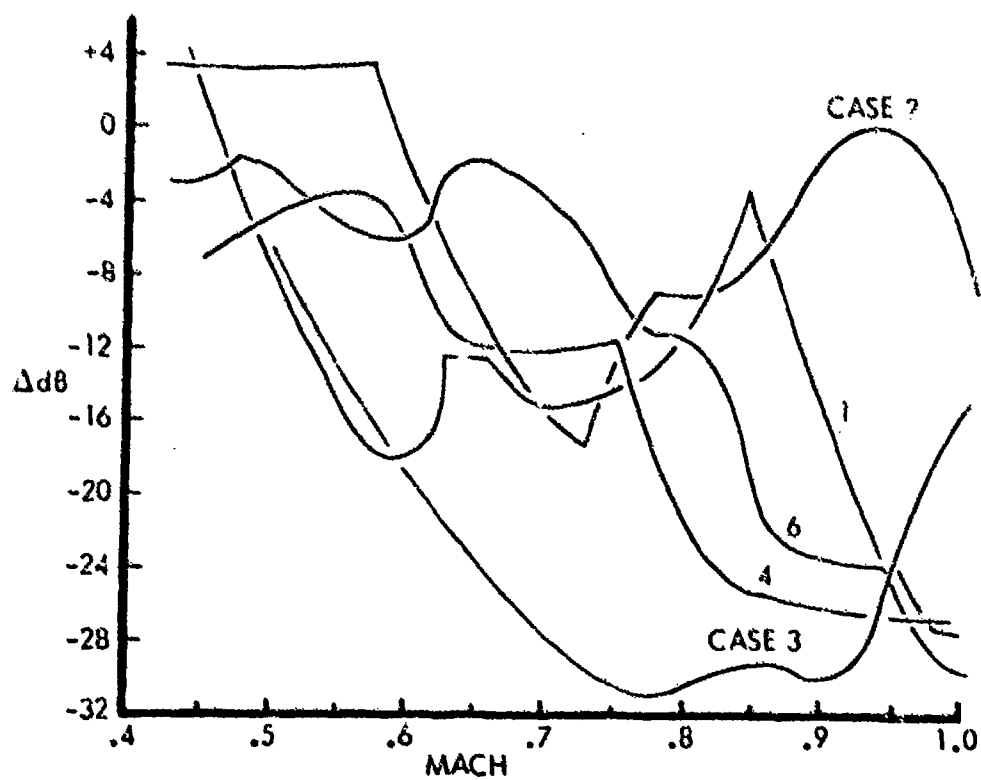


Figure 70. Effect of Selected Alleviation Device(s) on Maximum Oscillatory SPL

CMCA Case #	Launch Altitude Feet	Unsuppressed Max. SPL dB	Suppressed Max. SPL dB
1	25000	160	149
	37000	155	144
2	25000	156	146
	37000	150	141
3	25000	158	128
	37000	153	123
4	25000	151	130
	37000	146	125
5	No Oscillation		
6	25000	162	147
	37000	157	142

Figure 71. Predicted Maximum Levels Of CMCA Missile Bay Oscillation With And Without Alleviation; Launch At Mach 0.8; 25000 And 37000 Feet Altitude